INVESTIGATION OF WETTING AND PHYSICAL PROPERTIES OF (96.5-x)Sn-2Ag-0.5Cu-1In-(x)Al QUINARY LEAD-FREE SOLDER ALLOY SYSTEMS

2024
PhD THESIS
PHYSICS

Masoud Giyathaddin OBAID

Thesis Advisor
Assoc. Prof. Dr. Ahmet Mustafa ERER

INVESTIGATION OF WETTING AND PHYSICAL PROPERTIES OF (96.5-x)Sn-2Ag-0.5Cu-1In-(x)Al QUINARY LEAD-FREE SOLDER ALLOY SYSTEMS

Masoud Giyathaddin OBAID

Thesis Advisor
Assoc. Prof. Dr. Ahmet Mustafa ERER

T.C.
Karabük University
Institute of Graduate Programs
Department of Physics
Prepared as
PhD Thesis

KARABÜK
June 2024

I certify that in my opinion the thesis submitted by Masoud Giyathaddin OBAID titled "INVESTIGATION OF WETTING AND PHYSICAL PROPERTIES OF (96.5-X)Sn-2Ag-0.5Cu-1In-(x)Al QUINARY LEAD-FREE SOLDER ALLOY SYSTEMS" is fully adequate in scope and in quality as a thesis for the degree of PhD.

Assoc. Prof. Dr. Ahmet Mustafa ERER ....
Thesis Advisor, Department of Physics

This thesis is accepted by the examining committee with a unanimous vote in the Department of Physics as a PhD thesis. June 11, 2024

Examining Committee Members (Institutions)		Signature
Chairman	: Prof. Dr. Kadir DEMİR (ZBEU)	....
Member	: Prof. Dr. Necla ÇAKMAK (KBU)	....
Member	: Prof. Dr. Hayrettin AHLATCI (KBU)	....
Member	: Assoc. Prof. Dr. Hakan ALICI (ZBEU)	....
Member	: Assoc. Prof. Dr. Ahmet Mustafa ERER (KBU)	....

The degree of PhD by the thesis submitted is approved by the Administrative Board of the Institute of Graduate Programs, Karabuk University.

Assoc. Prof. Dr. Zeynep ÖZCAN ....
Director of the Institute of Graduate Programs

"I declare that all the information within this thesis has been gathered and presented in accordance with academic regulations and ethical principles and I have according to the requirements of these regulations and principles cited all those which do not originate in this work as well."

Masoud Giyathaddin OBAID

ABSTRACT

Ph. D. Thesis

INVESTIGATION OF WETTING AND PHYSICAL PROPERTIES OF (96.5-x)Sn-2Ag-0.5Cu-1In-(x)Al QUINARY LEAD-FREE SOLDER ALLOY SYSTEMS

Masoud Giyathaddin OBAID

Karabük University
Institute of Graduate Programs
Department of Physics

Thesis Advisor:
Assoc. Prof. Dr. Ahmet Mustafa ERER
June 2024, 115 pages

In this study, aluminum (Al) was added to a SAC205-1In in order to produce (96.5-x)Sn-2Ag-0.5Cu-1In-(x)Al, quinary solder alloys that do not contain lead (Pb), where (x = 0.3 wt%, 0.5 wt%, 0.7 wt%, 0.8 wt%, and 0.9 wt%). By optimizing Sn-Al, manufacturing costs for new Pb-free solder alloys will be reduced. The produced quinary solder alloys were examined for X-RAY fluorescence (XRF) analysis, and the accuracy of the metal ratios in all new quinary lead-free solder alloys was determined by weight percentage. Differential scanning calorimeter (DSC) tests were conducted for all new quinary lead-free solder alloys. The results showed that adding Al to SAC205-1In (217.7 ^{0}C) slightly reduced the melting points. The lowest melting point among all new quinary solder alloys in this study was 214.3 ^{0}C for SAC205-1In-0.3Al. The melting point of the quinary lead-free solder alloy (SAC205-1In-0.3Al) decreased compared to SAC205-1In and SAC305.

The wetting experiments were performed on a Cu substrate in an Ar environment using the hybrid drop technique (pendant and sessile drop technique) at predetermined temperatures of 275 ^{0}C, 300 ^{0}C, and 325 ^{0}C to measure the wettability of the produced solder alloys. At a temperature of 325 ^{0}C, the lowest average contact angle of three positive wetting experiments of SAC205-1In-0.3Al was 39.88^{0}, indicating the highest wettability. SAC205-1In-0.3Al showed the lowest mean contact angle of 42.87^{0} at 325 ^{0}C, while the mean contact angle for SAC205-1In-0.5Al was 43.06^{0}, for SAC205-1In-0.7Al was 50.45^{0}, for SAC205-1In-0.8Al was 43.94^{0}, and for SAC205-1In-0.9Al was 44.78^{0}. The results of the wetting experiments revealed that the contact angle decreases as the temperature increases for all new quinary lead-free solder alloys. This study involved conducting XRD and SEM-EDX analyses to study the microstructure properties of the new quinary solder alloys and how adding aluminum (Al) affects the formation of IMCs in the alloy. The analysis results confirmed the formation of various IMCs, such as Ag_3Sn, Ag_2Al, Ag_3Al, Al_2Cu, AlCu, Cu_3Sn, and Cu_6Sn_5. Adding (Al) to the SAC solder alloys resulted in the formation of Ag-Al and Cu-Al IMC and reduced the growth of Ag3Sn and Cu6-Sn5 IMC. Additionally, this study examined how adding aluminum to the SAC205-1In-xAl solder alloys in a 1M hydrochloride acid HCl solution affects their corrosion behavior. HCL acid is known to have a faster corrosion rate than other electrolytes due to the presence of chlorine (Cl-) and hydrogen (H+) ions compared to other electrolytes like salt and alkaline solutions, which only have one type of ion, produced solder alloys exhibited slightly different corrosion potentials when Al was added, in comparison to the corrosion potentials of SAC305 and SAC205-1In. The corrosion rates followed a pattern where, adding 0.8 wt% Al reduced the corrosion rate, but as less aluminum was replaced with tin, the corrosion rate slightly increased. Furthermore, the corrosion rates of SAC205-1In were enhanced by the addition of Al. This study also utilized a two-point probe technique to examine the electrical resistivity of cross-sectioned samples of developed quinary lead-free solder alloys. The results indicated that as the percentage of aluminum weight increased, so did the electrical resistivity, peaking at 0.9 wt%. Compared to the previous SAC305 solder alloy, all the quinary lead-free solder alloys exhibited a slightly higher electrical resistivity. The solder alloy with 0.3Al added is the best conductor for the current, as it has the lowest electrical resistivity value $1.07 \times 10^{-6}\ \Omega.m$. Meanwhile, shear test

was carried out to assess the reliability of the solder joints. The maximum shear strength was measured as 155.94 MPa for the SAC205-1In-0.8Al solder alloy.

Key Words : Wettability, Hybrid drop technique, Melting point, Corrosion rate, Shear strength, Inter metallic compounds, Resistivity.

Science Code : 20206

ÖZET

Doktora Tezi

(96,5-X)SN-2AG-0,5CU-1IN-(X)AL BEŞLİ KURŞUNSUZ LEHİM ALAŞIMI SİSTEMLERİNİN ISLATMA VE FİZİKSEL ÖZELLİKLERİNİN ARAŞTIRILMASI

Masoud Giyathaddin OBAID

Karabük Üniversitesi
Lisansüstü Eğitim Enstitüsü
Fizik Anabilim Dalı

Tez Danışmanı:
Doç. Dr. Ahmet Mustafa ERER
Haziran 2024, 115 sayfa

Bu çalışmada SAC205-1In’a alüminyum (Al) ilave edilerek beşli birer kurşunsuz lehim alaşımı olan (96.5-x)Sn-2Ag-0.5Cu-1In-(x)Al (x = 0.3 wt%, 0.5 wt%, 0.7 wt%, 0.8 wt%, ve 0.9 wt%) üretilmiştir. Sn-Al optimizasyonu sağlanarak yeni beşli kurşunsuz lehim alaşımlarının üretim maliyeti düşürülecektir. Üretilen beşli lehim alaşımları X-Işını Floresans (XRF) analizine tabi tutuldu ve tüm yeni beşli kurşunsuz lehim alaşımlarındaki metal oranlarının doğruluğu ağırlık yüzdesi ile belirlendi. Tüm yeni beşli kurşunsuz lehim alaşımları için diferansiyel taramalı kalorimetre (DSC) testleri yapıldı. Sonuçlar, SAC205-1In'a Al eklenmesinin erime noktalarını hafifçe düşürdüğünü gösterdi. Bu çalışmadaki tüm yeni beşli lehim alaşımları arasında en düşük erime noktası SAC205-1In-0.3Al için 214.3 ^{0}C oldu. Beşli kurşunsuz lehim

alaşımı SAC205-1In-0.3Al'un erime noktası, SAC205-1In ve SAC305'e kıyasla azaldı.

Islatma deneyleri, üretilen lehim alaşımlarının ıslanabilirliğini ölçmek için önceden belirlenmiş 275 ^{0}C, 300 ^{0}C ve 325 ^{0}C sıcaklıklarda Hibrit damla tekniği kullanılarak Ar ortamında bir Cu altlık üzerinde gerçekleştirildi. 325 ^{0}C sıcaklıkta SAC205-1In-0.3Al'un üç pozitif ıslatma deneyinin en düşük ortalama temas açısı 39.88^0 ile en yüksek ıslanabilirliği gösterdi. Ortalama temas açısı 325 ^{0}C'de SAC205-1In-0.5Al için 43.06^0, SAC205-1In-0.7Al için 50.45^0, SAC205-1In-0.8Al için 43.94^0 ve SAC205-1In-0.9Al için 44.78^0 olurken SAC205-1In-0.3Al en düşük ortalama temas açısı olarak 42.87^0 göstermiştir. Islatma deneylerinin sonuçları, tüm yeni beşli kurşunsuz lehim alaşımları için sıcaklık arttıkça temas açısının azaldığını ortaya çıkardı. Bu çalışma, yeni beşli lehim alaşımlarının mikroyapı özelliklerini ve alüminyum (Al) ilavesinin alaşımdaki IMC oluşumunu nasıl etkilediğini incelemek için XRD ve SEM-EDX analizlerinin yapılmasını içermektedir. Analiz sonuçları Ag_3Sn, Ag_2Al, Ag_3Al, Al_2Cu, AlCu, Cu_3Sn ve Cu_6Sn_5 gibi çeşitli IMC'lerin oluşumunu doğrulamaktadır. SAC lehim alaşımlarına Al eklenmesi, Ag-Al ve Cu-Al IMC'nin oluşmasını sağlamış ve Ag_3Sn ve Cu_6Sn_5 IMC gelişimini azaltmıştır. Ek olarak bu çalışma, 1M hidroklorür (HCl) asit çözeltisindeki SAC205-1In-xAl lehim alaşımlarına alüminyum eklemenin korozyon davranışlarını nasıl etkilediğini incelemiştir. HCL asidinin, yalnızca tek tür iyona sahip olan tuz ve alkalin çözeltileri gibi diğer elektrolitlerle karşılaştırıldığında, klor (Cl^-) ve hidrojen (H^+) iyonlarının varlığı nedeniyle diğer elektrolitlerden daha hızlı korozyon oranına sahip olduğu bilinmektedir. Üretilen lehim alaşımları, Al eklendiğinde SAC305 ve SAC205-1In'un korozyon potansiyellerine kıyasla biraz farklı korozyon potansiyelleri göstermiştir. Korozyon oranları, ağırlıkça %0.8 Al ilavesinin korozyon hızını azalttığı bir model izlemiştir, ancak daha az alüminyumun kalayla değiştirilmesiyle korozyon hızı biraz artmıştır. Ayrıca SAC205-1In'un korozyon oranları Al ilavesiyle arttırılmıştır. Bu çalışmada ayrıca, geliştirilen beşli kurşunsuz lehim alaşımlarının kesit örneklerinin elektriksel özdirencini incelemek için iki noktalı sonda tekniği kullanılmıştır. Sonuçlar, alüminyum ağırlık yüzdesi arttıkça elektrik özdirencinin de arttığını ve ağırlıkça % 0.9'a ulaştığını göstermiştir. Önceki SAC305 lehim alaşımıyla karşılaştırıldığında tüm beşli kurşunsuz lehim alaşımları biraz daha yüksek bir

elektriksel özdirenç sergilemiştir. 0.3Al ilaveli lehim alaşımı, $1.07 \times 10^{-6} \Omega \cdot m$ ile en düşük elektriksel özdirenç değerine sahip olduğundan akım için en iyi iletken olmuştur. Bunun yanında lehim bağlantılarının güvenilirliğini belirlemek için kesme testi yapılmıştır. Maksimum kesme dayanımı 155.94 MPa olarak SAC205-1In-0.8Al lehim alaşımı için ölçülmüştür.

Anahtar Kelimeler **:** Islanabilirlik, Hibrit damla tekniği, Erime noktası, Korozyon hızı, Kesme dayanımı, İntermetalik bileşikler, Özdirenç.

Bilim Kodu **:** 20206

ACKNOWLEDGMENT

Starting with a heart full of gratitude, I sincerely thank God for completing my thesis. I am also deeply thankful to my supervisor, Assoc. Prof. Dr. Ahmet Mustafa ERER, for generously sharing his time, invaluable advice, and insightful ideas that helped me choose a thesis subject, navigate the research process and develop a solid plan for completing the thesis to the best of my ability.

I want to thank my Ph.D. thesis committee members, Prof. Dr. Necla ÇAKMAK and Prof. Dr. Hayrettin AHLATCI, for their constructive feedback, thought-provoking questions, and unwavering support throughout my academic journey. Your contributions have significantly enhanced the quality of my thesis.

I am also grateful to the physics department staff at the College of Science at Karabuk University for their assistance and kind treatment during my entire study period. I also thank my friends and colleagues at Karabuk University, especially Dr. Serkan OGUZ, for their invaluable help completing this thesis.

Also, I thank the staff of all physics laboratories and the library of Karabuk University for their cooperation and help during my studies.

Lastly, I want to convey my sincere gratitude to my mother, father, wife, and entire family for their unwavering support and encouragement throughout this academic pursuit.

This work was supported by the Karabuk University Scientific Research Project (BAP). Within the scope of the Comprehensive Research Project, it was supported with the project number 'KBÜBAP- 21-KP-091'.

CONTENTS

Page

APPROVAL ii
ABSTRACT iv
ÖZET vii
ACKNOWLEDGMENT x
CONTENTS xi
LIST OF FIGURES xiv
LIST OF TABLES xviii
SYMBOLS AND ABBREVITIONS INDEX xx

PART 1 1
INTRODUCTION 1

PART 2 5
LITERATURE REVIEW 5

PART 3 13
THEORETICAL BACKGROUND 13
- 3.1 SOLDERING AND WETTABILITY 13
- 3.2 YOUNG'S EQUATION 14
- 3.3 UTILIZATIONS OF CONTACT ANGLES 16
- 3.4 METHODS OF MEASURING CONTACT ANGLES 17
  - 3.4.1 Sessile Drop Method 17
  - 3.4.2 Captive Bubble Approach 18
  - 3.4.3 Droplet Sliding on a Tilted Surface 18
  - 3.4.4 Drop Dimensions Approach 19
  - 3.4.5 Wilhelmy Plate Approach 20
- 3.5 MAXIMUM BUBBLE PRESSURE METHOD 21
- 3.6 DROP VOLUME OR DROP WEIGHT METHOD 22

Page

3.7 CAPILLARY RISE METHOD 23
3.8 THE FACTORS THAT AFFECT THE MEASUREMENT OF CONTACT ANGLE 24
3.9 SURFACE TENSION OF METALS 26
3.10 ADSORPTION 26
3.10.1 Physical Adsorption 27
3.10.2 Chemical Adsorption 28
3.11 KINITIC ADSORPTION 28
3.12 BIOSORPTION 28
3.13 DEVELOPMENT OF SOLDER ALLOYS 29
3.13.1 Sn-Pb Solder Alloys 29
3.13.2 Lead Free Solder Alloys 30
3.14 Sn-Ag-Cu LEAD FREE SOLDER ALLOYS 32
3.14.1 Effect Of Ag And Cu On SAC Lead Free Solder Alloys. 33
3.14.2 Effect Of Al On SAC Lead Free Solder Alloys. 34

PART 4 36
METHODOLOGY 36
4.1 PRODUCTION OF LEAD-FREE SOLDER ALLOYS 36
4.2 X-RAY FLUORESCENCE (XRF) METHOD 38
4.3 X-RAY DIFFRACTION (XRD) 38
4.4 DIFFERENTIAL SCANNING CALORIMETER (DSC) ANALYSIS 39
4.5 WETTING EXPERIMENTS 40
4.6 SEM-EDX ANALYSIS OF SAC205-1In-xAl SOLDER ALLOYS ON Cu SUBSTRATE. 43
4.7. CORROSION EXPERIMETNS 46
4.8 ELECTRICAL RESISTIVITY MEASUREMENTIS 47
4.9 SHEAR STRENGTH TESTS 49

PART 5 52
RESULT AND DISCUSSION 52
5.1 X-RAY FLUORESCENCE (XRF) ANALYSIS 52

Page

5.2 DIFFERNTIAL SCANNING CALORIMETER (DSC) ANALYSIS 53
5.3 X-RAY DIFFRACTION (XRD) ANALYSIS 55
5.4 WETTABILITY ANALYSIS 57
5.4.1 Contact Angles Measurements Of SAC205-1In-0.3Al 57
5.4.2 Contact Angles Measurements Of SAC205-1In-0.5Al 59
5.4.3 Contact Angles Measurements Of SAC205-1In-0.7Al 61
5.4.4 Contact Angles Measurements Of SAC205-1In-0.8Al 63
5.4.5 Contact Angles Measurements Of SAC205-1In-0.9Al 65
5.5 SEM-EDX ANALYSIS OF SAC205-1In-xAl SOLDER ALLOYS ON Cu-SUBSTRATE. 70
5.6 CORROSION ANALYSIS 76
5.6.1 Characteristics Of New Solder Alloys.. 76
5.6.2 Potentiodynamic Polarization Analysis.. 79
5.6.3 Post-Corrosion Descriptions.. 81
5.7 ELECTRICAL RESISTIVITY ANALYSIS.. 85
5.8 SHEAR STRENGTH RESULTS.. 88

PART 6 91
CONCLUSION 91

PART 7 96
SUMMARY 96

REFERENCES 98

APPENDIX A. 110
MEASUREMENTS OF THE CONTACT ANGLE OF SAC205-1In-XAl OBTAINED FROM WETTING EXPERIMENTS 110
APPENDIX B. 114
ELECTRICAL RESISTIVITY MEASUREMENTS OF SAC205-1In-xAl 114

RESUME 115

LIST OF FIGURES

Page

Figure 3.1. Three forces maintain the equilibrium of a liquid droplet on a solid surface (γSL), (γSV), and (γLV). 14

Figure 3.2. A diagram of the sessile-drop technique [133]. 18

Figure 3.3. Contact angle measurements using the sliding drop on an inclined plate method [69]. 19

Figure 3.4. Calculating the contact angle using the drop dimensions method. 20

Figure 3.5. The maximum bubble pressure method [69]. 22

Figure 3.6. Liquid surface tension measurement, a. A pendant drop is produced by suspending the liquid from the end of a narrow tube. b. Injecting the gas is done using a syringe with a needle attached to the tip [69].......... 23

Figure 3.7. A diagram of the capillary rise method [76]. 24

Figure 3.8. Phase diagram of Sn-Pb [93].......... 29

Figure 3.9. Phase diagram of Sn-Ag binary solder alloy.......... 31

Figure 3.10 SEM micrographs with high magnification of SAC solder joints having two different weight percentages of Ag. a) Ag 3%wt, b) Ag 4 %wt [105]. 33

Figure 3.11. Results of microscopic analysis conducted on a) Sn-3.0Ag-0.5Cu and b) Sn-3.9Ag-0.5Cu [106].......... 34

Figure 3.12. SEM of IMC layer formed in (a), (b) SAC0305, (c), (d) SAC0305-1Al, (e), (f) SAC0305-2Al, (g), (h) SAC0305-2Al-2Si solder joint. (b), (d), (f), and (h) are the magnified images of (a), (c), (e), and (g) [109]. 35

Figure 4.1. Melting materials in a controlled atmosphere unit (Furnace). 36

Figure 4.2. Displays the quinary lead free-solder alloys that have been produced. .. 37

Figure 4.3. Electric furnace used for homogenization process.......... 37

Figure 4.4. Preparing the samples for XRF and XRD analysis. 38

Figure 4.5. The device used for the XRD analysis "RIGOKU - ULTIMA IV.......... 39

Figure 4.6. DTA/TGA/DSC Laboratory for determining melting temperature of solder alloys. 40

Figure 4.7. Illustrates the components of the experimental apparatus used in the hybrid drop technique. 40

Figure 4.8. The device used for the SEM-EDX analysis " ZEISS ULTRA PLUS FESEM SE2. 44

Page

Figure 4.9. Shows the preparing SACIn-xAl solder/Cu interface at temperatures of 2750C, 3000C, and 3250C for SEM-EDX analysis................................ 45

Figure 4.10. Forcipol 2v, a Grinder-Polisher device.. 45

Figure 4.11. Electrical resistivity measurements were taken using the Keith 2400 source meter and two-point probe technique. 47

Figure 4.12. Shows Cu-substrate dimensions and the process of soldering. 50

Figure 4.13. The device used for shear strength test Zwick Roell Z050 device at static test laboratory of Karabük University Iron and Steel Institute....... 51

Figure 5.1. The weight percentage of elements in produced solder alloys 53

Figure 5.2. DSC analysis of SAC205-1In-xAl , a) SAC-In-0.3Al , b) SAC-In-0.5Al, c) SAC-In-0.7Al, d) SAC-In-0.8Al, e) SAC-In-0.9Al............................ 55

Figure 5.3. XRD analysis of lead-free solder alloys SAC205-1In-xAl indicates the formation of IMCs: a) SAC205-11In-0.3Al, b) SAC205-1In-0.5Al, c) SAC205-1In-0.7Al, d) SAC205-1In-0.8Al, and e) SAC205-1In-0.9Al. . 56

Figure 5.4. Shows the measurements of the left and right contact angles for SAC205-1In-0.3Al droplet on a Cu-substrate at intervals 600th-second a) Exp. (3) at 275 °C, b) Exp. (6) at 300 °C, c) Exp. (8) at 325 °C........................... 59

Figure 5.5. Shows the measurements of the left and right contact angles for SAC205-1In-0.5Al droplet on a Cu-substrate at intervals 600th-second a) Experiment (10) at 275 °C, b) Experiment (13) at 300 °C, c) Experiment (16) at 325 °C.. 60

Figure 5.6. Shows the measurements of the left and right contact angles for SAC205-1In-0.7Al droplet on a Cu-substrate at intervals 600th-second a) Experiment (21) at 275 °C, b) Experiment (23) at 300 °C, c) Experiment (26) at 325 °C.. 62

Figure 5.7. Shows the measurements of the left and right contact angles for SAC205-1In-0.8Al droplet on a Cu-substrate at intervals 600th-second a) Experiment (29) at 275 °C, b) Experiment (31) at 300 °C, c) Experiment (35) at 325 °C.. 64

Figure 5.8. Shows the measurements of the left and right contact angles for SAC205-1In-0.9Al droplet on a Cu-substrate at intervals 600th-second a) Experiment (38) at 275 °C, b) Experiment (41) at 300 °C, c) Experiment (43) at 325 °C.. 67

Figure 5.9. The average contact angles of three wetting-positive experiments at specified intervals (0, 5, 10, 15, 30, 60, 90, 120, 150, 300, and 600 seconds) of a SAC205-1In-xAl solder droplet on a Cu substrate at temperatures of 275°C, 300°C, and 325°C. 68

Figure 5.10.SEM images of SAC205-1In-0.3Al solder alloy/Cu interface at different temperatures: a) 2750C, b) 3000C, c) 3250C. 72

Page

Figure 5.11.SEM images of SAC205-1In-0.5Al solder alloy/Cu interface at different temperatures: a) 2750C, b) 3000C, c) 3250C. 72

Figure 5.12.SEM images of SAC205-1In-0.7Al solder alloy/Cu interface at different temperatures: a) 2750C, b) 3000C, c) 3250C. 72

Figure 5.13.SEM images of SAC205-1In-0.8Al solder alloy/Cu interface at different temperatures: a) 2750C, b) 3000C, c) 3250C. 73

Figure 5.14.SEM images of SAC205-1In-0.9Al solder alloy/Cu interface at different temperatures: a) 2750C, b) 3000C, c) 3250C. 73

Figure 5.15.SEM-EDX results of the SAC205-1In-0.3Al solder/Cu interface at predetermined temperatures: a) 2750C, b) 3000C, and c) 3250C............ 73

Figure 5.16.SEM-EDX results of the SAC205-1In-0.5Al solder/Cu interface at predetermined temperatures: a) 2750C, b) 3000C, and c) 3250C............ 74

Figure 5.17.SEM-EDX results of the SAC205-1In-0.7Al solder/Cu interface at predetermined temperatures: a) 2750C, b) 3000C, and c) 3250C............ 74

Figure 5.18.SEM-EDX results of the SAC205-1In-0.8Al solder/Cu interface at predetermined temperatures: a) 2750C, b) 3000C, and c) 3250C............ 75

Figure 5.19.SEM-EDX results of the SAC205-1In-0.9Al solder/Cu interface at predetermined temperatures: a) 2750C, b) 3000C, and c) 3250C............ 75

Figure 5.20.SEM images of SAC-1In-xAl solder alloys before the electrochemical measurements in 1M HCL solution (a) SAC205-1In-0.3Al, (b) SAC205-1In-0.5Al, (c) SAC205-1In-0.7Al, (d) SAC205-1In-0.8Al, and (e) SAC205-1In-0.9Al.. 77

Figure 5.21.EDX analysis of SAC205-1In-0.3Al alloy before immersion in 1M HCL 77

Figure 5.22.EDX analysis of SAC205-1In-0.5Al alloy before immersion in 1M HCL 78

Figure 5.23.EDX analysis of SAC205-1In-0.7Al alloy before immersion in 1M HCL 78

Figure 5.24.EDX analysis of SAC205-1In-0.8Al alloy before immersion in 1M HCL 78

Figure 5.25.EDX analysis of SAC205-1In-0.9Al alloy before immersion in 1M HCL 79

Figure 5.26.Potentiaodynamic polarization curves, a) Potentiodynamic polarization curves of SAC205-1In-xAl (x = 0.3, 0.5, 0.7, 0.8, and 0.9 wt%), b) potentiodynamic polarization curves magnified image. 80

Figure 5.27.SEM images of SACIn-xAl solder alloys after immersion in 1M HCL solution: (a) SAC205-1In-0.3Al, (b) SAC205-1In-0.5Al, (c) SAC205-1In-0.7Al, (d) SAC205-1In-0.8Al, and (e) SAC205-1In-0.9Al. 82

Figure 5.28.EDX analysis of the SAC205-1In-0.3Al solder alloy after immersion in a 1M HCL solution. 83

Page

Figure 5.29.EDX results of the SAC205-1In-0.5Al solder alloy after immersion in a 1M HCL solution. 83

Figure 5.30.EDX results of the SAC205-1In-0.7Al solder alloy after immersion in a 1M HCL solution. 84

Figure 5.31.EDX results of the SAC205-1In-0.8Al solder alloy after immersion in a 1M HCL solution. 84

Figure 5.32.EDX results of the SAC205-1In-0.9Al solder alloy after immersion in a 1M HCL solution. 85

Figure 5.33.Maximum electrical resistivity of new quinary lead-free solder alloys SAC205-1In-xAl (x=0.3, 0.5, 0.7, 0.8 , and 0.9 wt%) and SAC305. 86

Figure 5.34.Average Electrical resistivity of SAC205-1In-xAl (x=0.3 wt%, 0.5 wt%, 0.7 wt%, 0.8 wt%, 0.9 wt%.. 87

Figure 5.35.Shear strength values of produced solder alloys SAC205-1In-xAl 90

Figure Appendix A.1. Contact angle measurements of SAC205-1In-0.3Al............ 110

Figure Appendix A.2. Contact angle measurements of SAC205-1In-0.5Al............ 111

Figure Appendix A.3. Contact angle measurements of SAC205-1In-0.7Al............ 111

Figure Appendix A.4. Contact angle measurements of SAC205-1In-0.8Al............ 112

Figure Appendix A.5. Contact angle measurements of SAC205-1In-0.9Al............ 112

Figure Appendix A.6 Mean contact angles of SAC205-1In-xAl............................ 113

LIST OF TABLES

Page

Table 3.1. The melting points of some binary lead-free solder alloys [16] 30

Table 3.2. Melting points of some ternary solder alloys 32

Table 4.1. The specifications of each component of the experiment device. 41

Table 4.2. List of the hybrid drop technique experiments that are conducted at different temperature for each quinary lead-free solder alloys formed by the addition of Al to SAC205-1In. 43

Table 4.3. Displays the solder alloys produced with their corresponding wetting experiment numbers for SEM-EDX analysis.. 45

Table 5.1. Results of XRF analysis show the wt% of the chemical composition of produced quinary lead-free solder alloys Sn-2Ag-0.5Cu-1In-xAl......... 52

Table 5.2. The melting temperatures of the produced quinary lead-free solder alloys according to the results of DSC. 54

Table 5.3. Displays the average left and right contact angles for each wetting experiment of SAC205-1In-0.3Al at 2750C, 3000C, and 3250C. 58

Table 5.4. Shows the average contact angle measurements for three wetting experiments of SAC205-1In-0.3Al performed at 2750C, 3000C, and 3250C. 59

Table 5.5. Displays the average left and right contact angles for each wetting experiment of SAC205-1In-0.5Al at 275 0C, 300 0C, and 325 0C. 60

Table 5.6. Shows the average contact angle measurements for three wetting experiments of SAC205-1In-0.5Al performed at 2750C, 3000C, and 3250C. 61

Table 5.7. Displays the average left and right contact angles for each wetting experiment of SAC205-1In-0.7Al at 275 0C, 300 0C, and 325 0C. 62

Table 5.8. Shows the average contact angle measurements for three wetting experiments of SAC205-1In-0.7Al performed at 275 0C, 300 0C, and 325 0C. 63

Table 5.9. Displays the average left and right contact angles for each wetting experiment of SAC205-1In-0.8Al at 2750C, 3000C, and 3250C. 64

Table 5.10. Shows the average contact angle measurements for three wetting experiments of SAC205-1In-0.8Al performed at 275 0C, 300 0C, and 325 0C. 65

Table 5.11. Displays the average left and right contact angles for each wetting experiment of SAC205-1In-0.9Al at 275 0C, 300 0C, and 325 0C. 66

Page

Table 5.12. Shows the average contact angle measurements for three wetting experiments of SAC205-1In-0.9Al performed at 275 0C, 300 0C, and 325 0C. 67

Table 5.13. Mean contact angles of new quinary lead-free solder alloys at predetermined temperatures of 275 0C, 300 0C, and 325 0C 69

Table 5.14. The corrosion parameters of the produced solder alloy SAC205-1In-xAl 81

Table 5.15. The maximum electrical resistivity of the new quinary lead-free solder alloys SAC205-1In-xAl obtained experimentally and SAC305. 86

Table 5.16. The average electrical resistivity of SACIn-xAl (x=0.3 wt%, 0.5 wt%, 0.7 wt%, 0.8 wt%, 0.9 wt%). 87

Table 5.17. Shear strength test results of produced solder alloys SACIn-xAl. 89

Table Appendix B. 1. Electrical resistivity measurements of SAC205-1In-xAl where (x=0.3, 0.5, 0.7, 0.8, and 0.9 wt%). 114

SYMBOLS AND ABBREVITIONS INDEX

SYMBOLS

Cu : Copper

Pb : Lead

Hg : Mercury

Cd : Cadmium

Sn : Tin

Bi : Bismuth

Zn : Zinc

Ag : Silver

Ni : Nickel

In : Indium

Al : Aluminum

Ga : Gallium

Co : Cobalt

Pt : Platinum

Au : Gold

P : Phosphorus

Sb : Antimony

Ge : Germanium

NaCl : Sodium Chloride

Ti : Titanium

Fe : Iron

Ar : Argon

TiO2 : Titanium Dioxide

HCl : Hydrochloric Acid

ρ : Electrical Resistivity

A : Area

Al2O3 : Aluminum Oxide

G : Geometric Resistivity Correction

T : Thickness

γ : Surface Tension

θ : Angle

$\emptyset_t$: Tilt angle

h : Height

R : Radius of the spherical segment

Rb : Contact Radius of the liquid drop

Δp : Density Difference between the liquid and the vapor

ΔP : Young-Laplace Pressure Difference

g : Gravity Acceleration Constant

a : Capillarity Constant

P : Pressure

W_{drop} : Force Balance

m : Mass

r : Radius

V : Volume

R : Resistance

I : Current

V : Voltage

S : Distance between probs

T_1 : Correction Factor to apply for finite thickness (t) of the sample

ρ : Electrical Resistivity

G : Geometric Correction Factor

Fmax : Maximum Shear Force

ε_{max} : Maximum Shear Elongation

Fbreak : Breaking Shear Force

ε_{break} : Breaking Shear Elongation

ABBREVITIONS

SAC	: Tin-Silver-Copper
EU	: European
RoHs	: Restriction Of Hazardous Substances
WEEE	: Waste Of Electric And Electronic Equipment
XRF	: X-Ray Fluorescence
XRD	: X-Ray Diffraction
DSC	: Differential Scanning Calorimeter
SEM	: Scanning Electron Microscope
EDX	: Energy-Dispersive X-Ray Spectroscopy.
IMC	: Intermetallic compounds
icorr or CCD	: Corrosion Current Density
Ecorr	: Corrosion Potential
Cr	: Corrosion Rate
CNTs	: Coated Carbon Nanotubes
SL	: Solid and Liquid
SV	: Solid and Vapor or Gas
LV	: Liquid and Vapor
CA	: Contact Angle
SMT	: Surface Mount Technology
PTH	: Plated-Through-Hole
BGA	: Ball Grid Array
GIXRD	: Grazing Incidence X-Ray Diffraction
XRR	: X-Ray Reflectivity
DTA	: Differential Thermal Analysis
TGA	: Thermal Gravimetric Analysis

PART 1

INTRODUCTION

Solder alloys like Sn-Pb have been used to construct electronic devices for a long time. Numerous positive qualities of this alloy include affordability, low melting point, good manufacturability, and excellent wetting on copper (Cu) substrates. However, extensive research has been conducted to find a Pb-free solder acceptable for electronic assemblies because of the toxicity of Pb to human health and the environment [1]. Due to environmental concerns, governmental regulations, and competition, there has been a sustained shift toward using lead-free soldering. SAC solder alloy is widely acknowledged and recommended as the preferred lead-free alloy for interconnecting electronic components in the electronics industry [2]. The use of risky materials Pb, Hg, and Cd is restricted by various environmental legislations. These environmental directives encouraged the widespread manufacturing of soldiers without lead in electronics and electrical equipment industries. To replace solders, contain lead, many lead-free solder compositions have been developed, including Sn - Cu , Sn – Ag, Sn - Bi, Sn - Zn, Zn - Bi, Sn – Ag - Cu, Sn – Zn - Bi, Sn – Cu - Bi, Sn – Cu - Ni, and more. Researchers in the electrical and electronic sectors are facing difficulties due to creating IMCs, which increase the melting temperature of lead-free solder [3]. To find replacements for the standard Sn-Pb solder alloy, various alloys containing components like Sn, Ag, Cu, Bi, In, and Zn have been identified as potential options [4,5]. However, it is yet to be determined if replacements for all applications will be reached.

Due to its high reliability and desirable mechanical characteristics, SAC solder alloys were among the most widely used Pb-free solders. Three challenges that must be addressed are the high cost, high melting temperature, and poor wettability of the Sn-Ag-Cu solders. To tackle these disadvantages of SAC and improve its performance, we added an Al element to SAC205-1In in this study. Technological product

and electrical and electronic devices, which are an indispensable part of our lives, are widely used and will directly impact the environment and human health as waste material when they malfunction. For soldering operations, Solder alloys containing lead threaten human health and environmental pollution as the Pb element is toxic. According to the EU's RoHS and WEEE directives, seven elements, including Pb, were restricted and banned in many countries in 2006 [6]. Using solder with a high silver content increases its cost [7].

The directives of RoHS and WEEE aim to produce and advance solder alloys that don't contain lead. Finding alternative lead-free solder alloys with wetting properties, mechanical properties, and costs similar to or better than the previously used Sn-Pb alloy is essential. Several lead-free solder alloys, including Sn-Ag, Sn-Cu, Sn-Zn, Sn-Bi, Sn-In, and SAC, have been produced as replacements for Sn-Pb.

There are certain disadvantages linked with the SAC group of alloys. Compared to the Sn-Pb solder alloy, which has a melting temperature of 183°C, these alloys are less desirable because of their high melting temperatures of 217–219°C. Moreover, the high Ag ratio in these alloys raises the cost of production. The desired results were obtained from Sn-2Ag-0.5Cu-1Bi and Sn-2Ag-0.5Cu-1In solder alloys produced before. They are more suitable for melting temperatures and production costs and have higher wetting capabilities than SAC305 alloys [8,9]. Wetness is defined by the ability of the molten solder to spread on its substrate during the reflow process [10].

Sn-Ag and SAC solders, with higher melting points than the Sn-Pb alloy, are being investigated as alternatives to Sn-Pb. Both types will need higher soldering temperatures when used in the industrial field [11]. The wetting and melting temperature characteristics of lead solder alloy Sn-Pb are still not achieved, as the solder alloy development is ongoing. The addition of aluminum to the Sn-Cu-Al solder alloy enhances its wettability [12]. Two approaches could enhance the properties of lead-free solder alloys. The first method involves adding elements like rare earth components to the SAC alloy to improve its wetting properties and overall performance. The second method involves adding metal, ceramic, and polymer

nanoparticles or particles to achieve different properties of the SAC solder. The type and size of the added particles determine the resulting properties [13]. SnPb solder melts at 183°C, whereas SAC solder melts at 227°C. However, adding an element like titanium or zinc to the SAC lead-free solder alloys can reduce the alloy's melting temperature to as low as three °C [14]. When searching for an alternative to Pb-based soldering materials, it is essential to ensure that the substitute solders' properties are equal or superior to Sn-Pb solders. The ideal lead-free alternatives have established criteria, including a melting temperature similar to Sn-Pb solders, better wettability for suitable metallization in the manufacturing process, similar or better electrical conductivity to transmit electrical signals efficiently, adequate mechanical properties to ensure the reliability of electronic products, and is nontoxic and relatively inexpensive [15]. Soldering has become an essential technique for producing electronic devices since the advent of the electronic age in the 20th century. All electronic components like resistors, capacitors, transistors, and integrated circuits are connected to the printed circuit board using soldering. In today's technology, portable electronic devices, modern automobiles, space vehicles, and power plants are equipped with countless soldered electronic components [16].

This research explores the effects of adding aluminum (Al) to the lead-free solder alloy Sn-2Ag-0.5Cu-1In. The study involves producing a quinary Pb-free solder alloy (96.5-x)Sn–2Ag-0.5Cu-1In–xAl, where x is (0.3 wt%, 0.5 wt%, 0.7 wt%, 0.8 wt%, and 0.9 wt%). It further investigates the performance of the produced alloys, including their physical properties, wettability, inter-metallic phases, microstructures, and melting temperatures by using advanced techniques such as hybrid drop technique, X-ray fluorescence analysis (XRF), X-ray diffraction (XRD), differential scanning calorimeter (DSC), scanning electron microscope, and energy-dispersive X-ray spectroscopy (SEM + EDX). Furthermore, the potentiodynamic polarization technique is used to determine corrosion rates; electrical conductivity analysis is used to determine the resistivity of the alloys, and shear strength analysis is used to investigate the reliability of solder joints of the alloy. Thus, this study is significant in lead-free solder alloy production by introducing new quinary lead-free solder alloys that have never been produced before and providing a comprehensive analysis of the production parameters required to achieve an industrial output of these alloys.

The research makes essential contributions to the literature by discussing the advantages and disadvantages of the newly produced alloys compared to similar alloys and comparing each test and analysis result of the produced alloys with each other and the previous results in the literature. This level of detail and analysis provides valuable insights into the characteristics, properties, and performance of the new quinary lead-free solder alloys, which can inform future research and improve the production processes of these alloys.

PART 2

LITERATURE REVIEW

About 2000 years ago, tin-lead (Sn-Pb) solders were initially utilized for metal connections. Soldering is required for every electronic device and circuit assembly, connectivity, and packaging [17]. Lead is a toxic substance and can build up in human organisms throughout time by establishing solid connections to proteins and impeding the body's regular processing and operation [18]. Solder alloys containing lead were commonly used in electrical and electronic equipment. However, because of lead's toxic nature, these soldiers are being phased out in response to the RoHS directives starting from July 2006. Leads' harmful effects have forced countries like Japan and countries in the European Union to implement laws that either ban or limit the use of solders containing lead. As a result, these directives encourage the production of new Pb-free solders [4,19]. Therefore, several studies were conducted to produce lead-free solder alloys and, simultaneously, to try to reduce silver quantity from lead-free alloys (SAC) to reduce its production cost and improve its properties [20]. In 2003 a study was carried out by Terashima *et al.* to investigate the effect of silver content on the thermal fatigue resistance of Sn-xAg-0.5 Cu. It was observed that solder alloys containing less Ag content (1 to 2 wt%) exhibited a higher rate of failure when subjected to thermal fatigue testing compared to alloys containing more Ag content (3 to 4 wt%). Furthermore, the study showed that the endurance resistance of the solder junctions was strongly correlated with the content of silver. Solder junctions containing a higher ratio of silver have better endurance resistance [21].

Many studies looked at the thermal and microstructure characteristics of Sn-In-(Ga, Zn, Bi) solder alloys. According to the findings, adding those alloying elements resulted in a lower temperature of melting and varied the microstructure of the produced solder alloys [22]. In 2001, researchers Huh *et al.* examined the effects of

mixing Ag to Sn-0.7 Cu on its microstructural and tensile properties. Their findings revealed that adding Ag increased the size of Cu_6Sn_5 particles, while Ag_3Sn particles dispersed finely in the

eutectic network band. Furthermore, the ductility of the Sn-0.7 Cu alloy can be significantly enhanced by adding Ag [23]. In 2008, a study conducted by Amagai discovered that nanoparticles such as Pt, Co, and Ni were more helpful in promoting the creation of IMCs and improving drop test results when compared to other nanoparticles like Ge, In, P, Cu, Ag, Zn, Au, Al, and Sb. The study also revealed that adding 0.05% aluminum as nanoparticles did not impact the interfacial IMC. A few other studies were conducted to determine the effect of adding aluminum on mechanical and interfacial properties, microstructure, and its interaction with a copper substrate [24]. Moser et al. verified that adding (In) to SAC alloy affected the wettability, giving good wet diffusion connections on the surface of the substrate [25]. The formation of an IMC at the point of contact between the copper and solder during soldering can impact the solderability and wetting. Typically, the existence of an IMC at the solder-substrate interface is indicated by high wetting [26]. In 2009, Rosalbino et al. investigated the way that two different kinds of solder alloys corrode, namely Sn–3Ag–3Cu and SAC305, in a 0.1 M solution of NaCl. Potentiodynamic polarization was employed to measure the corrosion resistance of each alloy and compare the results. It was found that the Sn–3Ag–3Cu alloy exhibited better resistance to corrosion than the Sn–3Ag–0.5Cu solder in the NaCl solution. After the electrochemical tests, On the surface of both alloys, the researchers also found tin oxyhydroxychlorides or oxychlorides [27]. In 2011, Moser et al. studied characteristics wetting of Sn-2.86Ag-0.40Cu alloys on a Cu substrate when a flux was present. The study found that the CA decreased as the alloy's In content increased. The wetting balance results agreed with those of the sessile drop studies. It was discovered that the wetting of SAC-In alloys on copper substrate was good [28]. Kannachai et al.'s 2009 study found that adding Indium (up to 3 wt%) to SAC0307 lead-free solder alloy lowers its temperatures at solidus and liquidus, reduces the time of wetting, and raises the microhardness, tensile strength, and wetting force. The size of the Sn-rich phase is reduced, and the dispersion of IMCs becomes more regular with the addition of In up to 0.3 wt% [29]. A 2012 study

examined the effects of incorporating a small amount of Ti into Sn3.5Ag0.5Cu solder, specifically on its mechanical properties and microstructure. The research findings revealed that even adding less than 1.0 wt% of Ti could reduce the melting temperature and refine the microstructure of the solder alloy. The microstructural analysis showed that the refinement of b-Sn and the formation of Ti_2Sn_3 IMCs in the SAC-XTi solder alloys improved the mechanical properties [30]. In 2012, Fallahi et al. conducted a study aimed to enhance the reliability of SAC solder by adding iron and indium. The researchers created four different types of solders by incorporating Fe or In into the solder. The melting point of the SAC solder alloy decreased when indium was added, and the study findings also showed that adding Fe and In in small quantities improved the wettability and shear strength of the SAC solder [31]. Sn-Ag-Cu, a lead-free solder, demonstrates remarkable potential for the production of environmentally friendly products. When Sn-Ag-Cu comes into contact with a copper substrate, it initiates the production of two distinct layers of IMCs at the point of contact (Cu_6Sn_5 and Cu_3Sn). The initial layer, Cu_6Sn_5, takes shape during the soldering process and features a unique scallop-like structure. Subsequently, at the junction of Cu6Sn5 and Cu base, the second layer, Cu3Sn, appears.. However, it's important to note that the thickness of Cu_3Sn is considerably smaller than that of Cu6Sn5, and its formation is comparatively slower [32]. In 2013, an investigation was carried out by Koleňák et al. to investigate the effects of incorporating a tiny quantity of aluminum (0.1 wt%) on the properties of SAC 405. The experimental findings indicate that adding aluminum reduced the wettability of the SAC 405 solder little. Moreover, the shear strength of the solder is reduced moderately, with an average drop of 8 MPa, and the melting temperature of SAC 405-(0.1 wt% Al) solder became 221°C [33]. In 2014, Lee et al. performed an analysis to examine the impact of adding different amounts of Aluminum (Al) (0, 0.01, 0.05, and 0.1 wt. %) to the SAB25 solder alloy on the wettability of the solder and the production of IMCs. The study found that adding 0.01 Al wt.% to the SAB25 alloy improved the solder's wettability and produced the best wetting properties for the solder. On the other hand, The IMCs' growth rate decreased due to an increase in the nucleation rate of Ag3Sn [34]. SnAgCu solder alloys are an alternative to Sn-Pb solder due to their reliability and mechanical properties. However, Sn-Ag-Cu solders need improvement in high temperature of melting and low wettability. To solve these problems,

researchers incorporate several components into an alloy. (such as In, Ti, Sb, Zn, Fe, Bi, Ga, Ni, Al, and rare earth) to SAC solders [35]. In 2015, a group of researchers conducted a study on the influence of adding 0.1 and 0.5 wt% Al to Sn-1Ag-0.5Cu solder on a Cu substrate. To evaluate the wettability of the solders, they employed wetting balancing and spread area techniques. The study showed that adding 0.1 wt.% Al improved the wettability of the Sn-1Ag-0.5Cu solder on the Cu substrate [36]. In 2016, Leong et al. conducted a study investigating the effect of adding a small amount of aluminum (0.1-0.5 wt.%) to Sn-1Ag-0.5Cu on the solder and copper substrate structure. The mixing of aluminum resulted in the formation of Cu-Al particles, known as Cu_3Al_2 IMCs, which were found close to the surface/edges of the solder. It is found that these particles had greater modulus and durability. The results showed that adding minor aluminum repressed the formation of Cu_6Sn_5 IMCs [37]. In 2016, Maslinda et al. did a study to examine the effect of adding different percentages of Al (0.5, 1, 1.5, 2 wt%) to the microstructure, IMC formation, wettability, and mechanical properties of SAC0305 solder. The results showed that adding Al increased the melting and crystallization temperature of the solder while decreasing the undercooling degree. Although the wettability of the solders decreased with increasing Al, it remained within the acceptable range. The addition of Al also encouraged the formation of Ag–Al and Cu–Al IMC while suppressing the formation of Ag_3Sn and Cu_6-Sn_5 IMC. Furthermore, Under both low and high speed shear conditions, the solder's shear strength was increased when Al was mixed to SAC0305 [38]. In 2016, Sun et al. conducted a study that manually mixed Al particles ranging from 0 to 0.4 wt% into Sn–1Ag–0.5Cu solder paste. The aim was to explore the effect of aluminum on the melting temperature, wettability, mechanical features, and microstructure of solder (SAC105) on a copper substrate. The study concluded that adding Al cannot significantly change the melting point of the solder, but it can improve its wettability and mechanical properties. However, adding more Al nanoparticles can decrease the mechanical and wettability properties [39]. Errer et al. conducted a study in 2018 on the wetting characteristics of SAC-1Bi and SAC305 solder alloys on a Cu-substrate, employing the highly precise sessile drop manner. The dependable findings revealed that SACBi alloys displayed better wetting characteristics than SAC305 alloys [8]. Sayyadi and colleagues conducted a study to reduce the production cost of SAC357 by reducing the percentage of silver.

Additionally, they added the Bi element to the solder of SAC257 in varying weight percentages of 1wt%, 2.5wt%, and 5wt%. According to the study, the solder's melting point was reduced by adding bismuth. Additionally, as the wt% of bismuth increased, the wettability of the solder alloys improved. Furthermore, the strength of the solder alloys at tensile showed an increase by incorporating bismuth up to 2.5wt% [40]. Liao et al. studied the corrosion behavior of Sn-3.0Ag-0.5Cu alloy; when exposed to 0.5 mol NaCl in an electrolyte layer of 200-μm, the SAC305 alloy mostly displayed pitting corrosion as opposed to pure tin, which behaved uniformly under the same corrosive conditions. The formation of a crystal boundary between β-Sn and intermetallic compounds accelerated the process of passivating film rupture into a metallic base, as the galvanic corrosion impact of the compounds optimally dissolved the β-Sn phase [41]. Kumar et al.'s research analyzed the mechanical and microstructural characteristics of solder alloys SAC305 and SAC405, aiming to compare their properties. It is found that the strength at tension, density, and hardness all increased with an increase in Ag concentration [42]. To enhance the properties of the SAC alloy, researchers have added indium to the ternary solder alloy. The results displayed that mixing 1.0 wt.% of indium decreased the solder alloy's contact angles (θ). The CA were measured by using the technique of sessile drop on a copper substrate in the Ar atmosphere. The smallest CA was 35.55° recorded at 310°C. Adding indium to the solder alloys reduces the temperature of melting and enhances the wettability of the alloy [9]. In 2019, Nasir and colleagues carried out a study on the strengthening of the Sn-3.0Ag-0.5Cu alloy with 1.0 wt. % TiO_2. The researchers observed that TiO_2 nanoparticles resulted in the reduction of Cu_6Sn_5 and Ag_3Sn intermetallic compound phases. As a result, the hardness values increased up to 26.2% compared to the pure alloy [43].

Subri et al. examined the behavior of corrosion of Sn-1Ag-0.5Cu with added Fe and Bi in NaCl-based solutions. The results showed that adding 1.0 wt% Bi and 0.05 wt% Fe improved the resistance of alloy to the corrosion because of the reduction in micro-galvanic interaction between the anodic Sn matrix and cathodic Ag_3Sn intermetallic compounds, which also caused a decrease in Ecorr towards a more noble value [44]. Gharaibeh et al. showed that using SAC solder alloys presents various challenges. One of the main issues is the risk of electrochemical corrosion,

which can undermine the reliability of electronic components. Researchers indicated that Icorr measures could be taken to assess the corrosion rate. Additionally, with higher corrosion potential values and relatively positive values, Ecorr can display better corrosion behavior. [45].

Ali et al. revealed that adding 1, 2, and 3 wt% of Bi to SAC305 improved its mechanical characteristics by inhibiting the development of intermetallic compounds. The microstructure was rectified, and the performance was most significantly improved when 3wt.% Bismuth was added to SAC305 [46]. Kaushik et al. investigated the electrochemical corrosion behavior of commonly used lead-free solder alloys: low-Ag (SAC105) and high-Ag (SAC387). Electrochemical potentiodynamic polarization experimens in a 0.5 M solution of NaCl showed that the high-Ag solder offers better corrosion resistance than the low-Ag solder [47]. Dheeraj et al. conducted a study in 2022 to examine the influence of adding Al to the properties of electrochemical of Sn-0.7Cu-xAl where (x = 0, 1, 2, and 3 wt.%) in NaCl solution. The results indicated that adding Al to the SC07 improved the resistance of the alloy to corrosion and the microstructure of the alloy, which is essential for preventing electronic component failures. The potentiodynamic polarization test appeared that the SC07 alloy had the highest corrosion rate (10.7030 $\times 10^{-2}$ mm/year), while SCA071 alloy had the lowest corrosion rate (0.1604 $\times 10^{-2}$ mm/year) [48].

Gao and Cui conducted a study to examine the impact of adding different ratios (0, 0.05, 0.1, 0.2, and 0.5 wt%) of Ni-coated carbon nanotubes (CNTs) to Sn-3.0Ag-0.5Cu lead-free solder. The research showed that the addition of Ni-CNTs to the Sn-3.0Ag-0.5Cu solder alloy enhanced the shear strength of the solder. Furthermore, the Sn-3.0Ag-0.5Cu-0.05 (Ni-CNTs) combination demonstrated the best wettability, microhardness, and shear strength [49]. In 2007, Kuang et al. accomplished a study to analyze shear loads of solder balls made of SAC305 and 63Sn37Pb alloys. Two different load speeds, 200 μm/s and 300 μm/s, were employed to observe the influence of loading on the shear strength. According to the experimental findings, SAC305 solder balls produced a more ductile joint than the traditional 63Sn37Pb alloy [50].

Under the influence of 1 M HCl, the corrosion properties of SAC305 and SAC-xIn where (x is 0.5, 1, and 2 wt%) were examined. The examination reveals that the total rates of corrosion correspond to a condition where a 0.5% indium replacement for silver results in a noticeably lower corrosion rate. However, when more indium replaces silver, the corrosion rate rises [51].

Resistivity is a term used to describe how well a matter can resist the flow of current. Conductivity, on the other hand, is a measure of how easily a material can allow electric current to pass through it and inversely related to resistivity. Morevere, low resistivity values refers to the higher conductivity suitable for a solder [52]. The electrical resistivity of alloys increases linearly with the rise in temperature and concentration of In [53, 54]. Microhardness and electrical resistivity increase when an aluminum phase forms in solder alloys. It is found that the Young's modulus decreased and electrical resistivity was raised in the SZ9 eutectic melt-spun ribbons due to the aluminum concentration. [55].

There is a connection between the resistivity (ρ) of a material and the geometric shape of the material (G). The geometric resistivity correction factor is used by physists to calculate the resistivity (ρ). This correction factor rely on geometric dimensions of the sample, the thickness (t) of the sample, the position, the surface area (A), and the array of probes on the sample [56]. Ismail and colleagues conducted a study on the electrical resistivity of a specific type of solder joint, identified as SAC305, in which carbon nanotube (CNT) was incorporated in amounts as much as 0.04 wt%. They utilized the four-point probe technique to make their measurements. The study revealed that adding CNT to the max 0.03 wt% increased the electrical resistivity of the SAC305 solder junction. However, at 0.04 wt%, a slight decrease was observed. The four-probe technique effectively eliminated the errors during the measurement because of spreading resistance under each probe, probe resistance, and contact resistance between each metal probe and the material [57]. Various environmental factors, such as weather conditions, moisture, physical situations, and substances containing hydroxide, can impact electronic devices and deteriorate the resistance of solder alloys against corrosion [58]. As per the research by Fayeka et al., the corrosion resistance of the Sn-3.0 Ag solder alloy decreased when the Ag

content decreased from 3.0 to 1.0 weight percent. Conversely, when the percentage of copper in the same alloy was increased by 0.5 weight percent, the corrosion resistance improved [59]. Incorporating aluminum has been found to improve the passivation properties of SAC105. The creation of Al_2O_3 and $AlCuO_4$ species has been observed to significantly mitigate the corrosion reaction of solder in the presence of NaCl [60]. Hamidah et al. showed that the corrosion rate for HCL is higher than for other electrolytes because hydrochloric acid (HCL) consists of two separate types of ions (hydrogen and chlorine ions) that aggressively destroy the metal components [61]. The experimental study investigated the effect of adding Al and Bi on the corrosion behavior of lead-free solder alloys. As per the findings, adding Al caused the most significant values for corrosion current density. [62].

The researchers studied the electrical resistivity of two types of solder alloys Sn-3Ag-0.5Cu with high Ag content and Sn-1Ag-0.5Cu with low Ag content. They used the four-point probe technique to measure the electrical resistivity and found that as the Ag content decreased in the alloy, the electrical resistivity increased [63]. Shnawah et al. showed in their study that aluminum (Al) can be added to SAC105 alloy to reduce the formation of certain particles that can negatively affect the alloy's performance. Adding 0.2% Al decreases the density of Ag_3Sn particles and replaces Cu6-Sn5 particles with Al-Ag and Al-Cu particles. When adding 0.5% Al, Ag_3-Sn and Cu_6-Sn_5 particles are suppressed. Adding 1% Al eliminates the formation of Cu_6Sn_5 and Ag_3Sn particles and produces Al-rich particles (Al-Ag and Al-Cu). The electrical resistivity of the solder alloy is impacted by the existence of Al, which affects the Ag_3Sn concentration [64]

.

PART 3

THEORETICAL BACKGROUND

3.1 SOLDERING AND WETTABILITY

Soldering is a process of using an additional metal called solder that has a temperature of melting less than the metals being connected to create a metallurgical bond. Soldering combines two materials by heating them with a filler metal until it melts and flows into the joint [65]. Electronic circuits depend on the solder alloy for mechanical, thermal, and electrical support. For a solder alloy to be dependable and suitable for all electronic assemblies, it must fulfill several characteristics. A solder alloy is usually a substance that must wet and form intermetallic compounds when it comes into contact with copper, nickel, and other metallic substrates [66,67].

Several properties must be considered regarding the manufacturing performance and reliability of solders. These properties include melting temperature, wettability, cost, environmental friendliness, availability, compatibility with current manufacturing processes, recycling potential, paste-making potential, and both thermal and electrical conductivity, fatigue properties, the ability of resistance to corrosion, enhanced shear characteristics, and formation of intermetallic compounds. Wetting is a physical phenomenon that occurs when a liquid spreads and wets a solid surface and maintains contact with it. The volume of wetting, known as wettability, is defined by the cohesive and adhesive forces that result from the molecular bonds between the liquid and the solid particles. Small contact angles with nearly complete wetting are produced when the adhesion forces are more significant than the cohesion forces [68].

3.2 YOUNG'S EQUATION

Young's equation is a fundamental concept in physics with practical applications in various industries, and it makes it possible to find out the angle of contact between a liquid and a solid surface; it is considered an essential parameter in many industrial processes. A solid's surface molecules are less mobile than those of any liquid. As a result, the faces needed for the macroscopic reduction of surface free energy are typically absent from the solid surface. Since most solids cannot adhere to such equilibrium states, their surface configuration is essentially a frozen-in archive of an arbitrary past. Because of this, solids have some flaws, humps, and fissures, and the laws governing liquid capillarity do not apply to them.

The empirical technique is commonly used to observe the tension of solid surfaces. It involves estimating the tension of the solid surface by looking at the liquid's tension that comes into contact with it. When the droplet of a liquid comes into contact with the surface of a solid, there is a state of balance created due to three opposing forces, the surface tensions between solid and liquid (SL), between solid and vapor (SV), and between liquid and vapor (LV). (See Figure 3.1.).

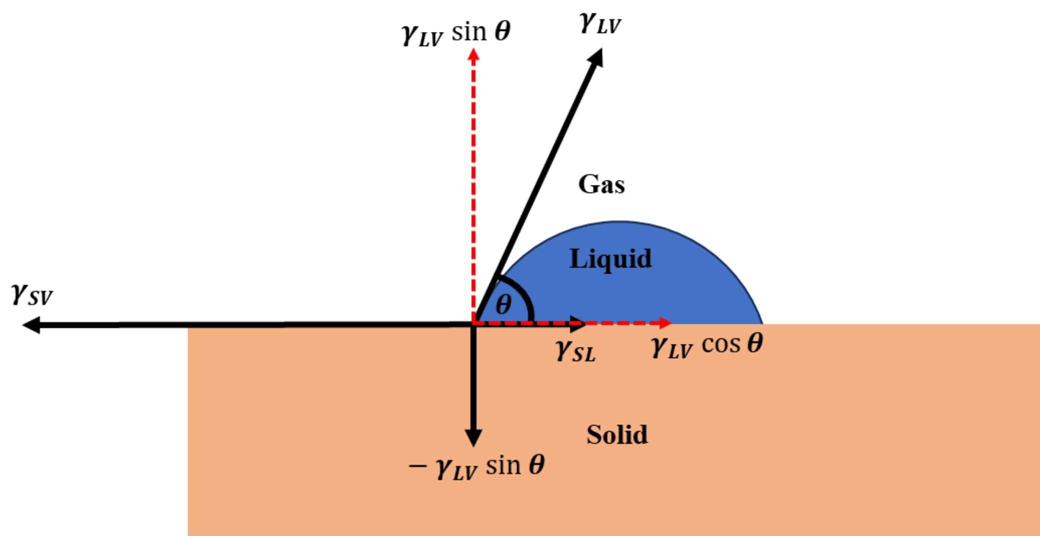

Figure 3.1. Three forces maintain the equilibrium of a liquid droplet on a solid surface (γ_{SL}), (γ_{SV}), and (γ_{LV}).

A liquid droplet that appears at the junction of a solid surface, a gas, and a liquid establishes what is known as the contact angle (θ). To determine this angle, one measures the distance between the planes of tangency where the solid and liquid surfaces meet at the point of contact. The contact angle indicates how much a liquid can wet a solid surface. It quantifies the liquid's capacity to spread over the surface of the solid.

When a solid surface and a liquid come into contact, its interaction can be evaluated by the CA (θ). If (θ) is low, the liquid and solid strongly interact, enabling the liquid to spread and thoroughly wet the surface of the solid well. On the other hand, high values of (θ) indicate a weak interaction and poor surface wetting. The liquid is partially wet when the angle is less than 90 degrees. When (θ) is more than 90 degrees, the wetting becomes very poor and the liquid is not wetting the surface of the solid, making it non-wetting, whereas when (θ) is zero, it indicates total wetting. When the solid surface exhibits low energy, the force of attraction it exerts on the liquid molecules is notably weaker than the force of attraction between the liquid molecules themselves [69].

In 1805, T. Young became the pioneer scientist to characterize contact angle equilibrium. Equation 3.1 illustrates the interfacial contact between the solid surface, gas or vapor, and liquid phase using the vector sum of forces at the three-phase intersection point.

$$\gamma_{SV} = \gamma_{SL} + \gamma_{LV} \cos\theta \quad (3.1)$$

[69]

Where (γ) is the surface tension and (θ) is the contact angle. if ($\gamma_{SV} > (\gamma_{SL} + \gamma_{LV})$, this means that there is a solid present with a high surface energy, and then Young's equation indicates ($\cos\theta = 1$), whereas ($\theta = 0$), which refers the total spreading of the liquid (complete wetting). However, the vertical component (γ_{LV} $\sin\theta$) as shown in Figure 3.1. is equilibrium with a ($-\gamma_{LV}$ $\sin\theta$) that is equivalent to the strain field on the solid surface.

3.3 UTILIZATIONS OF CONTACT ANGLES

Contact angles have various industrial applications. These applications range from surface coatings to adhesives and studying material properties. The measurement of contact angles can provide valuable information about the wettability and material's surface tension which can be beneficial to optimize the performance of materials in various industrial processes.

The measurement of contact angles can help us understand the relationships between immiscible liquids that are not capable of being mixed together, solids, or liquids. It is crucial in various industries to comprehend their chemical and physical processes. Contact angle measurements can help assess the adhesion between composite structures and adhesive wetting on a substrate. Knowing the significance of contact angle is especially crucial in the paint and coating industries. Surface chemistry is also advantageous to ink adhesion to thermoplastic food packaging film products. As a result, contact angle measurements are required for the printing process. Many conventional metals and other heavier and weaker materials have been replaced by compound substances composed of supporting fibers and polymeric systems. Many recreational goods, automobiles, and aerospace products use them these days. Contact angle measurements can maximize the adhesion between the fiber and resin matrix system and determine the appropriate emulation of the resin matrix with suitable wetting properties against the fiber. Meanwhile, contact angle measurements in the textile industry can assess the wettability of individual fibers or fabrics and their washability and hydrophobicity.

The pharmaceutical, cosmetic, and medical sectors rely on CA measurements as a vital part of laboratory quality control processes. In dental surgery, ensuring strong adhesion between the tooth and dental materials is essential for successful procedures and patient well-being. Therefore, wettability and biocompatibility studies require contact angle measurements. Improving the efficiency of cleaning solutions intended for contact lenses requires making the surface-free energy ideal of both the lens and the solution. This optimization could result in enhanced formulation and performance of the cleaning solution. In addition, CA methods are applicable in evaluating the

cleanliness of semiconductor surfaces within the electronics industry. The assessment of contact angles holds particular promise in nanotechnology, where it can offer valuable insights and potential applications. [69), 70, 71, 72].

3.4 METHODS OF MEASURING CONTACT ANGLES

The process of contact angle measurement is utilized to determine the angle created between the surface of a solid and a stationary liquid droplet. A liquid droplet forms a specific contact angle when it falls and comes into connect with a solid surface. This angle is influenced by the cohesive forces among the liquid's molecules and the strength of adhesion forces between the liquid and the solid surface. A weak liquid-solid attraction results in a significant contact angle, while a more potent force leads to a smaller one. The critical components of wetting systems are the CA of the liquid on the substrate and the surface tension that wets the solid phase. Various methods are available for measuring and investigating the surface tension and CA of liquids. Some of these methods include the following.

3.4.1 Sessile Drop Method.

The method most frequently used for calculating contact angle is the method of sessile drop. This technique involves placing a droplet of liquid onto the surface of a solid substrate, as shown in Figure 3.2, creating a three-phase system with a solid, a liquid droplet, and a gas. The three interfaces are produced by a solid-liquid (material surface-droplet), Liquid-vapor (droplet-atmosphere), and Solid-vapor (material surface-atmosphere). Then, a video camera attached to a computer fitted with a magnifying lens is utilized or an angle measuring eye is used with a goniometer-microscope. This method also needs a suitable cold light source [73].

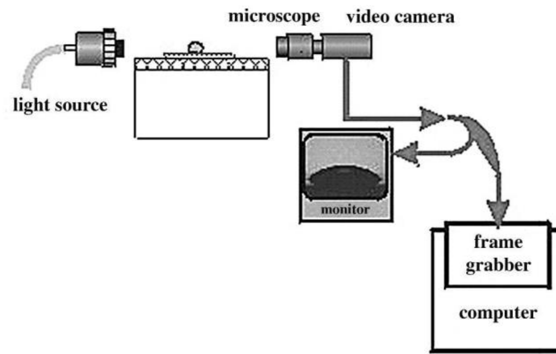

Figure 3.2. A diagram of the sessile-drop technique [133].

The angle created by the meeting of the tangent of the interface between vapor and liquid and an interface between solid and liquid is known as the contact angle. According to physicist Thomas Young, the system's interfacial tension can be related to the CA through a simple formula, as demonstrated in Equation 3.1.

3.4.2 Captive Bubble Approach

An inverted micrometer syringe is used for creating a bubble of a gas in a liquid and then placing it on the solid surface. The CA is measured by using a video camera or a goniometer when the solid is put in the test liquid. This method helps balance the pressure of saturated vapor of the liquid within the bubble at the solid-vapor contact. In the typical sessile drop method, an angle equal to (θ_r) results from the surrounding liquid front retreating when more air enters the bubble through the needle. Conversely, an angle equal to (θ_a) results from the liquid front advancing when air is removed from the bubble. Interestingly, the captive bubble method's (θ_e) measurement is closer to (θ_r) than (θ_a) [69,74].

3.4.3 Droplet Sliding on a Tilted Surface

When a stationary droplet forms on a solid surface. One end of the surface is held on a horizontal stage that can be tilted by a certain degree, causing the droplet to slide. When the solid surface plane approaches a critical inclination, the downhill and uphill edges of the drop approach the angles (θ_a) and (θ_r), respectively, as shown in Figure 3.3. Measuring the angles right before a drop starts to slide is essential. The

tilt angle, $\emptyset_t$ is additionally applicable to conclude thermodynamics. However, this approach is unreliable because it is difficult to determine a distinct and focused image of the drop at sliding. Inconsistent results are also obtained when rough substrates show an assertive behavior pinned by the liquid droplet, preventing it from sliding even at a tilt angle of $\emptyset_t$ = 90° [69].

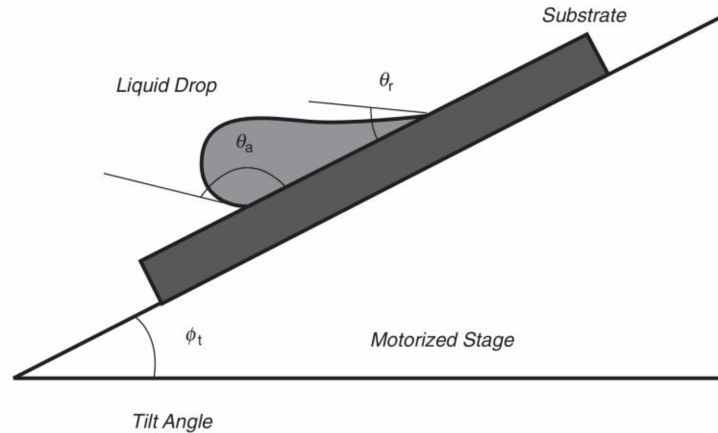

Figure 3.3. Contact angle measurements using the sliding drop on an inclined plate method [69].

3.4.4 Drop Dimensions Approach

The measurements of a sessile drop can be used to compute the contact angle indirectly. The drop must be small enough to allow for neglecting its shift from a spherical shape to perform such a computation. From plane trigonometry as shown in Figure 3.4, $h = R(1 - \cos\theta)$ where R is the radius of the spherical segment and h is the height of the drop. The liquid drop's contact radius, r_b, is given as ($r_b = R\sin\theta$).

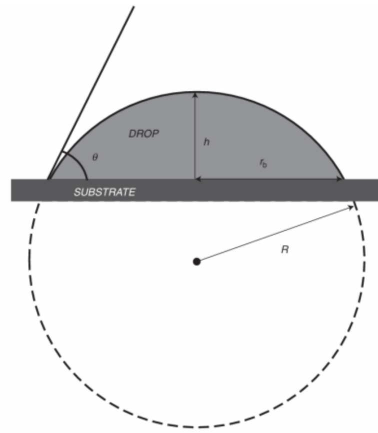

Figure 3.4. Calculating the contact angle using the drop dimensions method.

Equation (3.2) can be reliably used to calculate θ when measurements for h and rb are available. However, for large droplets, gravitation may distort (h) and (rb), rendering Equation (3.2) inappropriate. In such cases, more elaborate calculations are needed.

$$\frac{h}{r_b} = \frac{1-cos\theta}{sin\theta} = \tan\left(\frac{\theta}{2}\right) \tag{3.2}$$

[69]

3.4.5 Wilhelmy Plate Approach

In surface science, the Static Wilhelmy plate approach is frequently utilized to calculate surface tension in liquids and solids. To measure contact angle (θ) precisely, Neumann established the capillary rise on a vertical surface, which is the basis for the static Wilhelmy plate technique. This method involves using a moving microscope or cathetometer to measure the meniscus height caused by the wall's capillary rise of a perpendicular plate by partially submerging a Wilhelmy plate with a solid substrate coating on its surface in the testing liquid. If the surface tension or capillary constant of the tested fluid is confirmed, the CA can be obtained using an equation derived from the Young-Laplace formula (see Equation 3.3).

$$sin\theta = 1 - \frac{\Delta pgh^2}{2\gamma} = 1 - \left(\frac{h}{a}\right)^2$$ (3.3) [69]

The density difference between the liquid and the vapor is represented by Δp. while the acceleration due to gravity is denoted by g, and the capillarity constant is represented by (a).

3.5 MAXIMUM BUBBLE PRESSURE METHOD

With this technique, the greatest possible pressure needed to force a bubble outside of the capillary and into the liquid against the Young-Laplace pressure differential is measured to calculate the liquid's surface tension (ΔP). As seen in Figure 3.5, a bubble in the shape of a sphere part is created at the end of a vertical tube with an inner radius of (r) when the tube is immersed into a liquid and air is forced towards the upper part of the tube. The radius of curvature reduces as the bubble begins to grow due to an increase in internal pressure. The bubble becomes completely hemispherical as time passes, and its radius matches the capillary tubes. According to the Young-Laplace equation, the highest pressure is found within the bubble. As the bubble expands further, the pressure decreases as the radius increases, which can lead to instability. Subsequently, the bubble may detach from the capillary tube or burst due to air inflow [69].

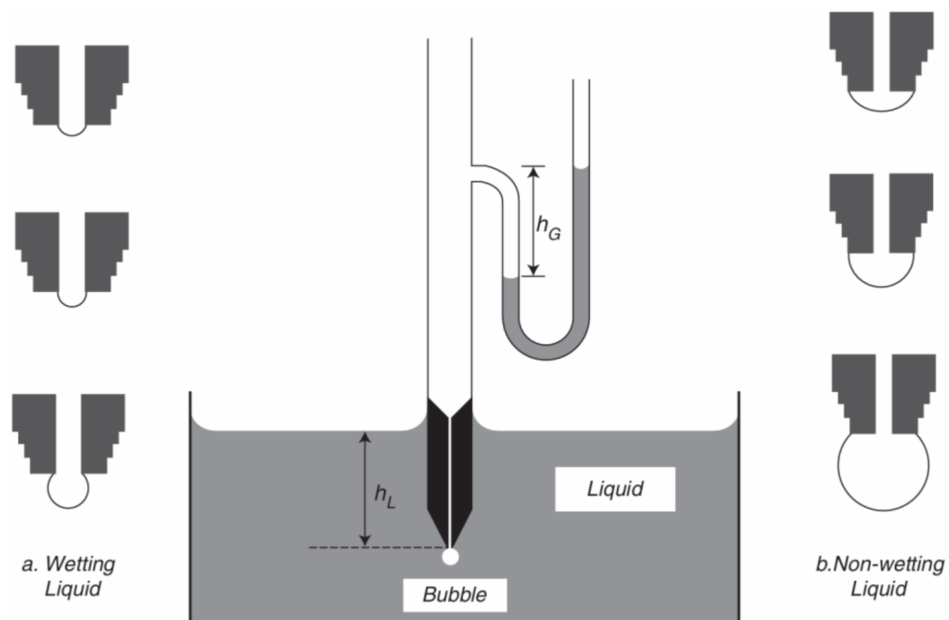

Figure 3.5. The maximum bubble pressure method [69].

Equations 3.4 and 3.5 indicate that the total pressure at its peak during this procedure is the combination of capillary and hydrostatic pressures.

$$P_{max} = P_{hyd} + P_{capil}$$

(3.4)

$$P_{max} = gh_L\Delta p + \frac{2\gamma}{r} \quad (3.5)$$

[69]

In order to obtain the surface tension of a liquid inside the tube, we need to calculate the distance (h_L) from the tip of the tube to the surface of the liquid. If the liquid wets the tube, the liquid fully covers the tube's lower border; hence, the radius (r) represents its internal radius. We must measure the maximum pressure (P_{max}) just before the bubble detaches to determine the surface tension value. Usually, As seen in Figure 6.5, P_{max} is typically obtained by determining the height of a water column (h_G) connected to the measurement tube.

3.6 DROP VOLUME OR DROP WEIGHT METHOD

This technique, which measures liquid surface tension, is an age-old detachment method initially described by Tate in 1864 and was previously referred to as the stalagmometer method [75]. A narrow glass cylinder with a radius of around 2 mm is used in the method, from which a slow stream of liquid drops falls. Surface tension causes the liquid stream to form into drops of critical sizes, which are then nipped off. Theoretically, As seen in Figure 3.6, a single drop grows until it reaches a volume where the forces of capillarity and gravity are equal. To compute the surface tension, one must ascertain the volume of a single drop encircled by air vapor [69]. Equation (3.6) provides the phrase for force balance at the point of separation.

$$W_{drop} = m_{dtop}g = V\rho g = 2\pi r\gamma \quad (3.6)$$ [69]

The formula is based on the variables drop's mass (m_{drop}), drop's volume (V) for its volume, and the interior radius (r) for the tube tip. It is essential to differentiate between wetting and non-wetting liquids in the context of this formula. For liquids that do not wet, (r) refers to the interior radius, while for wetting liquids like glass water, (r) refers to the external radius. Occasionally, the outside portion of the tip might be coated by using molten paraffin wax to forbid the liquid from sticking. In such circumstances, calculations can be made using the tube tip's interior radius.

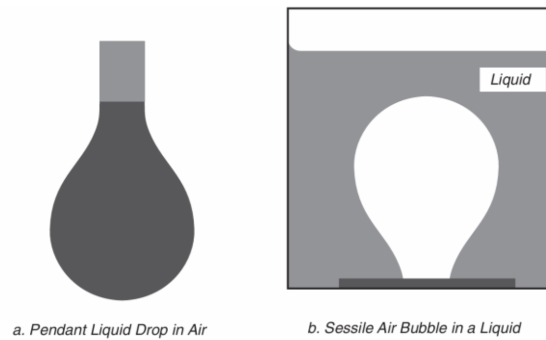

Figure 3.6. Liquid surface tension measurement, a. A pendant drop is produced by suspending the liquid from the end of a narrow tube. b. Injecting the gas is done using a syringe with a needle attached to the tip [69].

3.7 CAPILLARY RISE METHOD

For most liquids, the contact angle is nearly zero. However, due to the gravitational force, the liquid's free surface in a vessel can become horizontal. The liquid surface at the edge of the container can either be higher or lower than the horizontal level, depending on whether the liquid wets the liquid. In capillary tubes, the liquid rises or falls due to interfacial tension, known as capillarity. The liquid begins to rise due to the tension, and it becomes balanced with the effect of gravitational force. Wetting a solid surface with a liquid drop relies on the balance between adhesion and cohesion forces. In the situation, when the adhesion force among the solid matter molecules of the surface substrate and the molecules of the liquid is less than the cohesive forces among the molecules of the liquid, the liquid cannot wet and spread on the surface of the solid substrate.

On the other hand, when the adhesion force is bigger than the cohesive force, the liquid will be able to wet and spread on the surface of the matter substrate and form a concave shape. Conversely, the liquid will take a convex shape if the adhesion force appeared smaller than the cohesion force. (See Figure 3.7) [76, 77].

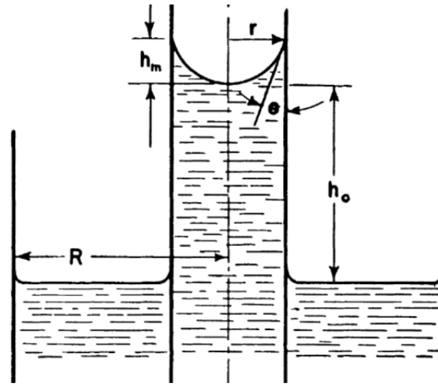

Figure 3.7. A diagram of the capillary rise method [76].

3.8 THE FACTORS THAT AFFECT THE MEASUREMENT OF CONTACT ANGLE

Various factors need to be considered when measuring contact angle using the sessile drop method.

- Roughness and Chemical Heterogeneity of the Surface: When a liquid droplet is placed on a smooth and flat surface, it usually takes a spherical shape. This shape has only one contact angle along the edge of the drop, which is a characteristic of the liquid and the surface. However, if the surface is not entirely smooth or the liquid is not uniform, the droplet's shape may deviate from this spherical shape, and the angle of contact may vary along the edge of the droplet. In such cases, assigning a single CA to the system becomes impossible [78]. The roughness of the surface affects the wetting because if the surface of a substrate is rough and not smoothed or planned, the actual area of the rough surface will be bigger than the area of the planned surface. As a result, when a liquid drop become in connect on a rough surface, the

interaction between the liquid and the solid will be more significant than it would be on a flat surface, even if the drop volume is the same in both cases.

- Outermost contamination: When tiny particles of some other matter surround the surface of a substrate or existence of liquid particles on the surface of the substrate, this could prevent a direct and significant interaction between the solid surface and the drop of a liquid. As a result, the measured contact angle might not be accurate. If the impurity is evenly distributed on the surface of the substrate, the measured CA may not represent the precise angle of the solid surface. On the other hand, if the impurity is unevenly distributed, the drop will be asymmetrical. Improper cleaning procedures often cause this contamination.

- The volume of the liquid drop: As per to published research, a drop's volume must be between 0.5 to 10 mm^3. However, some reports fail to mention the volume of the drop at all. Generally, researchers use tiny droplets in their experiments. However, if we compare the results of small drops with big drops or the drops of different sizes that were obtained, the effect of drop size will appear clearly. Therefore, it is crucial to consider the effect of drop size [79, 80, 81]. When a liquid drop falls onto a solid surface, the concentration of the liquid on the surface will vary depending on the time and distance along the solid in a band contact line. As a result, a gradient of surface free energy density will directly impact the horizontal force component and can lead to contact angle hysteresis.

- Time of the deposition: The liquid's surface tension denoted by γ_{LV}, typically decreases with an increase in temperature. Assuming that the surface tension correlated to a solid is not significantly influenced by changes in temperature, which means that γ_{SV} - γ_{SL} remains approximately constant, the surface tension should increase according to Young's equation when the temperature rises. This results in a decrease of (θ) with increasing temperature. However, the impact of temperature on the CA is minimal [69]. According to a study by Rudawska et al. in 2009, when measuring (CA) on a solid surface, it is crucial

to do so immediately after the drop has been deposited. All drops should be measured at the same time interval to minimize the volume lost by evaporation and any potential reaction between the solid surface and liquid drop [81].

- Mechanical vibration: Holding the sample motionless during the measuring process is crucial to avoid any vibration-induced deformation [73].

3.9 SURFACE TENSION OF METALS

There are challenges to measuring the surface tension of liquid metals because of their elevated temperatures and inclination to react with gases and solids. Small quantities of oxygen gas can, for example, lower the surface tension of numerous metals. Therefore, it is necessary to perform measurements in an atmosphere of inert gas to prevent any chemical reactions. Creating a new surface is almost always necessary to achieve accurate results. Pendant drop, sessile drop methods, maximum bubble pressure, and drop weight are commonly used to measure surface tension for liquid metals. However, Wilhelmy plate and capillary rise methods may be preferable due to the extremely high contact angles created between the molten metal and the substrate resulting from the strong cohesion of the liquid metal molecules. The surface tension of molten metals typically ranges from 400 to 4000 mNm^{-1} and is usually very high [69].

3.10 ADSORPTION

Adsorption is defined as the process of extracting chemical compounds from a bulk phase and an interface. Conversely, desorption entails molecules departing from an interface and transitioning to another phase. Absorption and adsorption are distinct processes. In adsorption, a substance permeates and disperses within the entire volume of a liquid or solid, unlike in absorption. When gases or liquids are adsorbed, the solid substance onto which the adsorption occurs is referred to as the adsorbent. The material attached to the solid surface in the adsorbed state is known as the adsorbate. The term "adsorptive" pertains to the liquid molecule, gas or vapor before

its adsorption. If the opposite happens, meaning the adsorbate molecules swiftly transition along the surface from one location to another, they are called non-localized [69]. Adsorption is a surface phenomenon that occurs when the molecules from the fluid (gas or liquid) are moved to the surface of a solid, creating an interface layer. This process is categorized into two types: physical and chemical [82]. The adsorption process occurs when gaseous, liquid, or solid material adheres to the surface of a solid or liquid substrate called adsorbent or sorbent [83]. There are various types of adsorption systems: liquid-liquid or liquid-gas and solid-liquid or solid-gas. The film, micelle, or emulsion constitutes the interfacial layer when the adsorbent is liquid. On the other hand, if the adsorbent is a solid substance, the approved mechanism for the adsorption process is the interfacial layer model.

The interfacial layer is the balance between the adsorbent and the bulk phase. It is divided into two regions - the first region is where the substrate is bound to the sorbent surface, while the second region is the surface layer of the sorbent. Adsorption of solids is generally sort depending on the force that binds the molecules of the adsorbed matter or atoms to the solid's surface molecules or atoms. Two principles elucidate the mechanism of the interfacial layer.

3.10.1 Physical Adsorption

The substrate and adsorbent are attracted to each other through weak van der Waals forces, known as physisorption. The bonding between the adsorbate and adsorbent is a weak Van der Waals force, with no alteration in the chemical structure of either adsorbate or adsorbent. Physical adsorption occurs due to physical forces. Its weak nature and multi-layered structure characterize this process. Unlike chemisorption, physical adsorption is nonspecific and occurs across the entire surface of the adsorbent. Factors such as surface area, pressure, temperature, and the characteristics of the adsorbate all impact physical adsorption.

The nature of the adsorbent is also a significant factor that affects this type of adsorption. Physical adsorption is reversible and is always an exothermic process.

The enthalpy of adsorption is the energy released during adsorption and typically ranges from 10-40 kJ/mol. Additionally, it does not require high-activation energy.

3.10.2 Chemical Adsorption

Chemical adsorption is a phenomenon caused by chemical forces (chemical bonds). It is known for being very strong between the adsorbent surface and molecules of the adsorbate, and it occurs through the exchange and sharing of electrons. It happens at reaction centers on the adsorbent and is usually a highly specialized single-layered phenomenon. The surface area, temperature, and nature of the adsorbate can all impact chemisorption, which depends on the adsorbent's nature. This adsorption type is generally irreversible and has a high enthalpy ranging from 40 – 300 kJ/mol. Additionally, it requires high activation energy [82].

3.11 KINITIC ADSORPTION

As per previous research, the kinetic adsorption process consists of two stages. Initially, the adsorbate needs to be transferred from the bulk solution to the surface of the adsorbent. Subsequently, the adsorbate undergoes diffusion in the pores of the sorbent, where it becomes arranged [85]. The stage that limits the adsorption rate determines the adsorption mechanism [86].

3.12 BIOSORPTION

Biosorption involves the attachment of specific biomolecules or biomass to particular ions or molecules in aqueous solutions. Various biomasses such as bacteria, yeast, fungi, agricultural waste, algae, industrial waste, and polysaccharides have been recognized as biosorbents for eliminating metals [87]. Biosorption is a physico-chemical process that does not rely on metabolism. It involves several mechanisms: adsorption, absorption, surface complexation, ion exchange, and precipitation. Biosorption plays a crucial role in the environment and traditional biotreatment processes. Biosorption is a subfield of biotechnology that uses biological materials such as dead or living bacteria, seaweed, plant materials, industrial and agricultural

wastes, and natural residues to extract or recover organic and inorganic chemicals from a solution. For many years, it has been considered a cost-efficient method for cleaning up, and it holds tremendous potential [88].

3.13 DEVELOPMENT OF SOLDER ALLOYS

3.13.1 Sn-Pb Solder Alloys

The well-known material properties and reliability of Sn-Pb solders have made them a popular choice in the electronics industry for many years. These solders possess excellent mechanical and electrical properties, making them ideal for circuit board assembly, wire bonding, and component attachment [89, 90]. However, it is essential to note that tin-lead solders have been associated with health and environmental concerns due to their toxicity. Regulations have been implemented to limit lead-based solders, replacements for solders containing lead are being explored. The impact of adding lead to tin is demonstrated as follows: The eutectic tin-lead system has a significantly lower melting point relative to pure tin and lead alone. Pure tin and lead have melting temperature of 232 °C and 327 °C, respectively, while the melting temperature of Sn-Pb solder alloy is 183 °C [91, 92]. The phase diagram of the SnPb alloy is displayed in Figure 3.8.

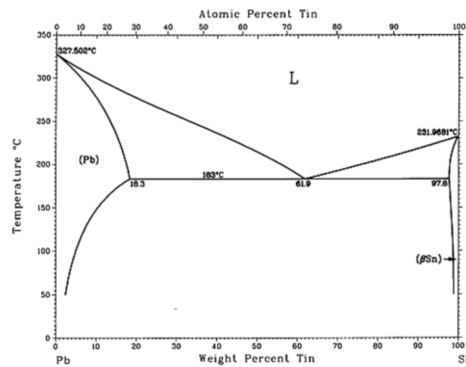

Figure 3.8. Phase diagram of Sn-Pb [93].

Adding lead to tin can help reduce surface tension, allowing the solder to flow more quickly over the surface of a substrate, leading to better spreading. The CA of eutectic (Sn-37Pb) on the Cu-substrate shows a significant improvement compared to pure tin, with a contact angle of approximately 11°. This improvement in wetting

is due to the incorporating of lead to the pure tin, while the CA of pure tin is 35° on the Cu-substrate. Various sources have supported these findings [94, 66, 92, 95]. Lead is an affordable and easily accessible element that significantly enhances tin's ductility and specific mechanical properties [91].

Lead is a toxic substance deemed dangerous to human health. Due to its distinct properties, it can build up in the body by creating powerful connections to proteins, disrupting our system's standard processing and operation. Lead poisoning occurs when the lead content of the blood is above 50 mg/dl [96), 97]. Direct and indirect risks are associated with producing and disposing of electronic assemblies. The direct risk involves the exposure of workers to solder vapor and fine lead-bearing particles in the electronic industry. On the other hand, the indirect risk arises from the leaching of waste electronic assemblies due to acidic rains, leading to contamination of underground waters [98].

The EU adopted the RoHS directive in February 2003 due to health concerns, and it became effective on July 1, 2006. Countries like Turkey [16], California, China, and Japan took similar measures. As a result, lead and lead-based products are prohibited in most developed countries' consumer electronics.

3.13.2 Lead Free Solder Alloys

The substitution of traditional Sn-Pb solders with various alloys, a topic of direct relevance to the field of materials science and environmental health, has been suggested by public health care and environmental awareness advocates. Many of these alternative solder alloys are based on Sn and include significant alloying elements like Zn, In, Au, Bi, Ge, Ag, and Sb. The table 3.1 shows the melting point of some binary systems, including Sn-Sb, Sn-Ag, Sn-Pb, Sn-Cu, and In-Sn.

Table 3.1. The melting points of some binary lead-free solder alloys [16]

Binary solder alloys	Melting point (^{0}C)	Reference
52In-48Sn	118	[134]
99.3Sn-0.7Cu	227	[134]

Sn-3.5Ag	221	[140]
Sn-37Pb	183	[16]
Sn-5Sb	235	[16]

The primary issue in the tin-silver solder alloy is the creation of large IMCs Ag3Sn. Another problem that may arise is the occurrence of tin whiskering, which is caused by high levels of tin concentration [66]. Figure 3.9 illustrates the binary phase diagram of tin-silver.

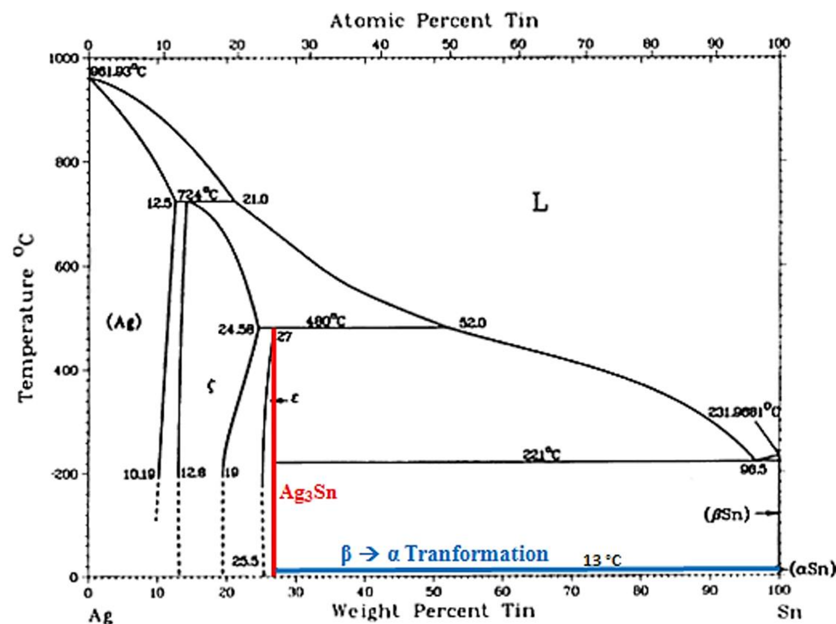

Figure 3.9. Phase diagram of Sn-Ag binary solder alloy

The Sn-Zn solder alloy, with a eutectic temperature of 198°C, shares a close similarity with the tin-lead alloy. Its eutectic composition, a crucial aspect of its properties, is composed of Zn-rich and Sn-rich lamellar phases. However, it is essential to note that due to the low alloying element concentration in Sn-Cu solder alloys, Sn whiskers may creat, and the transformation of white tin to gray tin may occur at low temperatures.

Although high-strength, low-temperature eutectic solder (138°C) is present in Sn-Bi solder alloys, it is unsuitable for most electronic applications where operating temperatures reach 150°C. Nonetheless, Sn-In solder alloy, with an eutectic

composition of In-49.1Sn and a eutectic temperature of 117°C, is preferred in some surface-mount technology (SMT) applications. However, like the Sn-Bi alloy, this alloy cannot be used in most electronic applications due to its low eutectic temperature. It is crucial to consider that these alloys have various issues, such as the formation of intermetallic compounds, tin whiskering, white tin to gray tin transformation, dewetting, high reactivity, and high cost.

Researchers have created ternary alloy systems to address the challenges faced by binary solder alloys. These systems mix three metals to produce alloys with improved properties. Table 3.2 presents some crucial ternary alloys and their corresponding melting temperatures.

Table 3.2. Melting points of some ternary solder alloys

Ternary solder alloys	Melting point (^{0}C)	Ref.
Bi - 26In - 17Sn	79	[135]
Bi - 41.7Sn - 1.3Zn	127	[136]
Sn - 56 Bi - 1Ag	137	[136]
Sn - 57Bi - 1.3Zn	127	[136]
Sn - 6Zn - 6Bi	127	[136]
Sn - 2.8Ag - 20In	178	[137]
Sn - 25Ag - 10Sb	233	[16]
Sn - 3.5Ag - 1Zn	217	[138]
Sn - 9Zn - 10In	178	[139]

3.14 Sn-Ag-Cu LEAD FREE SOLDER ALLOYS

SAC alloys are eutectic mixtures of tin, silver, and copper and are considered one of the most promising ternary alloys for replacing conventional Sn-Pb alloys. In 1996, a group of American researchers at Ames Laboratory discovered these SAC alloys for the first time, and studies on these alloys are continuous as they attempt to become more suitable for industrial use [16]. SAC alloys possess elevated heat shock, high mechanical and thermodynamic properties, and resistance to mechanical vibrations, enabling them to work efficiently at temperatures up to 150°C. These properties are better than those of traditional Sn-Pb solders [99,100]. The ternary SAC3709 was

determined experimentally, with eutectic phases of Sn, Ag3Sn, and Cu6Sn5. The temperature of melting of SAC alloy reaches 217 ^{0}C to 220 ^{0}C and is about 34°C higher than that of the Sn Pb solders, giving it the ability to work at higher temperatures and obtain better thermo-mechanical properties. SAC soldiers have a higher shear strength and stable microstructures than Sn-Pb alloys [101, 102].

Several types of solder that do not contain lead have been discovered recently. These solders include SC07, SA35, SAC3807, SABi3548, and SAC305, which have slightly different compositions but are all rich in Sn and have melting temperatures ranging from 210°C to 227°C. They are advised for a variety of soldering tasks, including surface mount technology (SMT), plated-through-hole (PTH), ball grid array (BGA), and flip-chip bumping. SAC305 is commonly utilized in the electronics industry. However, issues related to the creating of IMCs at high temperatures and costs still require further research [103, 104].

3.14.1 Effect Of Ag And Cu On SAC Lead Free Solder Alloys.

Adding Ag to Sn forms small Ag3Sn particles distributed uniformly in the Sn matrix while adding Cu forms rod-shaped Cu6Sn5 particles. The microstructure of SAC solder joints depends on the Ag wt%. Th density of Ag3Sn particles increases linearly with Ag content, and bigger Ag3Sn and Cu6Sn5 particles appear near the interfacial IMCs (see Figure 3.10 and 3.11). Mechanical tests showed that fatigue lifetime and shear strength depend on Ag content, with increased Ag % leading to increased strength and lifetime due to more Ag3Sn precipitates in the Sn matrix [105, 132].

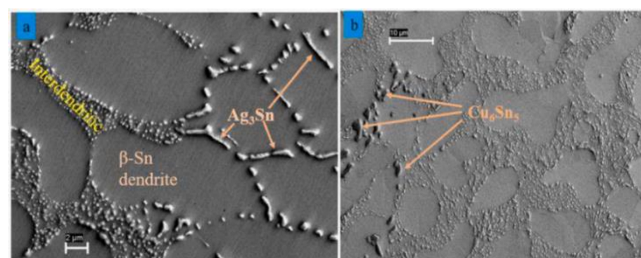

Figure 3.10. SEM micrographs with high magnification of SAC solder joints having two different weight percentages of Ag. a) Ag 3%wt, b) Ag 4 %wt [105].

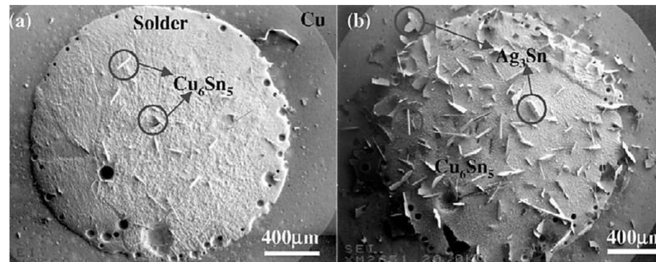

Figure 3.11. Results of microscopic analysis conducted on a) Sn-3.0Ag-0.5Cu and b) Sn-3.9Ag-0.5Cu [106].

If the silver content of the solder is less than three wt%, the creating of large Ag3Sn IMCs is significantly reduced [107]. Increasing Ag content in Sn forms Ag3Sn IMCs. A rise from 3.0 wt. % to 3.8 wt. % leads to a 28 vol. % increase in Ag3Sn content [108].

3.14.2 Effect Of Al On SAC Lead Free Solder Alloys.

The SAC0305 solder was mixed with aluminum (Al) to see how aluminum affected the wetting, mechanical, and microstructure characteristics. Findings appeared that the melting and crystallization temperature of the solder increased while the degree of undercooling decreased. Al refined the b-Sn dendrites and facilitated the formation of Cu–Al and Ag–Al IMCs, resulting in a less interdendritic region. The wetting angle and wetting time increased while the spreading area decreased with increasing Al. The shear strength of Al-added solders was slightly higher than that of the SAC0305 solder [38].

The study examined the effect of Al and Si on IMC formation at the solder and Cu interface. Four solder alloys were tested. Adding Si and Al dropped the thickness of IMC layer. 1.0 wt.% Al created a planar IMC shape, while 2.0 wt.% Al with 2.0 wt.% Si and 2.0 wt.% Al formed a scallop shape. Cu-Al IMC and Ag-Al IMC acted as impediments to the diffusion of Sn (See Figure 3.12). The suitable amount of Al and Si led to a thinner IMC layer, increasing the solder interconnect's reliability [109].

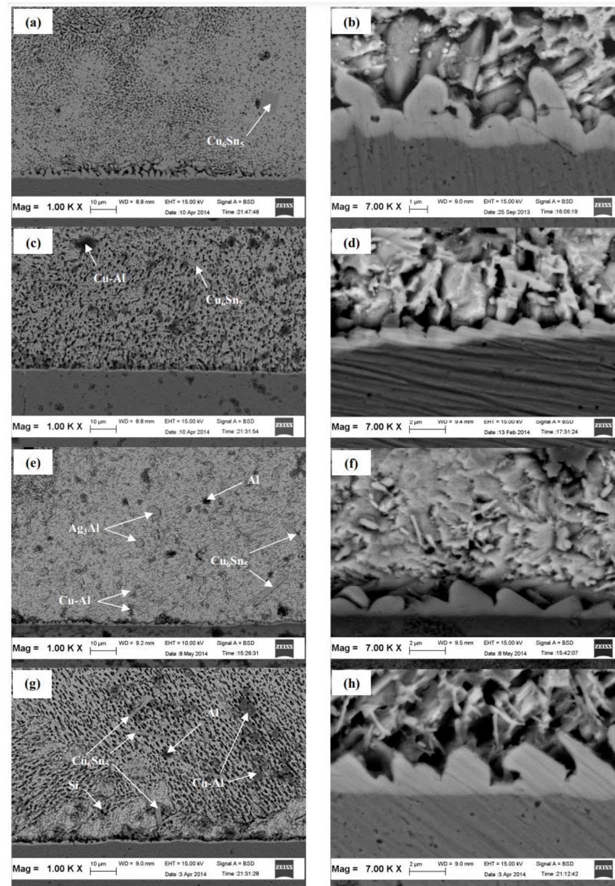

Figure 3.12. SEM of IMC layer formed in (a), (b) SAC0305, (c), (d) SAC0305-1Al, (e), (f) SAC0305-2Al, (g), (h) SAC0305-2Al-2Si solder joint. (b), (d), (f), and (h) are the magnified images of (a), (c), (e), and (g) [109].

PART 4

METHODOLOGY

4.1 PRODUCTION OF LEAD-FREE SOLDER ALLOYS

This study produced a quinary lead-free solder alloy (SAC205-1In-xAl) by adding varying amounts of aluminum (Al) to the SAC205-1In alloy. The amounts added were 0.3, 0.5, 0.7, 0.8, and 0.9 wt%. The melting process was done at the Karabük University Faculty of Engineering, Metallurgical and Materials Engineering Laboratory. The solder alloys were heated in a controlled-atmosphere melting unit (furnace) designed for microalloying to about 130-180°C higher than the melting point of the SAC205-1In alloy (see Figure 4.1). The objective was to optimize Sn-Al and develop new quinary lead-free solder alloys SAC205-1In-xAl (see Figure 4.2).

Figure 4.1. Melting materials in a controlled atmosphere unit (Furnace).

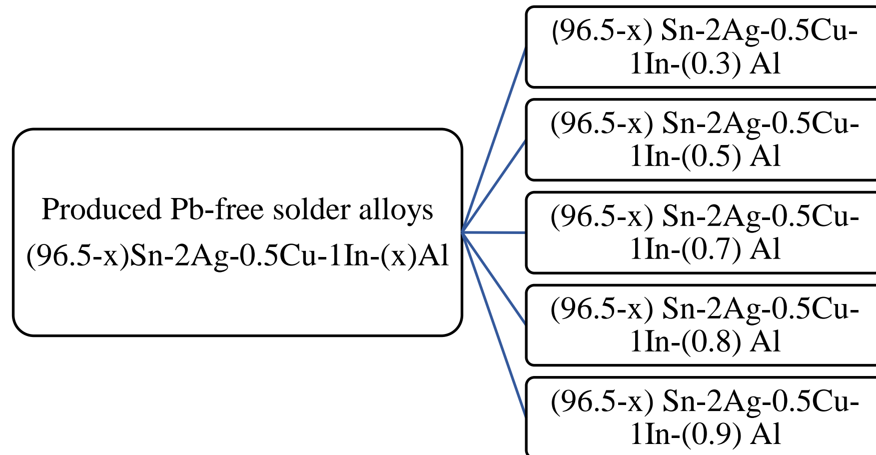

Figure 4.2. Displays the quinary lead free-solder alloys that have been produced.

Then, the quinary lead-free solder alloys produced were subjected to homogenization by placing them in an alumina paper and keeping them in a furnace for 48 hours at 180°C in the Karabuk University Laboratory for Metallurgical Materials Engineering Production. After 48 hours, the alloy samples were collected from the furnace and put directly into the cold water to improve the samples' homogenization process, as shown in Figure 4.3. This process was repeated until the desired ratios were achieved based on the study objectives. All elements utilized for producing the lead-free solder alloys had an approximate purity of 99.99%.

Figure 4.3. Electric furnace used for homogenization process

4.2 X-RAY FLUORESCENCE (XRF) METHOD

After the homogenization process was completed, pieces of the produced solder alloys were then prepared for X-ray fluorescence (XRF) analysis using the "RIGAKU ZSX Primus II" device at the Margem Laboratory of Karabük University Iron and Steel Institute. The X-ray fluorescence (XRF) method is widely used for elemental inspection of any substance without causing damage. It is frequently employed in scientific investigations to quantify the amount of impurities or essential elements in a sample [110]. According to the XRF analysis results, the metal accuracy ratios in the produced solder alloys by wt% were determined. The surfaces of the alloys were polished to have a flat surface before conducting XRF analysis to obtain correct measurements because the rough surfaces may lead to incorrect measurements. Pieces of solder alloys produced were catted and smoothed with 400, 600, 800, 1000, 1200, and 2000 mesh sandpaper before they were ready for the XRF and XRD analysis, as shown in Figure 4.4.

Figure 4.4. Preparing the samples for XRF and XRD analysis.

4.3 X-RAY DIFFRACTION (XRD)

The (XRD) analysis showed the effect of adding Al on the microstructure and the formation of intermetallic compounds in the alloy. In order to determine the phases and diffraction planes that may exist in the structure of the quinary lead-free solder alloys produced, XRD analysis was conducted at the Margem Laboratory of Karabuk University Iron and Steel Institute. The device used for the XRD analysis was "RIGOKU - ULTIMA IV (see Figure 4.5).

This device is capable of determining the crystal structure and phase analysis of powder, bulk, metal, and thin films, as well as performing measurements of non-

destructive residual stress, high-temperature (25–1500°C) analysis and degree of crystal tendency analysis, thin film analysis (GIXRD and XRR)-micro-point analysis. It has technical features such as analysis down 400 μ area.

Figure 4.5. The device used for the XRD analysis "RIGOKU - ULTIMA IV.

4.4 DIFFERENTIAL SCANNING CALORIMETER (DSC) ANALYSIS

The eutectic melting point is the minimum temperature at which a liquid phase remains stable under a specific pressure. In a eutectic system, two or more substances combine to form a uniform solid mixture. This mixture creates a super-lattice that melts or solidifies at a temperature lower than the melting point of any individual ingredient [111]. The melting temperature of quinary lead-free solder alloys produced was determined using a differential scanning calorimeter (Hitachi DSC 7000 Series) at the DTA/TGA/DSC Laboratory of the Margem Laboratory at Karabuk University's Iron and Steel Institute as shown in Figure 4.6. The melting temperatures play a crucial role in the soldering process. It is widely acknowledged that high melting temperatures characterize the eutectic SAC solder alloy family. However, recent developments have led to slight reductions in the melting temperatures of eutectic SAC-1In and SAC-1Bi solder alloys [8]. All DSC tests were conducted for produced eutectic SAC205-1In-xAl where (x = 0.3 wt%, 0.5 wt%, 0.7 wt%, 0.8 wt%, and 0.9 wt%) at a heating rate of 10 °C/min, within a temperature range of 25-400°C.

Figure 4.6. DTA/TGA/DSC Laboratory for determining melting temperature of solder alloys.

4.5 WETTING EXPERIMENTS

The wetting properties of the quinary solder alloys produced SAC205-1In-xAl where (x =0.3 wt%, 0.5 wt%, 0.7 wt%, 0.8 wt%, and 0.9wt%) were investigated by using the hybrid drop technique. The sessile drop technique is frequently used to assess the wetting properties of a molten alloy on a Cu substrate. [112]. Wettability is a crucial physicochemical parameter and has a wide range of uses like welding and soldering [113]. The researchers dropped the solder alloys onto a pure copper substrate (99.85% purity) of dimensions (12 × 18 × 3 mm) at 275 °C, 300 °C, and 325 °C. The experimental setup used for investigating the wetting characteristics of produced solder alloys is shown in Figure 4.7.

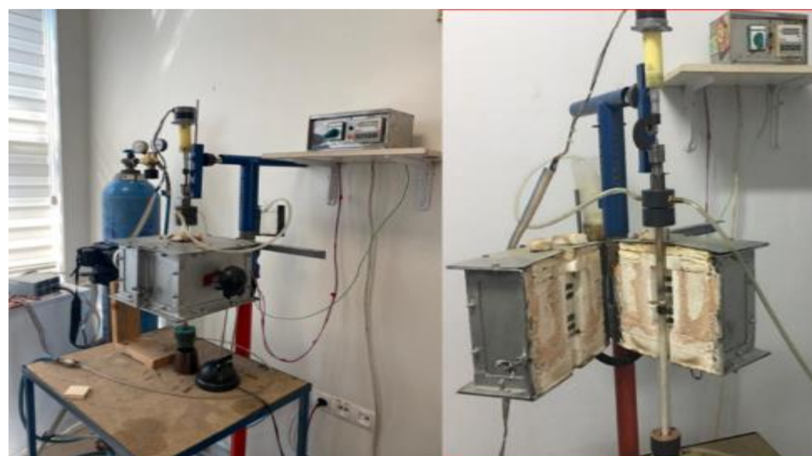

Figure 4.7. Illustrates the components of the experimental apparatus used in the hybrid drop technique.

The specifications for each component of the experimental device are included in Table 4.1.

Table 4.1. The specifications of each component of the experiment device.

Experiment setup parts	**Specifications**
Electric oven	Dimensions 300x300x200 mm
A durable ceramic tube closed at one end can withstand temperatures up to 1500°C.	The outer diameter is 15.60 mm, the inner diameter is 11.10 mm, and the length is 279 mm.
Steel bar	The diameter of the steel bar is 6.8 mm, and its length is 300 mm.
Stainless Steel tip	The diameter is 11.7 mm, and the length is 38 mm.
Quartz glass tube	The outer diameter is 24.72 mm, the inner diameter is 21.70 mm, and the total length is 450 mm.
Argon gas	99.999% purity
Stepper motor	has 1 hp power
Digital video camera	It has a shooting quality of 600 fps.
99.85% pure Cu substrate material	Dimensions are 12mm x 18mm x 3mm.

The Cu substrates underwent processing with bakelite material at the Metal Laboratory of KBÜ Faculty of Technology. The surface where the alloy drop of the Cu substrate will be placed was smoothed using 400, 600, 800, 1000, 1200, and 2000 mesh sandpapers.

In order to guarantee precise results from the experiments, it is imperative to clean and prepare all assembly components before commencing the experiments. Any formation of oxide resulting when the molten solder alloys drips on the Cu base substrate from the parts of the experiment set could adversely influence the experiment results. Thus, taking necessary precautions is critical to avoid such incidents.

Small particles weighing approximately 1.2 g - 1.7 g were cut from solder alloys produced from SAC205-1In-xAl, where x represents the weight percentages of 0.3, 0.5, 0.7, 0.8, and 0.9 for each wetting experiment. The particle was placed inside a ceramic tube with a closed end, and a hole of approximately 1mm in diameter was made for the solder alloy to melt and drip. A steel tip mounted on a steel bar was also placed inside the ceramic tube to prevent it from touching the material by pressing for the molten metal solder alloy to drip. The Cu substrate covered with Bakelite was cut using a jigsaw, and the surface on which the solder was to be dripped was cleaned of oxides using alumina material.

After cleaning the copper (Cu) substrate, it was placed on a graphite base in the experimental setup shown in figure 4.7. The solder alloy was put in a ceramic tube and placed in a quartz glass. The tip of the ceramic tube was placed at approximately 1 cm distance on the Cu substrate surface. The position where the drop would fall on the Cu substrate was left centered inside the furnace while the setup was being prepared. The apparatus was connected to an argon tube, allowing high-purity argon gas to circulate under and above the quartz glass to prevent oxidation during the soldering process. A digital camera capable of shooting 600 fps was placed in the most suitable position to capture the drop image. The experiment was then ready to begin.

After installing the essential controls, we circulated high-purity argon gas for 10 minutes from the lower end and 10 minutes from the upper end. Then, we set the furnace to the desired temperature (275 ^{0}C, 300 ^{0}C, and 325 °C) and monitored the solder until it melted. Since the oven has two sections (right and left), we allowed it to work for 30 minutes to ensure that both sections reached an equilibrium temperature. The right and left thermocouples showed the set temperature value.

After 50 minutes of starting the experiment, the solder alloy was ready to be dripped in molten form. A certain frequency was provided by the steel iron stepper motor, whose tip was connected to the stepper motor. During this time, a digital camera (Casio Made Pro EX-F1) was used to record a 10-minute video of the solder alloy being dripped onto the Cu substrate in a liquid form. Once all the procedures were

completed, the experimental setup was closed, and the process was terminated. To analyze the experiment, screenshots were taken at the intervals of 0th, 5th, 10th, 15th, 30th, 60th, 90th, 120th, 150th, 300th, and 600th seconds of the video recording. Using the "Corel DrawXX2" drawing program, the wetting angles of the solder alloy on the Cu substrate were measured and saved on the computer; however, the wetting angle diagrams were obtained using Sigma Plot15.0 Software.

The hybrid drop technique was used to conduct 45 experiments. Nine experiments were performed on each solder alloy produced of the five quinary lead-free solder alloys at predetermined temperatures 275 ^{0}C, 300 ^{0}C, and 325 ^{0}C as displayed in Table 4.2.

Table 4.2. List of the hybrid drop technique experiments that are conducted at different temperature for each quinary lead-free solder alloys formed by the addition of Al to SAC205-1In.

(x) Al (wt%)	Temperature (^{0}C)	Lead-free solder alloys (96.5-x)Sn-2Ag-0.5Cu-1In-(x)Al	Number of experiments
0.3	275	96.2Sn-2Ag-0.5Cu-1In-0.3Al	3
	300		3
	325		3
0.5	275	96Sn-2Ag-0.5Cu-1In-0.5Al	3
	300		3
	325		3
0.7	275	95.8Sn-2Ag-0.5Cu-1In-0.7Al	3
	300		3
	325		3
0.8	275	95.7Sn-2Ag-0.5Cu-1In-0.8Al	3
	300		3
	325		3
0.9	275	95.6Sn-2Ag-0.5Cu-1In-0.9Al	3
	300		3
	325		3
Total experiments			45

4.6 SEM-EDX ANALYSIS OF SAC205-1In-xAl SOLDER ALLOYS ON Cu SUBSTRATE.

Scanning electron microscopy and energy-dispersive X-ray spectroscopy (SEM + EDX) were then employed to evaluate the performance of the new alloy, microstructure, and IMC formation at the SACIn-xAl/Cu interface in the SEM

laboratory at the Margem Laboratory of Karabük University Iron and Steel Institute. The device used for the SEM-EDX analysis was ZEISS ULTRA PLUS FESEM SE2, Inlens, STEM, and EsB detectors. (see Figure 4.8). This device can receive the images of SEM by increasing the temperature of the sample to 750 ^{o}C by Hot-Stage Point, linear, and map-type chemical composite analysis utilizing an EDX detector. Coating of dielectric surfaces with Au, Au/Pt veC using a coating device. SEM-EDX provides a detailed elemental composition and high-resolution imaging of microscopic surface structures.

Figure 4.8. The device used for the SEM-EDX analysis " ZEISS ULTRA PLUS FESEM SE2.

After wetting experiments were completed, the samples were collected, and for each temperature 275 ^{0}C, 300 ^{0}C, and 325 ^{0}C, a sample with a better wettability was chosen for SEM-EDX analysis. At first, the sample was cut from its middle into two halves using a jigsaw. The two halves of the samples were covered with Bakelite material at the metal laboratory (see Figure 4.9). Then, the surface of the alloy samples was smoothed using 1000,1200, 1500, 2000, and 2500 mesh sandpaper, Then, the samples were polished with water-based diamond lubricant using Forcipol 2v, a Grinder-Polisher device, at a metallurgical laboratory at Karabuk University. (see Figure 4.10), Finally, until the samples became ready for SEM-EDX analysis, the samples were cleaned and washed by using alcohol, and then the samples were

dried by using an electric dryer; then we kept the samples in a closed container in the laboratory and so the samples became ready for SEM-EDX analysis.

Figure 4.9. Shows the preparing SACIn-xAl solder/Cu interface at temperatures of 275^0C, 300^0C, and 325^0C for SEM-EDX analysis.

Figure 4.10. Forcipol 2v, a Grinder-Polisher device.

Table 4.3 Displays the wetting experiment numbers through SEM-EDX for the chosen solder alloys at 275 ^{0}C, 300 ^{0}C, and 325 ^{0}C.

The table 4.3 lists the chosen samples of solder alloys for SEM-EDX analysis at 275^0C, 300^0C, and 325^0C, along with their corresponding wetting experiment numbers.

Table 4.3. Displays the solder alloys produced with their corresponding wetting experiment numbers for SEM-EDX analysis.

Solder alloys produced	275^0C	300^0C	325^0C
SAC205-1In-0.3Al	Exp.3	Exp.5	Exp.8
SAC205-1In-0.5Al	Exp.12	Exp.14	Exp.18
SAC205-1In-0.7Al	Exp.19	Exp.23	Exp.27
SAC205-1In-0.8Al	Exp.29	Exp.31	Exp.36

SAC205-1In-0.9Al	Exp.38	Exp.41	Exp.43

4.7. CORROSION EXPERIMETNS

We have conducted corrosion experiments to examine how adding Al affects the corrosion rate of SAC205-1In. To do this, we measured the corrosion rates of all newly produced solder alloys and compared them to the previously manufactured SAC305 and SAC205-1In. The main goal of corrosion tests is to determine the rate of corrosion, the current density, and the corrosion potential of the evolved solder alloys. We examined the features of corrosion for the SAC205-1In-xAl quinary lead-free solder alloy in a 1 M solution of HCL. Furthermore, the analysis of microstructure before and after corrosion for the SAC-1In-xAl where (x=0.3 wt%, 0.5 wt%, 0.7 wt%, 0.8 wt%, and 0.9 wt%) were done separately by using the device Carl Zeiss Ultra SEM at the Margem Laboratory of Karabuk University Iron and Steel Institute. The samples for corrosion tests were prepared using SiC sheets with mesh sizes ranging from 400, 600, 800, 1000, 1200, 2000, and 2500 to smooth the surfaces of the samples. Then, A diamond lubricating solution with a water base was used to polish the working electrode samples. Afterward, the samples were cleaned using alcohol and dried with a dryer. Finally, the prepared samples were stored in a closed container and were ready for the corrosion tests.

Before starting the polarization process, open-circuit monitoring was conducted for 10 minutes to ensure the working electrode surfaces were stabilized potentiostatically.

The experiments were conducted with a total of 3 electrode cells, comprising 1 reference electrode (Ag/ AgCl), a counter electrode (1 double graphite rod), and a working electrode (produced solder alloys). We used a harsh solution (1 M HCl) as the test medium due to the presence of two different types of ions in HCl acid, chlorine (Cl^-) and hydrogen (H^+), therefore, it corrodes more rapidly than other electrolytes. Unlike salt and alkaline solutions, which contain only a single type of ion that causes corrosion, potentials ranging from -1.0 V (Ag/AgCl) to +1.0 V (Ag/AgCl) were examined to identify potential sites for passivation and de-passivation. The scanning speed was adjusted to 1 mV/s [114].

4.8 ELECTRICAL RESISTIVITY MEASUREMENTIS

Electrical conductivity and resistivity are essential properties used to characterize lead-free solder alloys. The resistivity of solder alloys could be determined by applying a current source in order to produce an electric field within the sample. This electric field helps to determine the intensity of the current and (V) the potential drop that occurs between any two selected points. The resistivity of a material is then calculated by dividing the current (I) passing through the sample by the voltage (V) it generates according to Ohm's law. It is essential to consider the material's geometric properties when determining a homogeneous sample's electrical resistivity [115].

Resistivity measures how much a material prevents the electric current movement. Conductivity, on the other hand, measures how effectively a material can allow the movement of electric current through it and is the opposite of resistivity.

The electrical resistivity of SAC205-1In and quinary solder alloys that were produced in this study SAC205-1In-xAl where x = 0.3 wt%, 0.5 wt%, 0.7 wt%, 0.8 wt%, and 0.9 wt% was measured by using a two-point probe technique using a Keith 2400 source meter. The measurements of resistivity were taken by touching the surface layer of samples with two probes, as illustrated in Figure 4.11.

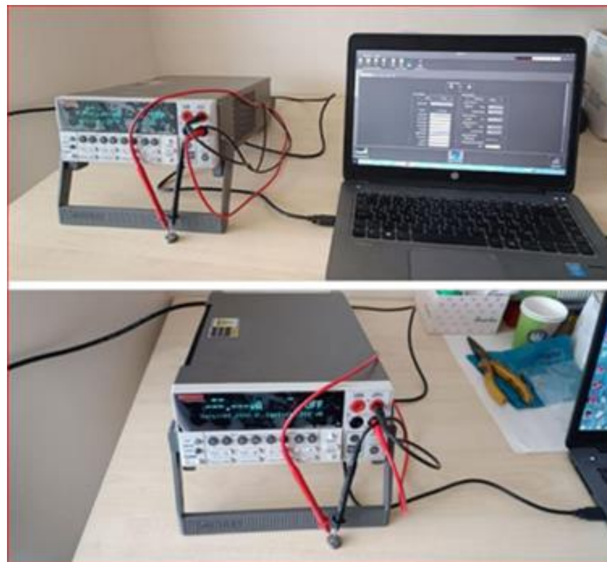

Figure 4.11. Electrical resistivity measurements were taken using the Keith 2400 source meter and two-point probe technique.

At room temperature, the electrical resistivity test was carried out by using an applied steady current of 1 A. For each sample, twenty measurements were taken. The electrical resistance R of an object is defined as the ratio between the difference voltage (*V*) that causes the current (*I*) to move through it. Electric resistance from the experimental measurements was calculated using Ohm's law as shown in equation. 4.1.

$$R = \frac{V}{I} \tag{4.1}$$

[116]

For calculating the resistivity of the sample, the geometrical dimensions of the sample must be known. Since the thickness of sample was taken approximately 3 mm, and the distance between the probs s =2mm.

$$\rho = \frac{V}{I} G \tag{4.2}$$

[117]

G: is the correction factor dependent on the sample shape and dimensions and arrangement of electrical contact [117].

The geometric factor G was derived by Uhlir [118, 119].

The formula was used for calculating the correction factor G is became as follow

$$G = 2\pi s \, T_1\left(\frac{t}{s}\right) \tag{4.3}$$

[117]

$2\pi s$: is the geometric factor for a semi-infinite volume,

s: Distance between probs

t: Sample thickness

$T_1\left(\frac{t}{s}\right)$: is an additional correction factor to apply for finite thickness (t) of the sample. It is value was determined as 0.835 from the table in Topase's article for calculating the correction factor (G) [117].

By substituting the value of s and $T_1\left(\frac{t}{s}\right)$ in equation (4.3), geometric correction factor becomes

$G = 2 \times 3.14 \times 2 \times 10^{-3} \times 0.835 = 10.4876 \times 10^{-3}$

According to equation (4.2), the electrical resistivity equation formula will become as follows.

$\rho = \frac{V}{I} G$

Hence

$\rho = RG$ (4.4) [117, 56]

By substituting the value of (G) in equation (4.4)

$\rho = (10.4876 \times 10^{-3}) R \ (m\Omega.m)$

$\rho = 10.4876 \times 10^{-6} R \quad (\Omega.m)$

(4.5)

The electrical resistivity measurements of produced solder alloys SAC205-1In-xAl where (x = 0.3 wt%, 0.5 wr%, 0.7 wt%, 0.8 wt%, and 0.9 wt%) and SAC205-1In were calculated by substituting the value of electrical resistance measurements (R) that obtained experimentally in equation 4.5, (see Appendix B).

4.9 SHEAR STRENGTH TESTS

For the shear test, Cu-substrate plates were prepared of dimensions 50 mm length, 15 mm width, and 1.5 mm thickness. The surfaces of the Cu substrate plates were smoothed with 1200 and 2000 mesh sandpaper and then cleaned with methanol alcohol to remove and prevent oxidation on its surface. For the shear test, quinary lead-free solder alloys SAC205-1In-xAl were soldered onto the Cu substrates plates, where x represented the weight percentage of Al (0.3%, 0.5%, 0.7%, 0.8%, and 0.9%). Small pieces of each solder alloy produced were placed between two Cu-substrate plates, which were then attached by soldering. Soldering between the copper plates was performed using two separate soldering irons, and a 15mm x

15mm region was soldered at a temperature of approximately 330-350°C (see Figure 4.12).

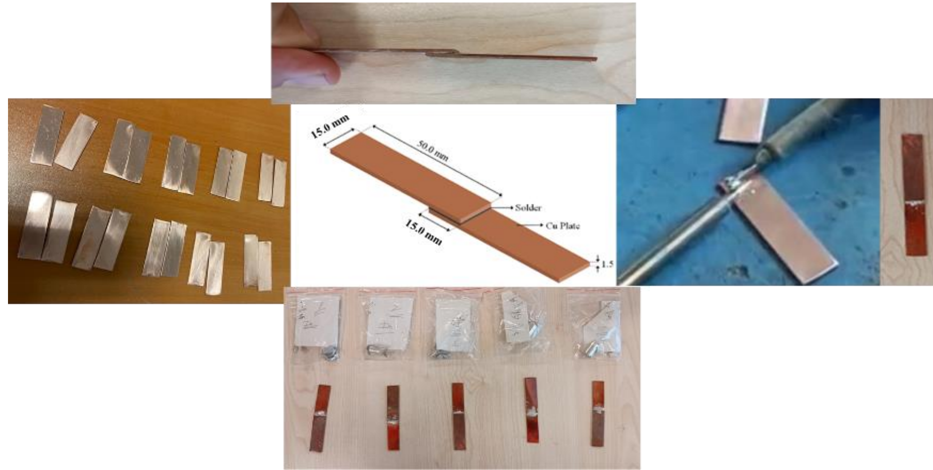

Figure 4.12. Shows Cu-substrate dimensions and the process of soldering.

Then the produced samples affected the cutting force. The shear strength values indicate the greatest load a material can withstand before shearing. These values are crucial in determining how effectively a material can resist forces that affect parallel to its surface. IMC materials are crucial for the mechanical strength and stability of solder junctions [120]. A solder junction needs to be very strong to sustain severe heat pressures or shock loads and remain practical for the long term. The newly produced quinary SAC205-1In-xAl (x=0.3%, 0.5, 0.7, 0.8 and 0.9 wt%) alloys that do not contain lead were sheared with a Zwick Roell Z050 device at static test laboratory of Karabuk University Iron and Steel Institute as shown in Figure 4.13.

Figure 4.13. The device used for shear strength test Zwick Roell Z050 device at static test laboratory of Karabük University Iron and Steel Institute.

The linked copper plates of each solder alloy produced SAC205-1In-xAl were then fastened to the jaws of a typical tensometer, where they were dragged with a shear force across the joint at a crosshead speed of 2.0 mm/min to observe the influence of loading speed on the shear strength and measuring the maximum shear force (F_{max}) and maximum elongation (ε_{max}).

PART 5

RESULT AND DISCUSSION

5.1 X-RAY FLUORESCENCE (XRF) ANALYSIS

After the production process of quinary lead-free solder alloys (96.5-x) Sn-2Ag-0.5Cu-1In-(x)Al (where x = 0.3 wt%, 0.5 wt%, 0.7 wt%, 0.8 wt%, and 0.9 wt%) completed at the production laboratory for Metallurgical Materials Engineering at Karabuk University. The new alloys produced were homogenized in an oven set at 180 °C. The sample alloys were put inside the furnace for a duration of 48 hours. Afterward, the homogenization process was completed, and the produced quinary lead-free solder alloys were subjected to X-ray Fluorescence (XRF) analysis using the 4KWX-Ray RhTube device equipped with wavelength distribution spectroscopy in the Karabuk University at Margem Laboratory to determine the accuracy of the metal ratios in the produced sample alloy in wt%. The chemical combinations of the investigated lead-free solder alloys are shown in weight percentage and listed in Table 5.1.

Table 5.1. Results of XRF analysis show the wt% of the chemical composition of produced quinary lead-free solder alloys Sn-2Ag-0.5Cu-1In-xAl.

Produced quinary lead-free solder alloys	Wt %				
	Sn	Ag	Cu	In	Al
96.2Sn- 2Ag- 0.5Cu- 1In- 0.3Al	96.2668	1.9713	0.4528	0.9993	0.3000
96Sn- 2Ag- 0.5Cu- 1In- 0.5Al	95.4494	2.1554	0.4900	0.9970	0.4843
95.8Sn- 2Ag- 0.5Cu- 1In- 0.7Al	95.7915	1.9395	0.4872	1.0240	0.7289
95.7Sn- 2Ag- 0.5Cu-1In- 0.8Al	95.6977	2.0048	0.4195	1.0928	0.8078
95.6Sn- 2Ag- 0.5Cu- 1In- 0.9Al	95.6414	2.0532	0.4835	1.0632	0.9112

Five quinary solder alloys were prepared by adding varying quantity of aluminum to the SAC205-1In to develop lead-free solder alloys. The corresponding ratios of elements in the produced solder alloys are displayed in Figure 5.1.

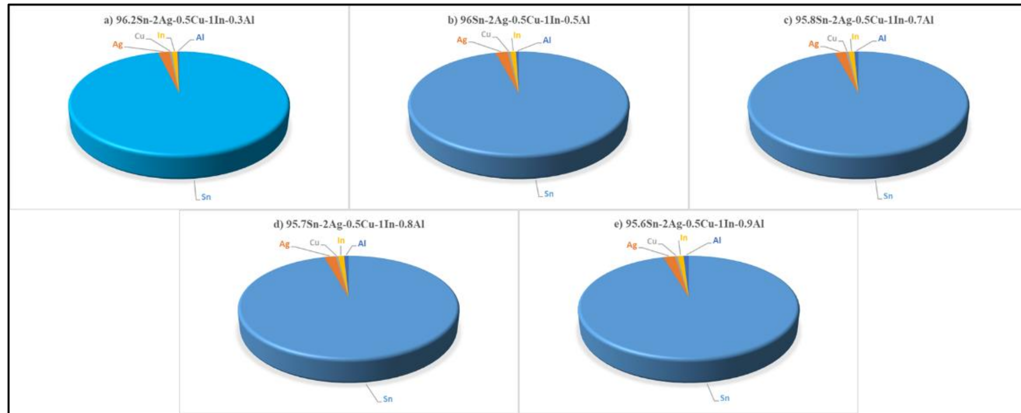

Figure 5.1. The weight percentage of elements in produced solder alloys

5.2 DIFFERNTIAL SCANNING CALORIMETER (DSC) ANALYSIS

Differential scanning calorimeter (DSC) tests were conducted in Margem laboratories at Karabuk University on quinary lead-free solder alloys ((96.5-x)Sn-2Ag-0.5Cu-1In-xAl) produced in this study with varying amounts of aluminum (x = 0.3, 0.5, 0.7, 0.8, and 0.9 wt%). The DSC analysis revealed that the melting points of the solder alloys, SAC-In-xAl where (x=0.3, 0.5, 0.7, 0.8, and 0.9 wt%), were as follows: 214.3°C, 219.7°C, 219.3°C, 219.1°C, and 220.5°C, respectively, as shown in Table 5.2 and Figure.5.2.

Previous studies have shown that the melting point of SAC305 was measured as 219.1°C [8], while the melting point of the SAC205-1In solder alloy was calculated as 217.7°C [9]. The reduction in melting point of quinary lead-free solder alloys SAC205-1In-0.3Al produced in this study is ranging about 3.8 to 4.8°C degrees to that of SAC205-1In and SAC305 solder alloys made in previous studies. Solder alloys with higher melting points require higher temperatures for soldering in industrial applications [11].

The melting point of the quinary lead-free solder alloy (SAC205-1In-0.3Al) decreased compared to SAC205-1In and SAC305, while the melting point of the other quinary lead-free solder alloy produced in this study was close to that of SAC205-1In.

Table 5.2. The melting temperatures of the produced quinary lead-free solder alloys according to the results of DSC.

Lead free solder alloy	Melting temperature ^{0}C
SAC205-1In-0.3Al	214.3
SAC205-1In-0.5Al	219.7
SAC205-1In-0.7Al	219.3
SAC205-1In-0.8Al	219.1
SAC205-1In-0.9Al	220.5
SAC305 [8]	219.1
SAC205-1In [9]	217.7

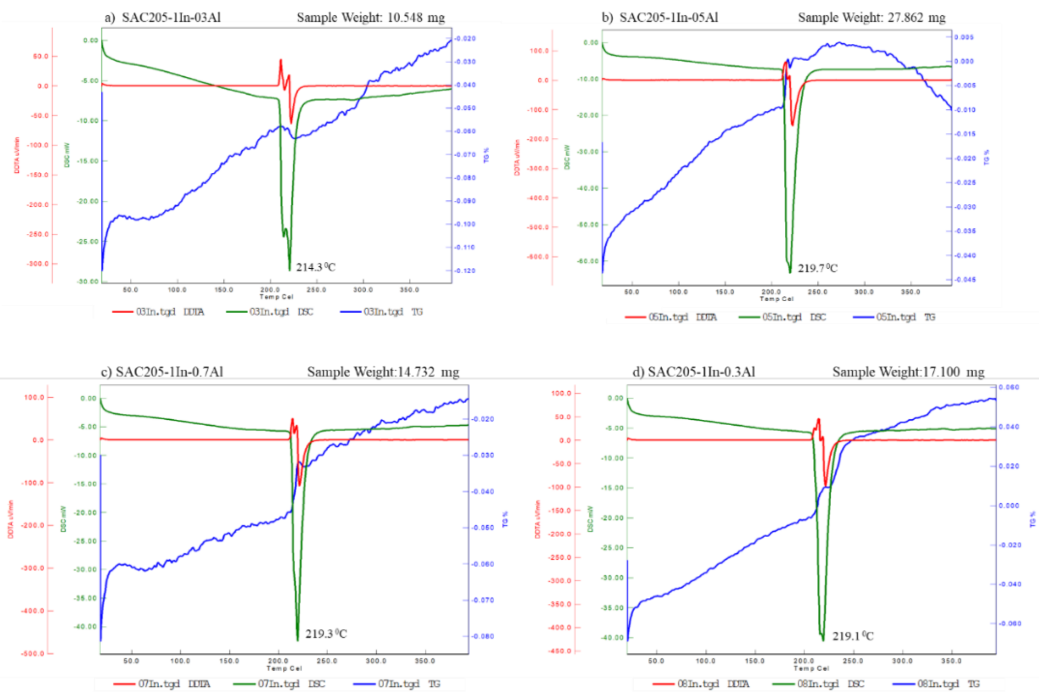

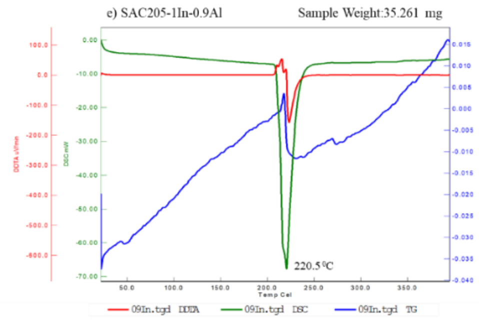

Figure 5.2. DSC analysis of SAC205-1In-xAl , a) SAC-In-0.3Al , b) SAC-In-0.5Al, c) SAC-In-0.7Al, d) SAC-In-0.8Al, e) SAC-In-0.9Al.

5.3 X-RAY DIFFRACTION (XRD) ANALYSIS

At the KBU Margem Laboratory, the XRD analysis was conducted on each quinary lead-free solder alloy SAC205-1In-xAl, where x represents 0.3 wt%, 0.5 wt%, 0.7 wt%, 0.8 wt%, and 0.9 wt%. This analysis's main goal was to figure out the kinds of IMCs that were present in the alloys. The results of the XRD analysis exhibited the impact of adding (Al) on the microstructure and the formation of IMCs in the alloy. The XRD results confirmed that the solder alloys contained various intermetallic compounds, such as Ag_3Sn, Ag_2Al, Ag_3Al, Al_2Cu, AlCu, Cu_3Sn, and Cu_6Sn_5. The presence of these IMCs in the solder alloys is depicted in Figure 5.3. The findings of this analysis will help better understand the properties and performance of the solder alloys, which can be used to improve their quality and reliability in various applications. The addition of (Al) to the SAC solder alloys leads to the formation of Ag-Al and Cu-Al IMC, enhances β-Sn dendrites, and reduces the growth of Ag3Sn and Cu6-Sn5 IMC [38]. When examining the microstructural properties, it becomes apparent that the Cu-Al IMC phase, which is abundant in Al, has replaced Cu6Sn5 and Ag3Sn IMCs [121].

X-ray diffraction (XRD) is a technique employed in science of materials to identify the crystallographic structure of a material. The principle of XRD is based on the fact that each crystal phase refracts X-rays in a characteristic order, which depends on the configuration of the atoms of crystal. XRD analysis helps to identify the microstructural properties of new quinary lead-free solder alloys (as depicted in Figure 5.3). The peak values in the XRD spectrums show the locations with the

highest intensity and prominence of Cu-Sn, Cu-Al, Ag-Al, and Ag-Sn phases. The phases observed in the SEM-EDX analysis were found to be proportional to their corresponding peak intensities in the XRD analysis.

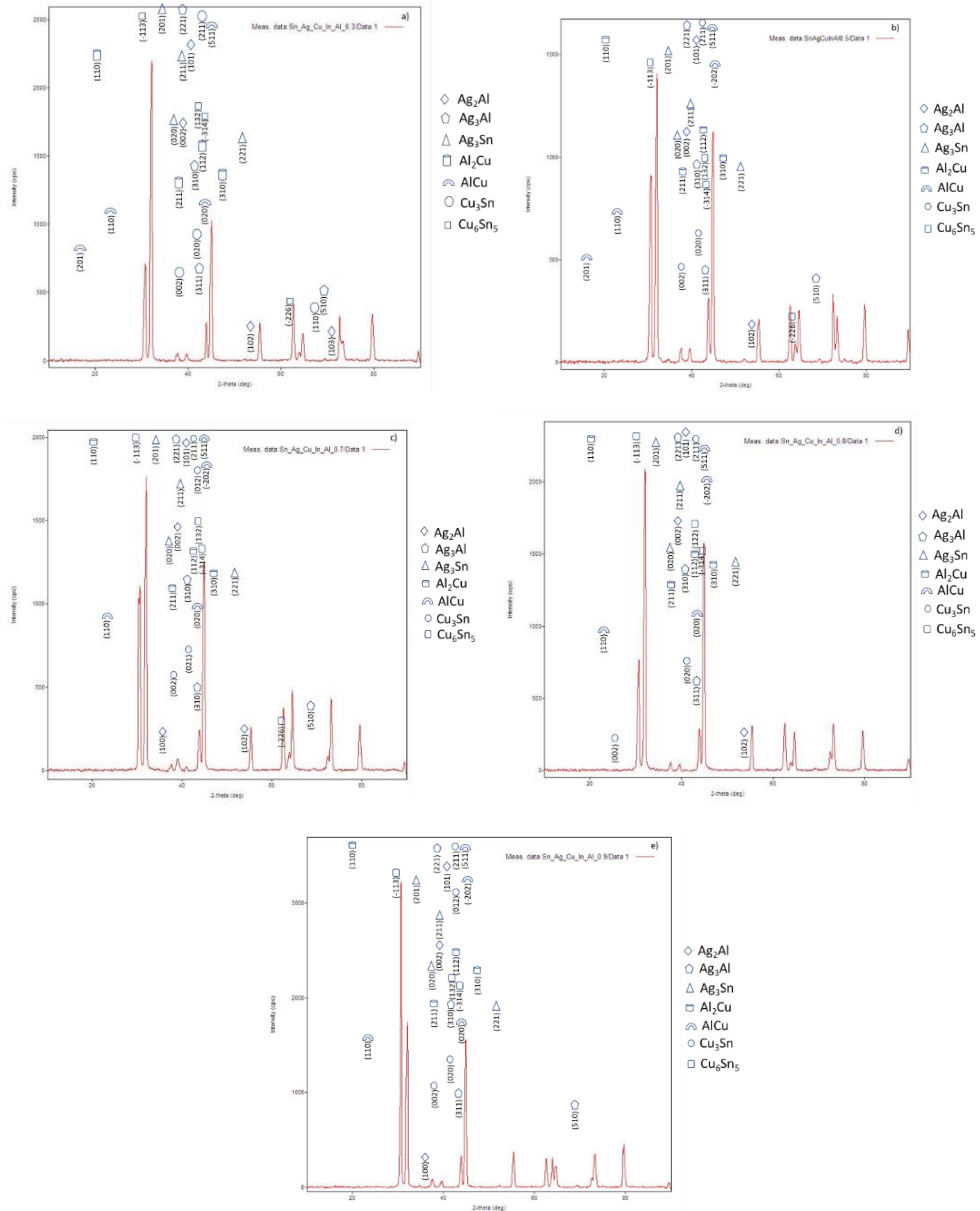

Figure 5.3. XRD analysis of lead-free solder alloys SAC205-1In-xAl indicates the formation of IMCs: a) SAC205-11In-0.3Al, b) SAC205-1In-0.5Al, c) SAC205-1In-0.7Al, d) SAC205-1In-0.8Al, and e) SAC205-1In-0.9Al.

5.4 WETTABILITY ANALYSIS

The wetting tests for the SAC205-1In-xAl (x is 0.3 wt%, 0.5 wt%, 0.7 wt%, 0.8 wt%, and 0.9 wt%) were conducted using the hybrid drop method on a 99.85% pure Cu substrate. The lead-free solder alloys melted inside the furnace and were then dropped onto the copper substrate at predefined temperatures (275 ^{0}C, 300 ^{0}C, and 325 °C). As soon as the droplets touched the Cu substrate, a 10-minute video recording was made using a high-speed camera with a camera featuring a shooting ability to capture 600 frames per second, the Casio Made Pro EX-F1. The video was captured at different intervals to observe the behavior of the drops on the substrate. The wetting angle versus time plots were obtained using Sigma Plot15.0 Software, and the wetting experiments data were obtained for three different positive wetting experiments for each temperature.

The wetting contact angle between the solder and Cu substrate was measured using the "Corel Draw XX2 software" with the help of screenshots of the video taken at specific seconds. Three wetting experiments were conducted using the hybrid drop method for each new quinary lead-free solder alloy at predetermined temperatures of 275, 300, and 325 °C. The average CA of the right and left was calculated.

5.4.1 Contact Angles Measurements Of SAC205-1In-0.3Al

Table 5.3 displays the average left and right contact angle measurements for all wetting experiments conducted on the new quinary lead-free solder alloy SAC205-1In-0.3Al at three different temperatures: 275 ^{0}C, 300 ^{0}C, and 325 ^{0}C. Among all the experiments, the lowest average of the left and right contact angles was recorded in experiment 8 at the 600th interval, with a value of 37.61^0, as indicated in Table 5.3 (See Figure Appendix A. 1). Additionally, Figure 5.4 depicts an image of some droplets of SAC205-1In-0.3Al on a Cu-substrate, along with the measurement of the CA at intervals of 600th. Then, the average contact angle of three wetting experiments of SAC205-1In-0.3Al for each predetermined temperature 275 ^{0}C, 300 ^{0}C, and 325 ^{0}C were calculated as shown in Table 5.4. The lowest average CA was observed as 39.88^0 at a temperature of 325 ^{0}C. All the information on the wetting

experiments conducted on SAC205-1In-xAl was registered, including essential details such as the mass of the Cu, the mass of the used solder alloy, the mass of the solder droplet on the Cu-substrate, the duration of the test, and the duration of the video recording. This information is crucial for analyzing and comparing the results of each experiment.

Table 5.3. Displays the average left and right contact angles for each wetting experiment of SAC205-1In-0.3Al at 275^{0}C, 300^{0}C, and 325^{0}C.

Average contact angles for both left and right sides of SAC205-1In-0.3Al droplet on Cu-substrate at a predetermined temperature									
Time (s)	275 ^{0}C			300 ^{0}C			325 ^{0}C		
	Exp.1	Exp.2	Exp.3	Exp.4	Exp.5	Exp.6	Exp.7	Exp.8	Exp.9
0	58.04	61.11	54.50	53.07	52.98	52.22	50.64	45.24	45.74
5	57.54	59.30	52.70	51.23	49.85	45.79	50.27	45.40	42.91
10	56.93	57.63	50.27	50.08	49.39	44.24	45.90	43.41	42.49
15	56.20	57.38	48.6	49.43	49.02	42.09	45.64	41.83	42.42
30	55.88	56.77	47.85	46.73	47.13	41.84	45.45	41.68	42.41
60	55.24	56.11	47.61	46.68	46.43	41.25	45.21	40.59	41.84
90	54.54	54.74	45.63	46.44	46.28	40.47	44.74	40.44	41.52
120	54.05	53.08	44.92	44.57	45.64	40.20	44.02	38.97	41.36
150	53.65	52.17	43.07	44.36	44.99	40.10	43.62	38.68	41.01
300	53.47	51.03	42.63	43.87	44.19	39.36	42.85	38.08	40.74
600	52.23	49.04	42.26	43.54	43.89	38.88	41.51	37.61	40.51

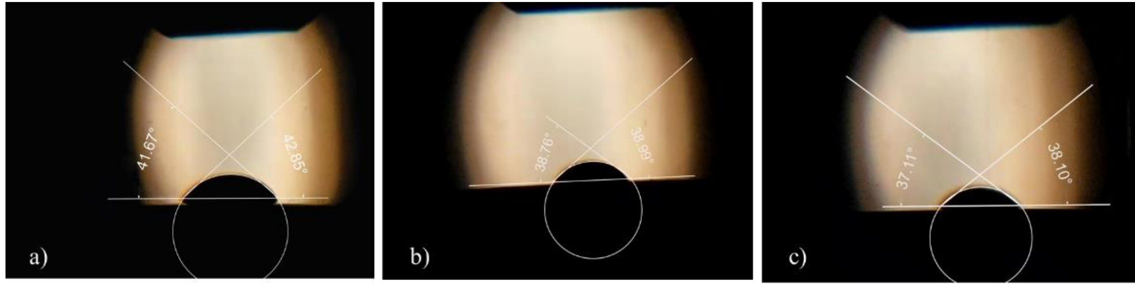

Figure 5.4. Shows the measurements of the left and right contact angles for SAC205-1In-0.3Al droplet on a Cu-substrate at intervals 600th-second a) Exp. (3) at 275 °C, b) Exp. (6) at 300 °C, c) Exp. (8) at 325 °C.

Table 5.4. Shows the average contact angle measurements for three wetting experiments of SAC205-1In-0.3Al performed at 275 ^{0}C, 300 ^{0}C, and 325 ^{0}C.

Contact angles measurements of SAC205-1In-0.3Al			
Time	avg. Contact angles of Exp.1,2, 3 at 275 ^{0}C	avg. Contact angles of Exp. 4,5,6 at 300 ^{0}C	avg. Contact angles of Exp. 7,8,9 at 325 ^{0}C
0	57.88	52.75	47.20
5	56.51	48.95	46.19
10	54.94	47.90	43.93
15	54.06	46.85	43.30
30	53.50	45.23	43.18
60	52.98	44.78	42.55
90	51.64	44.39	42.23
120	50.68	43.47	41.45
150	49.63	43.15	41.10
300	49.04	42.47	40.55
600	47.84	42.10	39.88
Mean contact angles	52.61	45.64	42.87

5.4.2 Contact Angles Measurements Of SAC205-1In-0.5Al

Table 5.5 shows the average contact angle measurements for wetting experiments on the new SAC205-1In-0.5Al solder alloy conducted at 275 ^{0}C, 300 ^{0}C, and 325 ^{0}C. Experiment 18 had the lowest average contact angle of 36.48^0 at the 600th second. The images of some droplets of a solder alloy SAC205-1In-0.5Al on a Cu-substrate with the measurements of the contact angle at a second of 600th are shown in Figure 5.5. however, Table 5.6 shows the average contact angle of three experiments at each temperature. The lowest average contact angle of 40.12^0 was observed at 325 ^{0}C. See

Figure Appendix A.2 which contains details on the contact angle measurements of all wetting experiments of SAC205-1In-0.5Al.

Table 5.5. Displays the average left and right contact angles for each wetting experiment of SAC205-1In-0.5Al at 275 ^{0}C, 300 ^{0}C, and 325 ^{0}C.

Average contact angles for both left and right sides of SAC205-1In-0.5Al droplet on Cu-substrate at a predetermined temperature									
Time (s)	275 ^{0}C			300 ^{0}C			325 ^{0}C		
	Exp. 10	Exp. 11	Exp. 12	Exp. 13	Exp. 14	Exp. 15	Exp. 16	Exp. 17	Exp. 18
0	55.12	56.22	58.37	46.52	50.28	62.41	53.47	50.61	44.78
5	54.06	55.86	57.71	43.32	48.76	60.29	45.20	49.75	43.48
10	53.41	54.99	56.75	42.61	48.58	59.66	43.86	46.51	41.39
15	51.74	54.93	56.11	42.48	47.48	59.01	43.70	46.26	41.41
30	47.34	54.69	56.02	42.26	47.24	58.74	42.90	45.88	38.70
60	46.16	54.66	55.42	41.96	46.37	58.30	42.51	45.58	38.31
90	44.13	54.41	54.97	41.74	45.97	57.71	42.36	45.29	37.93
120	43.50	53.64	54.71	41.34	45.61	57.37	41.86	45.06	37.52
150	43.14	53.04	54.30	40.72	45.25	57.22	41.67	44.46	37.39
300	42.22	52.91	52.85	40.41	44.87	56.24	41.73	43.96	37.12
600	40.14	52.68	49.61	39.53	44.30	55.68	40.76	43.11	36.48

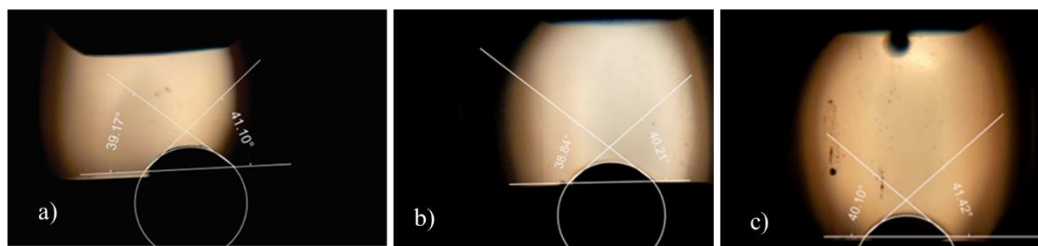

Figure 5.5. Shows the measurements of the left and right contact angles for SAC205-1In-0.5Al droplet on a Cu-substrate at intervals 600th-second a) Experiment (10) at 275 °C, b) Experiment (13) at 300 °C, c) Experiment (16) at 325 °C.

Table 5.6. Shows the average contact angle measurements for three wetting experiments of SAC205-1In-0.5Al performed at 275^0C, 300^0C, and 325^0C.

Contact angle measurements of SAC205-In-0.5Al

Time	avg. Contact angles of Exp. 10,11,12 at 275 ^{0}C	avg. Contact angles of Exp. 13,14,15 at 300 ^{0}C	avg. Contact angles of Exp. 16,17,18 at 325 ^{0}C
0	56.57	53.07	49.62
5	55.88	50.79	46.14
10	55.05	50.28	43.92
15	54.26	49.66	43.79
30	52.68	49.41	42.49
60	52.08	48.87	42.13
90	51.17	48.47	41.86
120	50.62	48.10	41.48
150	50.16	47.73	41.17
300	49.32	47.17	40.93
600	47.48	46.50	40.12
Mean contact angles	52.30	49.09	43.06

5.4.3 Contact Angles Measurements Of SAC205-1In-0.7Al

Table 5.7 presents the average left and right contact angles for all the wetting experiments conducted on the new quinary lead-free solder alloy SAC205-1In-0.7Al at three different temperatures: 275^0C, 300^0C, and 325^0C. Experiment 23, at the 600th second, recorded the lowest average of the left and right contact angles, which was 44.34^0, as mentioned in Table 5.7. Figure 5.6 shows droplets of SAC205-1In-0.7Al on a Cu-substrate with the measurement of the CA at a second of 600th. The average contact angle of three wetting experiments of SAC205-1In-0.7Al for each predetermined temperature 275^0C, 300^0C, and 325^0C were computed as presented in Table 5.8. At 325 ^{0}C, the lowest average CA was observed, 48.32^0. (See Figure Appendix A.3), which includes information about the contact angle measurements for all the wetting experiments involving SAC205-1In-0.7Al.

Table 5.7. Displays the average left and right contact angles for each wetting experiment of SAC205-1In-0.7Al at 275 ^{0}C, 300 ^{0}C, and 325 ^{0}C.

Average contact angles for both left and right sides of SAC205-1In-0.7Al droplet on Cu-substrate at a predetermined temperature									
Time (s)	275 ^{0}C			300 ^{0}C			325 ^{0}C		
	Exp.19	Exp.20	Exp.21	Exp.22	Exp.23	Exp.24	Exp.25	Exp.26	Exp.27
0	70.87	79.65	60.13	56.20	50.32	65.45	56.25	53.07	52.69
5	70.72	78.12	50.20	53.43	49.83	64.79	55.48	50.24	51.75
10	69.44	76.95	46.35	52.19	49.49	64.71	54.87	50.14	50.76
15	69.23	76.21	45.97	46.85	49.24	64.60	50.90	49.86	50.84
30	68.68	76.15	45.87	46.37	48.39	64.72	50.71	49.60	50.42
60	68.44	76.23	45.79	46.34	47.61	64.42	50.19	49.24	50.35
90	68.17	75.22	46.14	45.63	46.79	64.42	49.83	49.15	50.28
120	67.63	74.96	45.97	45.35	46.16	64.13	49.31	49.48	50.03
150	66.32	74.91	45.59	45.32	45.38	63.37	49.22	49.20	49.79
300	66.66	73.72	44.75	45.17	45.12	63.13	48.79	48.06	49.57
600	65.78	74.15	44.69	45.10	44.34	62.91	48.09	47.43	49.45

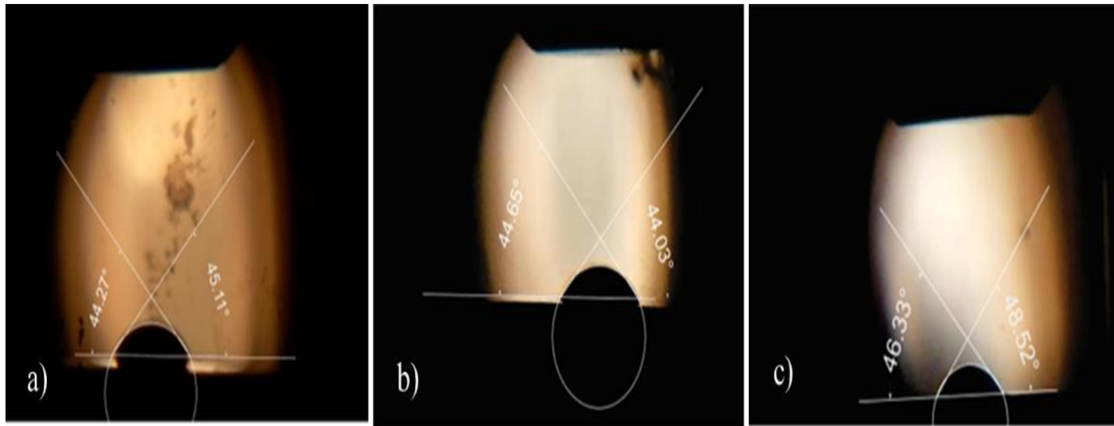

Figure 5.6. Shows the measurements of the left and right contact angles for SAC205-1In-0.7Al droplet on a Cu-substrate at intervals 600th-second a) Experiment (21) at 275 °C, b) Experiment (23) at 300 °C, c) Experiment (26) at 325 °C.

Table 5.8. shows the average contact angle measurements for three wetting experiments of SAC205-1In-0.7Al performed at 275 ^{0}C, 300 ^{0}C, and 325 ^{0}C.

Contact angle measurements of SAC205-In-0.7Al			
Time	avg. Contact angles of Exp.19,20,21 at 275 ^{0}C	avg. Contact angles of Exp. 22,23,24 at 300^{0}C	avg. Contact angles of Exp.25,26,27 at 325 ^{0}C
0	70.22	57.32	54.00
5	66.35	56.02	52.49
10	64.25	55.46	51.92
15	63.80	53.56	50.53
30	63.57	53.16	50.24
60	63.49	52.79	49.92
90	63.18	52.28	49.75
120	62.86	51.88	49.61
150	62.28	51.36	49.40
300	61.71	51.14	48.81
600	61.54	50.78	48.32
Mean contact angles	63.93	53.25	50.45

5.4.4 Contact Angles Measurements Of SAC205-1In-0.8Al

The average left and right contact angle measurements for all wetting experiments conducted on the new quinary lead-free solder alloy (SAC205-1In-0.8Al) were calculated at three various temperatures: 275 °C, 300 °C, and 325 °C, as shown in Table 5.9. Experiment 35 recorded the lowest average of the left and right contact angles at the 600th second with a value of 34.38^0. (See Figure Appendix A.4) which shows the CA measurements of all wetting experiments conducted on SAC205-1In-0.8Al. On the other hand, Figure 5.7 displays an image of some droplets of SAC205-1In-0.8Al on a Cu-substrate, along with the measurement of the CA at intervals of 600th seconds. The average contact angle of three wetting experiments of SAC205-1In-0.8Al for each predetermined temperature 275 °C, 300 °C, and 325 °C were calculated as shown in Table 5.10. The lowest average contact angle was identified at a temperature of 325 °C, with a value of 37.95.

Table 5.9. Displays the average left and right contact angles for each wetting experiment of SAC205-1In-0.8Al at 275^{0}C, 300^{0}C, and 325^{0}C.

Average contact angles for both left and right sides of SAC205-1In-0.8Al droplet on Cu-substrate at a predetermined temperature									
Time (s)	275 ^{0}C			300 ^{0}C			325 ^{0}C		
	Exp. 28	Exp. 29	Exp. 30	Exp. 31	Exp. 32	Exp. 33	Exp. 34	Exp. 35	Exp. 36
0	64.00	49.93	53.62	48.43	53.70	60.20	68.90	45.98	39.17
5	62.43	49.66	53.11	46.41	53.20	55.92	67.60	38.67	38.34
10	61.57	47.95	51.95	45.93	52.49	55.12	67.06	40.20	36.81
15	61.18	47.66	51.74	45.82	51.99	53.73	66.83	39.22	36.56
30	60.49	45.03	51.28	45.78	51.26	53.16	65.70	39.01	35.48
60	60.24	44.94	51.14	45.61	50.05	52.98	63.76	35.66	35.31
90	59.82	44.59	51.07	45.47	49.80	52.49	52.39	35.27	35.18
120	59.54	44.32	50.62	45.38	49.27	51.23	49.66	34.76	35.11
150	59.34	43.99	50.09	45.15	49.09	50.19	49.77	34.64	34.89
300	59.02	43.86	49.41	45.01	48.75	49.88	44.97	34.59	34.63
600	58.48	43.46	48.86	44.88	47.04	49.61	44.83	34.38	34.66

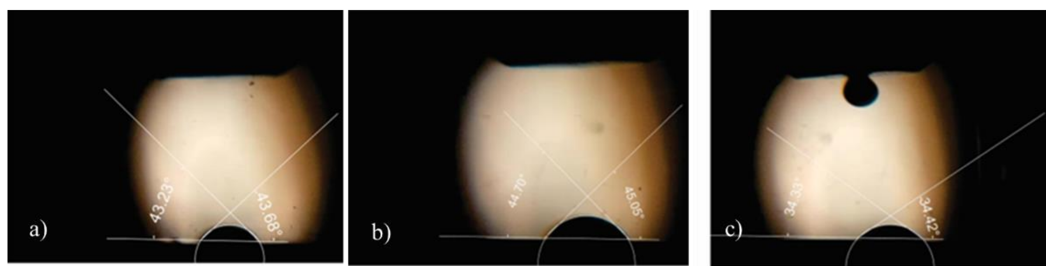

Figure 5.7. Shows the measurements of the left and right contact angles for SAC205-1In-0.8Al droplet on a Cu-substrate at intervals 600th-second a) Experiment (29) at 275 °C, b) Experiment (31) at 300 °C, c) Experiment (35) at 325 °C.

Table 5.10. Shows the average contact angle measurements for three wetting experiments of SAC205-1In-0.8Al performed at 275 ^{0}C, 300 ^{0}C, and 325 ^{0}C.

Contact angle measurements of SAC205-In-0.8Al			
Time	avg. Contact angles of Exp. 28,29,30 at 275 ^{0}C	avg. Contact angles of Exp. 31,32,33 at 300 ^{0}C	avg. Contact angles of Exp. 34,35,36 at 325 ^{0}C
0	55.85	54.11	51.35
5	55.06	51.84	48.20
10	53.82	51.18	48.02
15	53.52	50.51	47.53
30	52.26	50.07	46.73
60	52.10	49.55	44.91
90	51.83	49.25	40.94
120	51.49	48.62	39.84
150	51.14	48.14	39.77
300	50.76	47.88	38.06
600	50.26	47.17	37.95
Mean contact angles	52.55	49.85	43.94

5.4.5 Contact Angles Measurements Of SAC205-1In-0.9Al

Table 5.11 displays the average contact angle measurements for the wetting experiments on the new quinary lead-free solder alloy, SAC205-1In-0.9Al, at 275 ^{0}C, 300 ^{0}C, and 325 ^{0}C. Experiment 43 had the lowest average contact angle of 36.87^0 at the 600th second. However, Figure 5.8 display images of some droplets of SAC205-1In-0.9Al on a Cu-substrate, along with measurements of the contact angle at intervals of 600th. However, Table 5.12 presents the average contact angle of three experiments at each predetermined temperature: 275 ^{0}C, 300 ^{0}C, and 325 ^{0}C. The lowest average contact angle of 41.82^0 was observed at 325 ^{0}C. (See Figure Appendix A.5) which demonstrates the CA measurements of all wetting experiments of SAC205-1In-0.9Al.

Table 5.11. Displays the average left and right contact angles for each wetting experiment of SAC205-1In-0.9Al at 275 ^{0}C, 300 ^{0}C, and 325 ^{0}C.

Average contact angles for both left and right sides of SAC205-1In-0.9Al droplet on Cu-substrate at a predetermined temperature									
Time (s)	275 ^{0}C			300 ^{0}C			325 ^{0}C		
	Exp.37	Exp.38	Exp.39	Exp.40	Exp.41	Exp.42	Exp.43	Exp.44	Exp.45
0	55.18	52.39	65.09	56.39	47.59	53.97	41.61	53.10	51.27
5	52.43	48.81	64.56	53.60	46.85	54.20	40.32	52.29	48.86
10	51.70	45.29	63.95	52.75	46.35	52.63	39.97	52.04	48.48
15	50.74	45.70	62.95	52.69	45.96	50.76	39.13	51.60	46.95
30	50.41	45.67	62.44	51.66	44.47	50.82	38.15	50.65	46.64
60	49.12	44.54	62.14	51.01	43.64	48.94	37.83	50.36	45.74
90	48.82	44.46	61.47	50.48	43.55	48.25	37.61	48.58	45.02
120	48.44	44.14	61.16	49.26	43.31	47.98	37.39	48.11	44.90
150	47.80	43.77	60.86	48.99	43.04	47.87	37.23	47.64	44.49
300	46.95	43.58	60.33	48.41	42.25	47.65	36.97	45.32	44.13
600	46.30	43.36	60.40	48.16	41.53	47.44	36.87	45.14	43.47

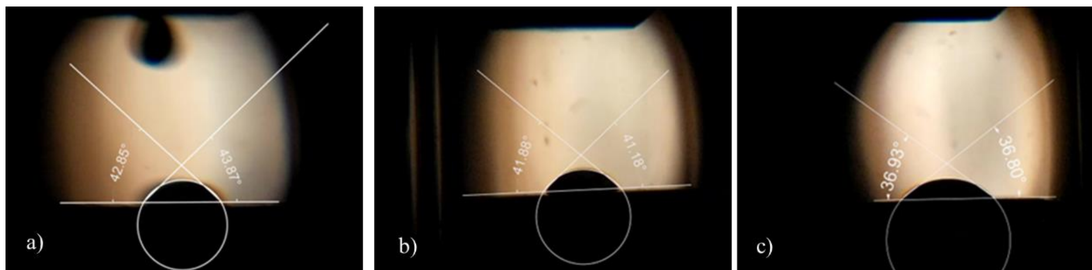

Figure 5.8. Shows the measurements of the left and right contact angles for SAC205-1In-0.9Al droplet on a Cu-substrate at intervals 600th-second a) Experiment (38) at 275 °C, b) Experiment (41) at 300 °C, c) Experiment (43) at 325 °C.

Table 5.12. Shows the average contact angle measurements for three wetting experiments of SAC205-1In-0.9Al performed at 275 ^{0}C, 300 ^{0}C, and 325 ^{0}C.

Contact angle measurements of SAC205-In-0.9Al			
Time	avg. Contact angles of Exp. 37,38,39 at 275 ^{0}C	avg. Contact angles of Exp. 40,41,42 at 300 ^{0}C	avg. Contact angles of Exp. 43,44,45 at 325 ^{0}C
0	57.55	52.65	48.66
5	55.26	51.55	47.15
10	53.65	50.58	46.83
15	53.13	49.80	45.89
30	52.84	48.98	45.14
60	51.93	47.86	44.64
90	51.58	47.42	43.73
120	51.25	46.85	43.46
150	50.81	46.63	43.12
300	50.29	46.10	42.14
600	50.02	45.71	41.82
Mean contact angles	52.57	48.56	44.78

The contact angles of new quinary lead-free solder alloys, SAC205-1In-0.3Al, SAC205-1In-0.5Al, SAC205-1In-0.7Al, SAC205-1In-0.8Al, and SAC205-1In-0.9Al have been measured for three positive wetting experiments. The average contact angles of all alloys change gradually over time instead of suddenly decreasing with temperature, as shown in Figure 5.9. The wetting angle graph exhibits a parabolic decrease in contact angle values over time, eventually stabilizing after the 60th second. Figure 5.9 shows that as the temperature increases, the wetting angle values decrease. Additionally, the wetting angle value rate reflects the solder alloy's tendency to spread on the Cu substrate [122]. Smaller wetting angles are seen in fast-spreading results.

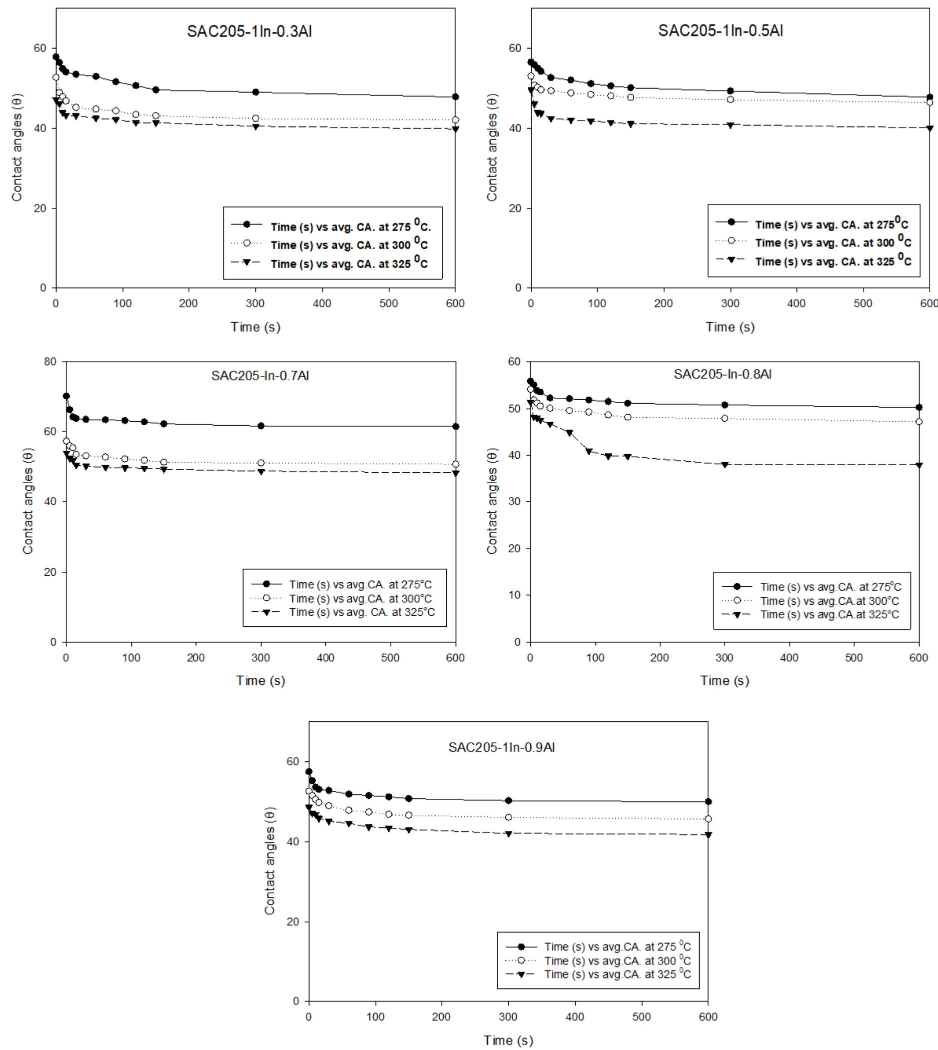

Figure 5.9. The average contact angles of three wetting-positive experiments at specified intervals (0, 5, 10, 15, 30, 60, 90, 120, 150, 300, and 600 seconds) of a SAC205-1In-xAl solder droplet on a Cu substrate at temperatures of 275°C, 300°C, and 325°C.

The capability of new quinary lead-free solder alloys, SAC205-1In-xAl, to spread on a Cu-substrate determines their wettability. Creating a reliable solder joint necessitates good wettability since it offers optimal contact and bonding between the substrate and the solder. Achieving better wetting requires careful control of the solder's composition and processing conditions and appropriate surface preparation of the substrate. Among all alloys, SAC205-1In-0.3Al showed the lowest mean contact angle at 42.87^0 at 325^0C. The mean contact angle for SAC205-1In-0.5Al was 43.06^0, for SAC205-1In-0.7Al was 50.45^0, for SAC205-1In-0.8Al was 43.94^0, and for SAC205-1In-0.9Al was 44.78^0, according to the contact angle measurements for

each alloy given in Tables 5.4, 5.6, 5.8, 5.10, and 5.12. The mean contact angle of new quinary lead-free solder alloys SAC205-1In-xAl was rearranged and mentioned in Table 5.13. In our research, we noticed that solder droplets, which are small amounts of molten metal used in soldering, spread more rapidly on the Cu substrate when the mean CA values are low. Conversely, when the mean CA values are high, they spread more slowly, providing insight into solder droplets' behavior on copper substrates.

Table 5.13. Mean contact angles of new quinary lead-free solder alloys at predetermined temperatures of 275 ^{0}C, 300 ^{0}C, and 325 ^{0}C

Lead free solder alloy	Mean CA. at Temperatures		
	275 ˚C	300 ˚C	325 ˚C
SAC-In-0.3Al	52.61	45.64	42.87
SAC-In-0.5Al	52.3	49.09	43.06
SAC-In-0.7Al	63.93	53.25	50.45
SAC-In-0.8Al	52.55	49.85	43.94
SAC-In-0.9Al	52.57	48.56	44.78

The wetting experiments showed that the contact angle decreases as the temperature increases for all new quinary lead-free solder alloys SAC205-1In-xAl. (See Figure 5.9, Table 5.13, and Figure Appendix A.6).

This study found that the SAC205-In-0.3Al solder alloy has the lowest melting point among all new quinary lead-free solder alloys. According to the DSC analysis, its melting temperature was 214.3 ^{0}C. The results of wetting experiments showed a correlation between the melting temperature and the degree of wettability. Adding aluminum to SAC205-1In lowered the melting point and improved the degree of wettability of new quinary lead-free solder alloys. At the same time, increasing the amount of Al from 0.3 wt% to 0.9 wt% causes a slight increase in the mean contact angle values and melting temperature of the alloy as shown in Table 5.13 and Table 5.12.

The contact angle value determines how well a liquid can wet a surface. If the contact angle value falls between 30 and 40 degrees, it means the surface is highly

wettable; when the CA is between 40 and 55 degrees, the wettability is satisfactory; when the CA is between 55 and 70 degrees, the wettability is poor, and when the CA exceeds 70 degrees, the wettability is very poor [11]. The range of average contact angles between 35 to 50 degrees for predetermined temperatures of 275 ^{0}C, 300 ^{0}C, and 325 ^{0}C indicates that the new quinary lead-free solder alloys SAC205-1In-xAl exhibit good and adequate wettability.

On the other hand, adding aluminum led to forming Cu-Al and Ag-Al IMCs. At the same time, Cu6Sn5 and Ag3Sn IMCs were suppressed. Cu-Al IMCs are an ideal choice for conductivity or binding compounds due to their thermal solid and electrical conductivity [64].

5.5 SEM-EDX ANALYSIS OF SAC205-1In-xAl SOLDER ALLOYS ON Cu-SUBSTRATE.

Understanding the microstructural characteristics of an alloy is crucial in determining its mechanical performance. SEM analyses of the alloys were carried out to analyze the microstructural properties of the new quinary lead-free solder alloys SAC205-1In-xAl and understand their mechanical performance and reliability. SEM-EDX analyses reveal the formation of several IMCs, such as Ag3Sn, Ag2Al, Ag3Al, Al2Cu, ALCu, Cu3Sn, and Cu6Sn5, at the interface of drop solder and Cu substrate, as shown in Figures 5.10, 5.11, 5.12, 5.13, and 5.14. The SEM-EDX analysis was used to examine the IMCs produced at the solder-to-Cu substrate interface, with each IMC being investigated at three different temperature values of 275°C, 300°C, and 325°C. The mechanical performance of an alloy is heavily influenced by its microstructural characteristics, so it is important to identify the microstructural characteristics of the new quinary lead-free solder alloy Sn-2Ag-0.5Cu-1In-xAl to determine its mechanical reliability and efficiency.

The Cu3Sn and Cu6Sn5 IMCs are essential in establishing the mechanical characteristics of solder alloys. CuSn is the main metallic phase that forms between the solder and the Cu substrate. During the soldering process, Cu6Sn5 is initially formed at the interface, which is then replaced by a combined layer of Cu3Sn and

Cu6Sn5. The thickness of the Cu3Sn layer is lower than that of the Cu6Sn5 layer, and it is formed between the Cu6Sn5 and Cu substrate. In accordance with the literature, the bonds of Al content with Cu content reduce the CuSn IMC phases, and the primary CuSn phases associated with Al-added SAC solder alloys are suppressed. Regions close to the Cu6Sn5 phase are observed to have SnCu and CuAl phases. With regard to the SEM examinations, for every lead-free solder alloy, the intermetallic components that were created at the contact point were increasingly noticeable as the temperature increased. [123, 124, 125].

The SnCu phase is represented by dark gray structures, the CuAl phase by black dotted structures, and the SnAg phase by white dendrite structures. As the temperature increased, the thickness of the SnCu and CuAl phases also increased and became more prominent. Similarly, SEM images showed that the size of the Cu3Sn and Cu6Sn5 phases increased with increasing temperature. The reliability of joints can be negatively affected by Cu6Sn5 IMC [126].

However, Cu6Sn5 IMC has a positive side: it can create a protective barrier on copper surfaces, making them highly corrosion-resistant. Cu3Sn IMC, on the other hand, improves electrical conductivity and is also highly corrosion-resistant. Many different alloys have been studied and debated in the literature as replacements to high Ag SAC alloys. Low Ag alloys have been found to have less Ag3Sn IMC in the bulk alloy, which corresponds to a decrease in mechanical strength. It seems evident that lower Ag alloys may be more capable of withstanding the effects of high strain rate deformation [127]. In bulk solder alloys, Ag-Al and Cu-Al IMC form faster due to the presence of Al. After forming Cu-Al and Ag-Al IMC, less Cu, and Ag are available to form IMC with Sn in bulk solder [38]. CuAl IMC is a popular choice for conductive or binding compounds due to its excellent thermal and electrical conductivity.

The images of SEM-EDX depicts the different phases of the new quinary solder alloys. The dark gray regions demonstrate the CuAl phase, while the lighter gray structures indicate the SnCu phase. The bar-shaped recessed structures represent the β-Sn phase. With increased temperature, the Cu3Sn and Cu6Sn5 phases formed at

the interface become more visible. Additionally, it has been reported that the size of CuSn phases also increases with the increase in temperature, as shown in the SEM-EDX Figures (See Figures 5.10. 511-5.19). The placement of the peaks in the EDX spectrums determines the element, while the intensity of the signal shows the degree of concentration of the element.

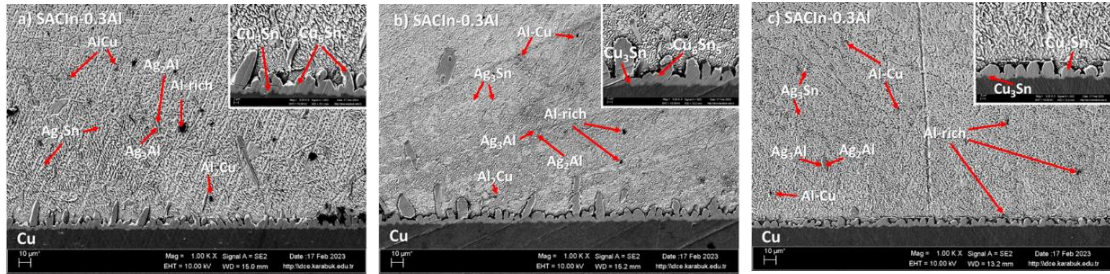

Figure 5.10. SEM images of SAC205-1In-0.3Al solder alloy/Cu interface at different temperatures: a) 275^{0}C, b) 300^{0}C, c) 325^{0}C.

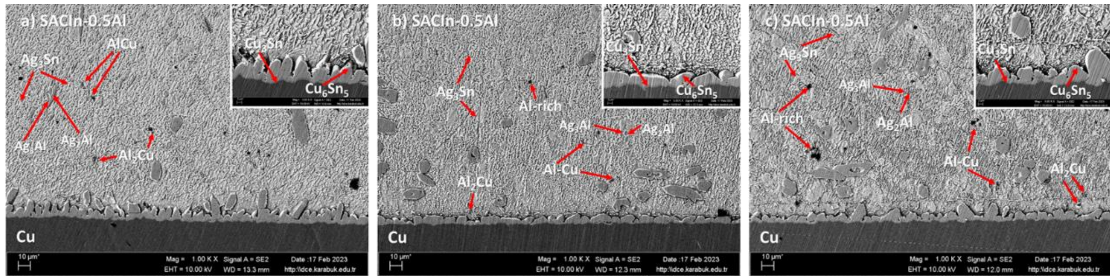

Figure 5.11. SEM images of SAC205-1In-0.5Al solder alloy/Cu interface at different temperatures: a) 275^{0}C, b) 300^{0}C, c) 325^{0}C.

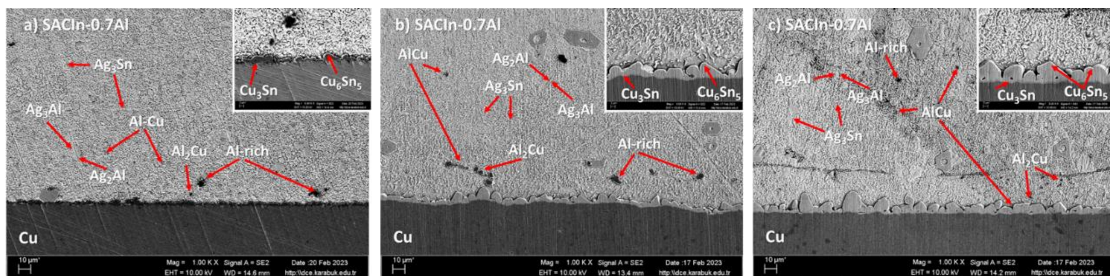

Figure 5.12.. SEM images of SAC205-1In-0.7Al solder alloy/Cu interface at different temperatures: a) 275^{0}C, b) 300^{0}C, c) 325^{0}C.

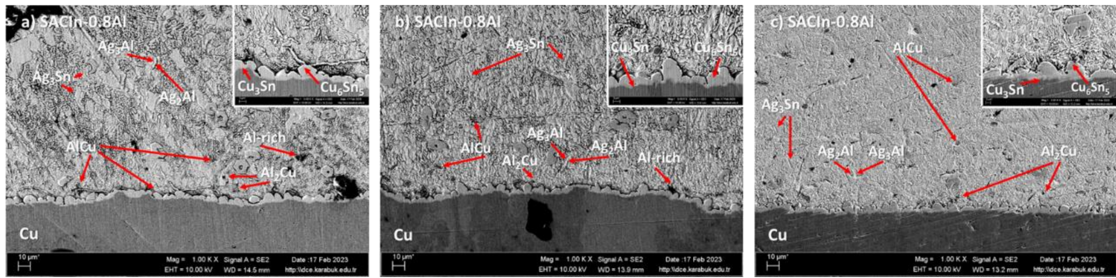

Figure 5.13. SEM images of SAC205-1In-0.8Al solder alloy/Cu interface at different temperatures: a) 275^{0}C, b) 300^{0}C, c) 325^{0}C.

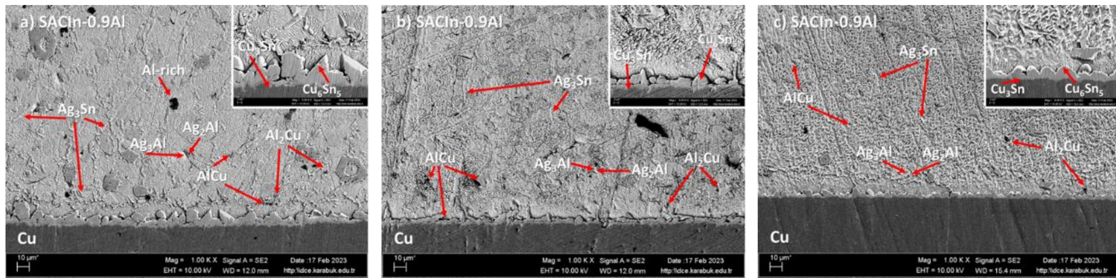

Figure 5.14. SEM images of SAC205-1In-0.9Al solder alloy/Cu interface at different temperatures: a) 275^{0}C, b) 300^{0}C, c) 325^{0}C.

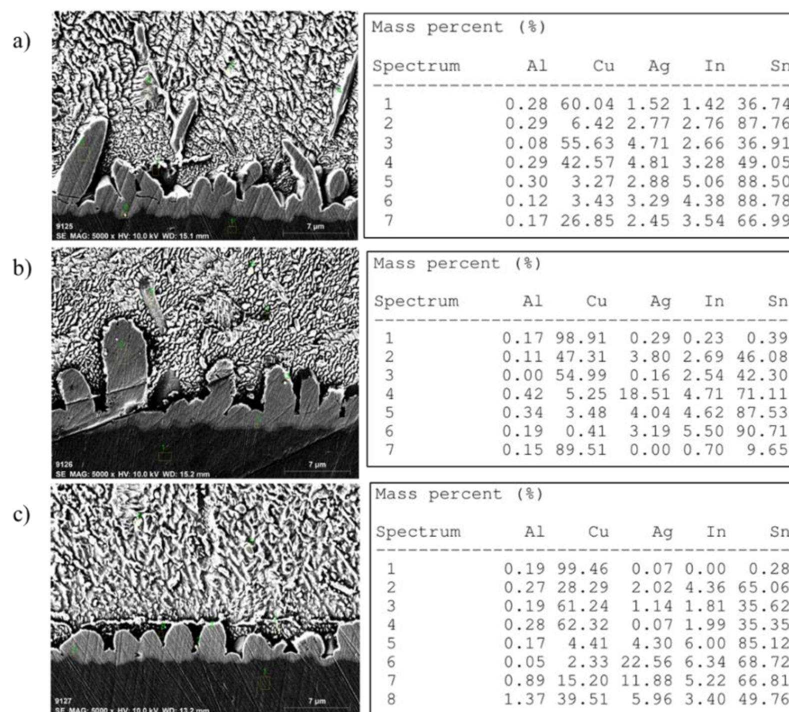

a)

Mass percent (%)

Spectrum	Al	Cu	Ag	In	Sn
1	0.28	60.04	1.52	1.42	36.74
2	0.29	6.42	2.77	2.76	87.76
3	0.08	55.63	4.71	2.66	36.91
4	0.29	42.57	4.81	3.28	49.05
5	0.30	3.27	2.88	5.06	88.50
6	0.12	3.43	3.29	4.38	88.78
7	0.17	26.85	2.45	3.54	66.99

b)

Mass percent (%)

Spectrum	Al	Cu	Ag	In	Sn
1	0.17	98.91	0.29	0.23	0.39
2	0.11	47.31	3.80	2.69	46.08
3	0.00	54.99	0.16	2.54	42.30
4	0.42	5.25	18.51	4.71	71.11
5	0.34	3.48	4.04	4.62	87.53
6	0.19	0.41	3.19	5.50	90.71
7	0.15	89.51	0.00	0.70	9.65

c)

Mass percent (%)

Spectrum	Al	Cu	Ag	In	Sn
1	0.19	99.46	0.07	0.00	0.28
2	0.27	28.29	2.02	4.36	65.06
3	0.19	61.24	1.14	1.81	35.62
4	0.28	62.32	0.07	1.99	35.35
5	0.17	4.41	4.30	6.00	85.12
6	0.05	2.33	22.56	6.34	68.72
7	0.89	15.20	11.88	5.22	66.81
8	1.37	39.51	5.96	3.40	49.76

Figure 5.15. SEM-EDX results of the SAC205-1In-0.3Al solder/Cu interface at predetermined temperatures: a) 275^{0}C, b) 300^{0}C, and c) 325^{0}C.

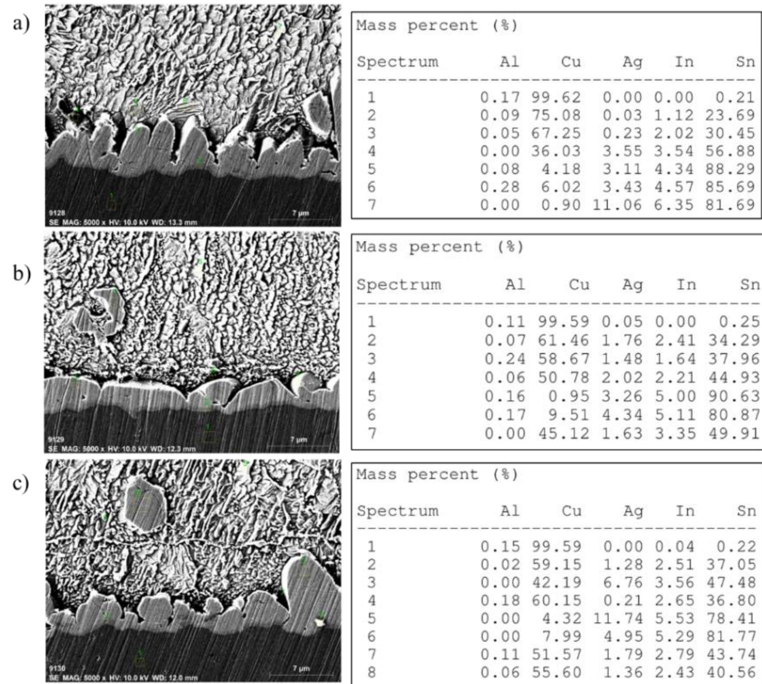

a)

Mass percent (%)

Spectrum	Al	Cu	Ag	In	Sn
1	0.17	99.62	0.00	0.00	0.21
2	0.09	75.08	0.03	1.12	23.69
3	0.05	67.25	0.23	2.02	30.45
4	0.00	36.03	3.55	3.54	56.88
5	0.08	4.18	3.11	4.34	88.29
6	0.28	6.02	3.43	4.57	85.69
7	0.00	0.90	11.06	6.35	81.69

b)

Mass percent (%)

Spectrum	Al	Cu	Ag	In	Sn
1	0.11	99.59	0.05	0.00	0.25
2	0.07	61.46	1.76	2.41	34.29
3	0.24	58.67	1.48	1.64	37.96
4	0.06	50.78	2.02	2.21	44.93
5	0.16	0.95	3.26	5.00	90.63
6	0.17	9.51	4.34	5.11	80.87
7	0.00	45.12	1.63	3.35	49.91

c)

Mass percent (%)

Spectrum	Al	Cu	Ag	In	Sn
1	0.15	99.59	0.00	0.04	0.22
2	0.02	59.15	1.28	2.51	37.05
3	0.00	42.19	6.76	3.56	47.48
4	0.18	60.15	0.21	2.65	36.80
5	0.00	4.32	11.74	5.53	78.41
6	0.00	7.99	4.95	5.29	81.77
7	0.11	51.57	1.79	2.79	43.74
8	0.06	55.60	1.36	2.43	40.56

Figure 5.16. SEM-EDX results of the SAC205-1In-0.5Al solder/Cu interface at predetermined temperatures: a) 275^0C, b) 300^0C, and c) 325^0C.

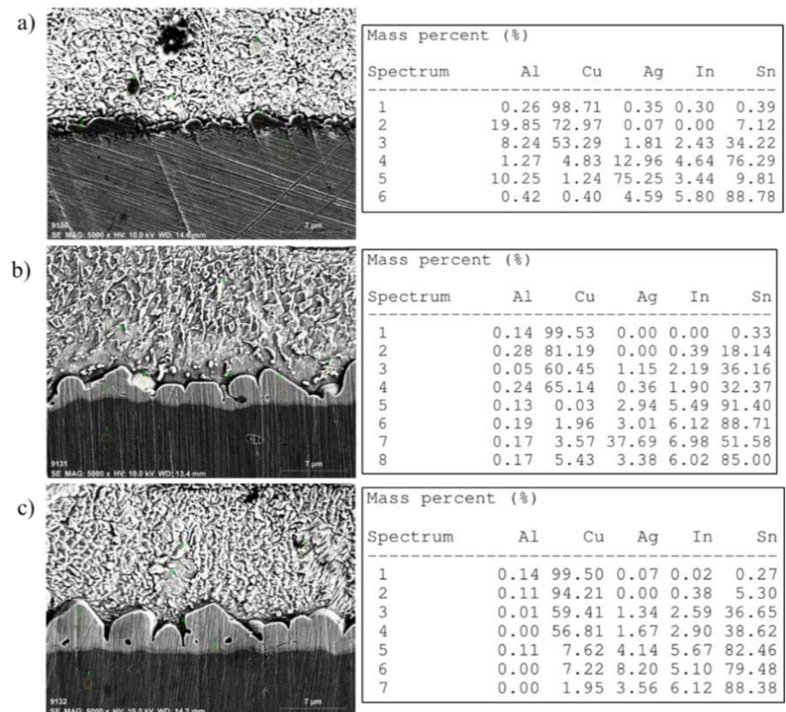

a)

Mass percent (%)

Spectrum	Al	Cu	Ag	In	Sn
1	0.26	98.71	0.35	0.30	0.39
2	19.85	72.97	0.07	0.00	7.12
3	8.24	53.29	1.81	2.43	34.22
4	1.27	4.83	12.96	4.64	76.29
5	10.25	1.24	75.25	3.44	9.81
6	0.42	0.40	4.59	5.80	88.78

b)

Mass percent (%)

Spectrum	Al	Cu	Ag	In	Sn
1	0.14	99.53	0.00	0.00	0.33
2	0.28	81.19	0.00	0.39	18.14
3	0.05	60.45	1.15	2.19	36.16
4	0.24	65.14	0.36	1.90	32.37
5	0.13	0.03	2.94	5.49	91.40
6	0.19	1.96	3.01	6.12	88.71
7	0.17	3.57	37.69	6.98	51.58
8	0.17	5.43	3.38	6.02	85.00

c)

Mass percent (%)

Spectrum	Al	Cu	Ag	In	Sn
1	0.14	99.50	0.07	0.02	0.27
2	0.11	94.21	0.00	0.38	5.30
3	0.01	59.41	1.34	2.59	36.65
4	0.00	56.81	1.67	2.90	38.62
5	0.11	7.62	4.14	5.67	82.46
6	0.00	7.22	8.20	5.10	79.48
7	0.00	1.95	3.56	6.12	88.38

Figure 5.17. SEM-EDX results of the SAC205-1In-0.7Al solder/Cu interface at predetermined temperatures: a) 275^0C, b) 300^0C, and c) 325^0C.

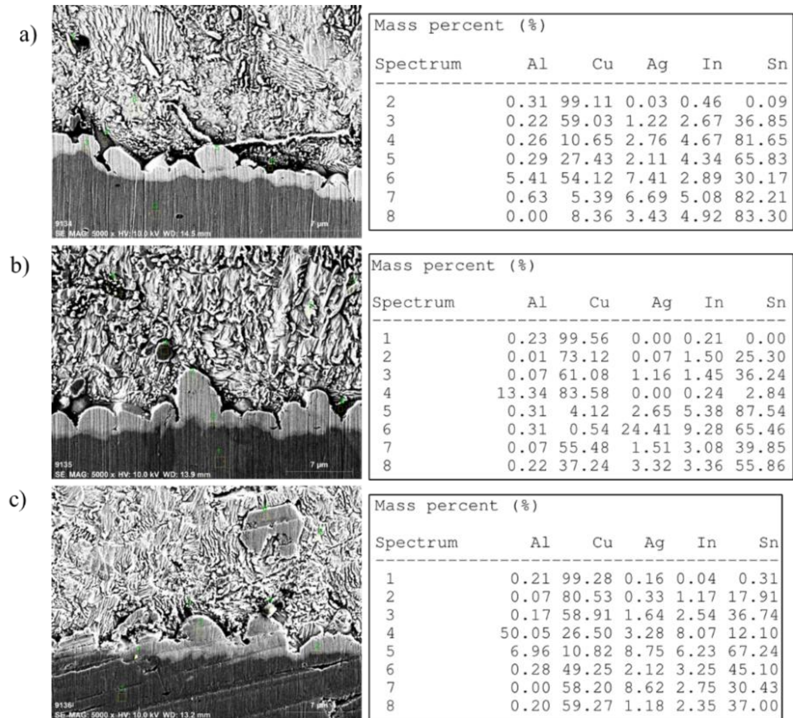

a)

Mass percent (%)

Spectrum	Al	Cu	Ag	In	Sn
2	0.31	99.11	0.03	0.46	0.09
3	0.22	59.03	1.22	2.67	36.85
4	0.26	10.65	2.76	4.67	81.65
5	0.29	27.43	2.11	4.34	65.83
6	5.41	54.12	7.41	2.89	30.17
7	0.63	5.39	6.69	5.08	82.21
8	0.00	8.36	3.43	4.92	83.30

b)

Mass percent (%)

Spectrum	Al	Cu	Ag	In	Sn
1	0.23	99.56	0.00	0.21	0.00
2	0.01	73.12	0.07	1.50	25.30
3	0.07	61.08	1.16	1.45	36.24
4	13.34	83.58	0.00	0.24	2.84
5	0.31	4.12	2.65	5.38	87.54
6	0.31	0.54	24.41	9.28	65.46
7	0.07	55.48	1.51	3.08	39.85
8	0.22	37.24	3.32	3.36	55.86

c)

Mass percent (%)

Spectrum	Al	Cu	Ag	In	Sn
1	0.21	99.28	0.16	0.04	0.31
2	0.07	80.53	0.33	1.17	17.91
3	0.17	58.91	1.64	2.54	36.74
4	50.05	26.50	3.28	8.07	12.10
5	6.96	10.82	8.75	6.23	67.24
6	0.28	49.25	2.12	3.25	45.10
7	0.00	58.20	8.62	2.75	30.43
8	0.20	59.27	1.18	2.35	37.00

Figure 5.18. SEM-EDX results of the SAC205-1In-0.8Al solder/Cu interface at predetermined temperatures: a) 275^0C, b) 300^0C, and c) 325^0C.

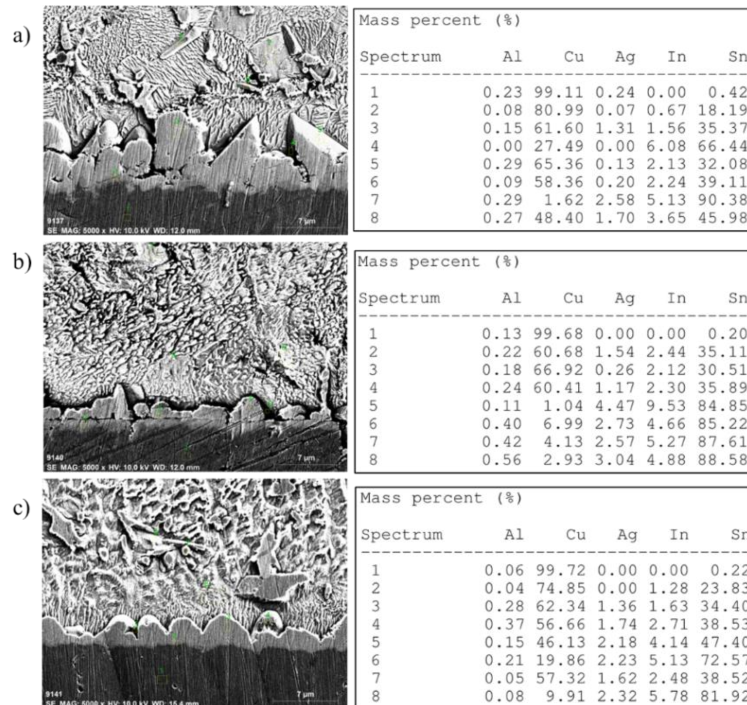

a)

Mass percent (%)

Spectrum	Al	Cu	Ag	In	Sn
1	0.23	99.11	0.24	0.00	0.42
2	0.08	80.99	0.07	0.67	18.19
3	0.15	61.60	1.31	1.56	35.37
4	0.00	27.49	0.00	6.08	66.44
5	0.29	65.36	0.13	2.13	32.08
6	0.09	58.36	0.20	2.24	39.11
7	0.29	1.62	2.58	5.13	90.38
8	0.27	48.40	1.70	3.65	45.98

b)

Mass percent (%)

Spectrum	Al	Cu	Ag	In	Sn
1	0.13	99.68	0.00	0.00	0.20
2	0.22	60.68	1.54	2.44	35.11
3	0.18	66.92	0.26	2.12	30.51
4	0.24	60.41	1.17	2.30	35.89
5	0.11	1.04	4.47	9.53	84.85
6	0.40	6.99	2.73	4.66	85.22
7	0.42	4.13	2.57	5.27	87.61
8	0.56	2.93	3.04	4.88	88.58

c)

Mass percent (%)

Spectrum	Al	Cu	Ag	In	Sn
1	0.06	99.72	0.00	0.00	0.22
2	0.04	74.85	0.00	1.28	23.83
3	0.28	62.34	1.36	1.63	34.40
4	0.37	56.66	1.74	2.71	38.53
5	0.15	46.13	2.18	4.14	47.40
6	0.21	19.86	2.23	5.13	72.57
7	0.05	57.32	1.62	2.48	38.52
8	0.08	9.91	2.32	5.78	81.92

Figure 5.19. SEM-EDX results of the SAC205-1In-0.9Al solder/Cu interface at predetermined temperatures: a) 275^0C, b) 300^0C, and c) 325^0C.

5.6 CORROSION ANALYSIS

The corrosion behavior of new quinary lead-free solder alloys SAC205-1In-xAl was examined under specific and controlled conditions in a 1M hydrochloric acid (HCl) solution, ensuring the reliability of the findings. Hydrochloric acid has a faster corrosion rate than other electrolytes due to chlorine (Cl-) and hydrogen (H+) ions that contrast with other electrolytes like salt and alkaline solutions, which contain only one type of ion that can cause corrosion. The microstructure analyses of the lead-free solder alloy SAC-1In-xAl were measured independently before and after corrosion. The study compared the corrosion rates of different solder alloys and determined the corrosion properties of newly developed solder alloys.

5.6.1 Characteristics Of New Solder Alloys

The images of SEM for the lead-free solder alloys SAC-2051In-xAl (x = 0.3, 0.5, 0.7, 0.8, and 0.9 wt%) show the alloy's microstructures that exhibit the formation of certain phases of IMCs such as Ag3Sn, Ag-Al phase IMC's that identified by Ag2Al and Ag3Al, the phase of Al-Cu IMC's that identified by Al2Cu and ALCu, and finally the phase of Cu-Sn IMC's which identified by Cu3Sn and Cu6Sn5 onto the solder surface, as seen in Figure 5.20 and Figure 5.28. The SEM analysis of the absorbent structures unveiled a β-Sn matrix with a Sn-rich region, along with the presence of large particles of the Sn-Cu intermetallic phase (Cu6Sn5) and smaller particles of the Ag3Sn intermetallic phase. Importantly, the observation revealed a complete eutectic structure with the Ag3Sn and Cu6Sn5 phases uniformly distributed within the β-Sn matrix. These findings are in agreement with reference [128, 129]. Al reduced the growth of Ag3Sn and Cu6Sn5 IMCs and supported the formation of Ag-Al and Cu-Al IMC because fewer Ag and Cu content would be able to form IMCs with the Sn when Al was added to SAC205-1In. The solder alloys containing Al displayed passivation behavior, as depicted in Figure 5.28. SEM and EDX analysis revealed the creation of dense passive layers on the Al-containing solder. These passivation films consisted of intermetallic compounds, including SnO, SnO2, Al2O3, and AlCuO4, effectively inhibiting reactions on the solder surface [60].

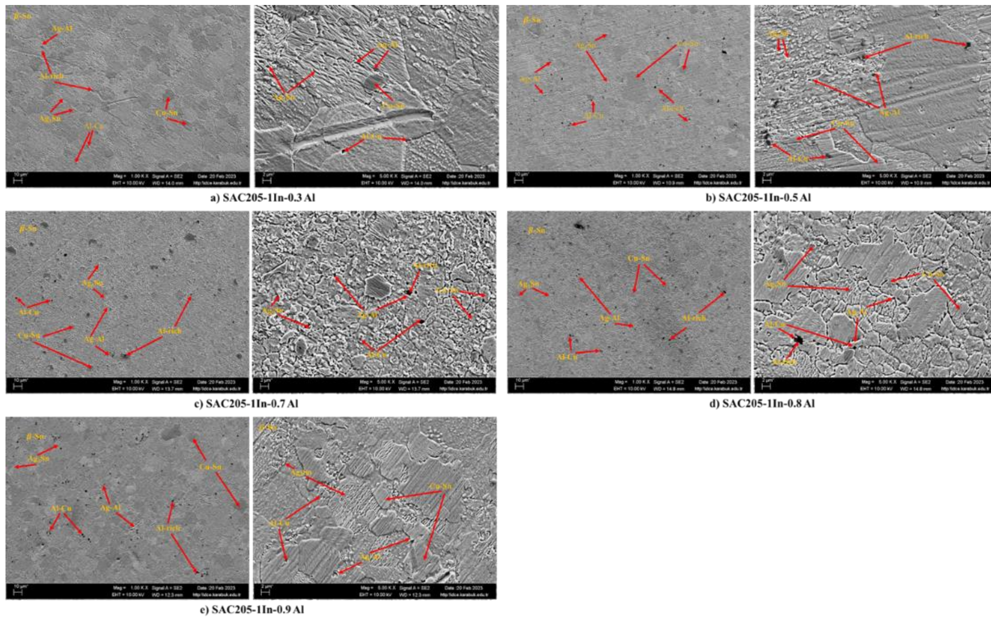

Figure 5.20. SEM images of SAC-1In-xAl solder alloys before the electrochemical measurements in 1M HCL solution (a) SAC205-1In-0.3Al, (b) SAC205-1In-0.5Al, (c) SAC205-1In-0.7Al, (d) SAC205-1In-0.8Al, and (e) SAC205-1In-0.9Al.

The EDX images in Figure 5.21, 5.22, 5.23, 5.24, and 5.25 show the mass percentage % of the elements in the new quinary lead-free solder alloys before immersion in a 1M HCL hydrochloride solution.

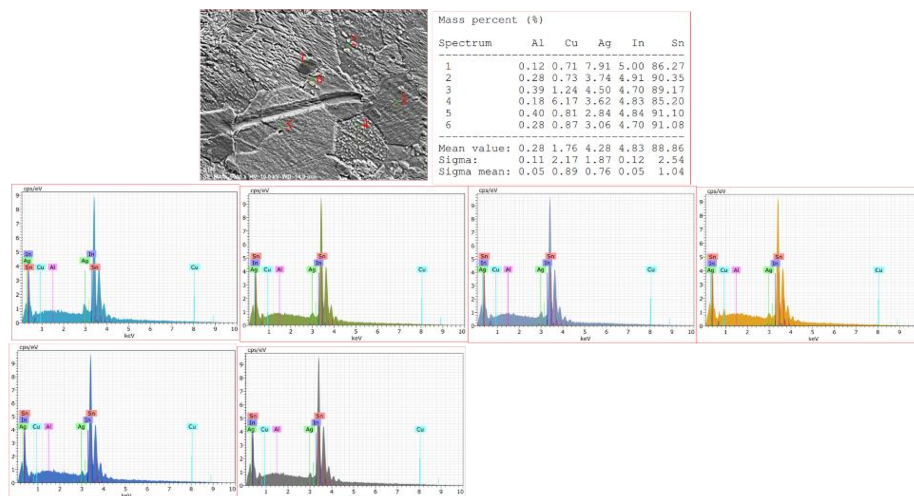

Mass percent (%)

Spectrum	Al	Cu	Ag	In	Sn
1	0.12	0.71	7.91	5.00	86.27
2	0.28	0.73	3.74	4.91	90.35
3	0.39	1.24	4.50	4.70	89.17
4	0.18	6.17	3.62	4.83	85.20
5	0.40	0.81	2.84	4.84	91.10
6	0.28	0.87	3.06	4.70	91.08
Mean value:	0.28	1.76	4.28	4.83	88.86
Sigma:	0.11	2.17	1.87	0.12	2.54
Sigma mean:	0.05	0.89	0.76	0.05	1.04

Figure 5.21. EDX analysis of SAC205-1In-0.3Al alloy before immersion in 1M HCL

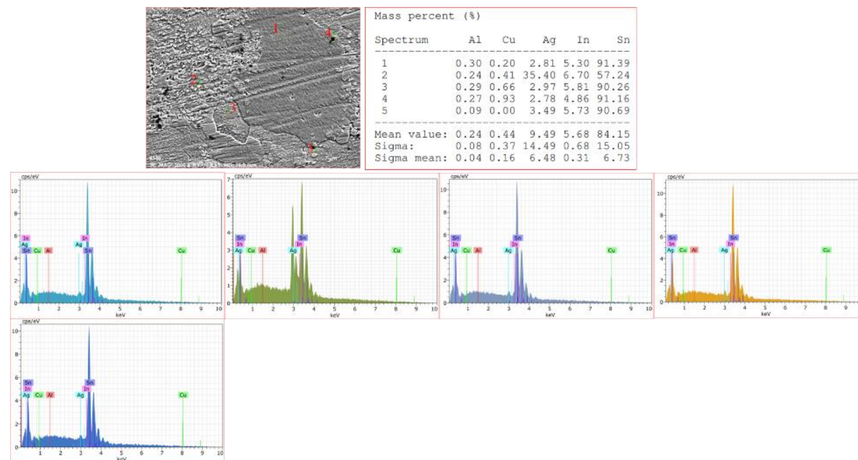

Mass percent (%)

Spectrum	Al	Cu	Ag	In	Sn
1	0.30	0.20	2.81	5.30	91.39
2	0.24	0.41	35.40	6.70	57.24
3	0.29	0.66	2.97	5.81	90.26
4	0.27	0.93	2.78	4.86	91.16
5	0.09	0.00	3.49	5.73	90.69
Mean value:	0.24	0.44	9.49	5.68	84.15
Sigma:	0.08	0.37	14.49	0.68	15.05
Sigma mean:	0.04	0.16	6.48	0.31	6.73

Figure 5.22. EDX analysis of SAC205-1In-0.5Al alloy before immersion in 1M HCL

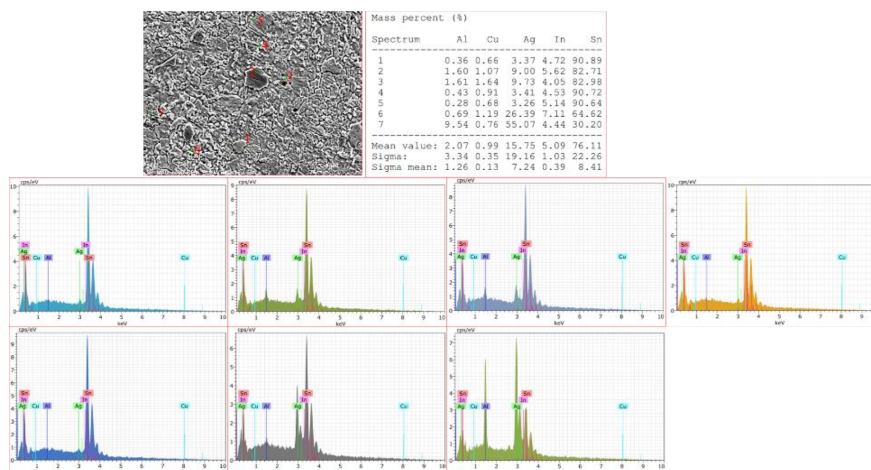

Mass percent (%)

Spectrum	Al	Cu	Ag	In	Sn
1	0.36	0.66	3.37	4.72	90.89
2	1.60	1.07	9.00	5.62	82.71
3	1.61	1.64	9.73	4.05	82.98
4	0.43	0.91	3.41	4.53	90.72
5	0.28	0.68	3.26	5.14	90.64
6	0.69	1.19	26.39	7.11	64.62
7	9.54	0.76	55.07	4.44	30.20
Mean value:	2.07	0.99	15.75	5.09	76.11
Sigma:	3.34	0.35	19.16	1.03	22.26
Sigma mean:	1.26	0.13	7.24	0.39	8.41

Figure 5.23. EDX analysis of SAC205-1In-0.7Al alloy before immersion in 1M HCL

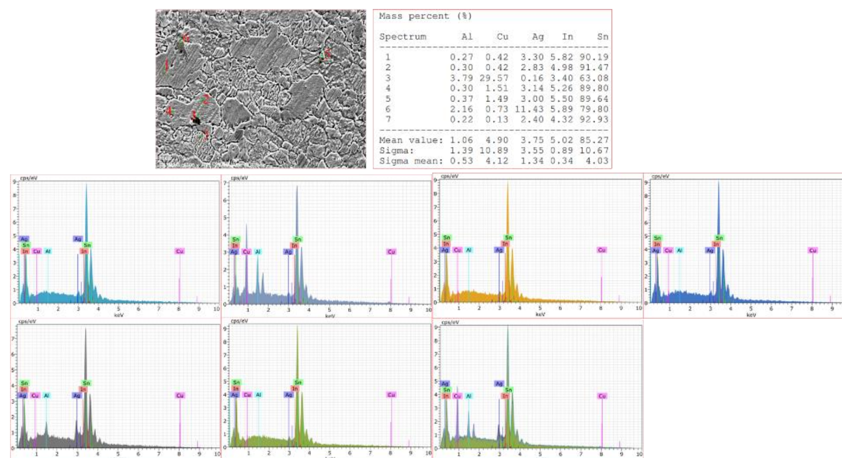

Mass percent (%)

Spectrum	Al	Cu	Ag	In	Sn
1	0.27	0.42	3.30	5.82	90.19
2	0.30	0.42	2.83	4.98	91.47
3	3.79	29.57	0.16	3.40	63.08
4	0.30	1.51	3.14	5.26	89.80
5	0.37	1.49	3.00	5.50	89.64
6	2.16	0.73	11.43	5.89	79.80
7	0.22	0.13	2.40	4.32	92.93
Mean value:	1.06	4.90	3.75	5.02	85.27
Sigma:	1.39	10.89	3.55	0.89	10.67
Sigma mean:	0.53	4.12	1.34	0.34	4.03

Figure 5.24. EDX analysis of SAC205-1In-0.8Al alloy before immersion in 1M HCL

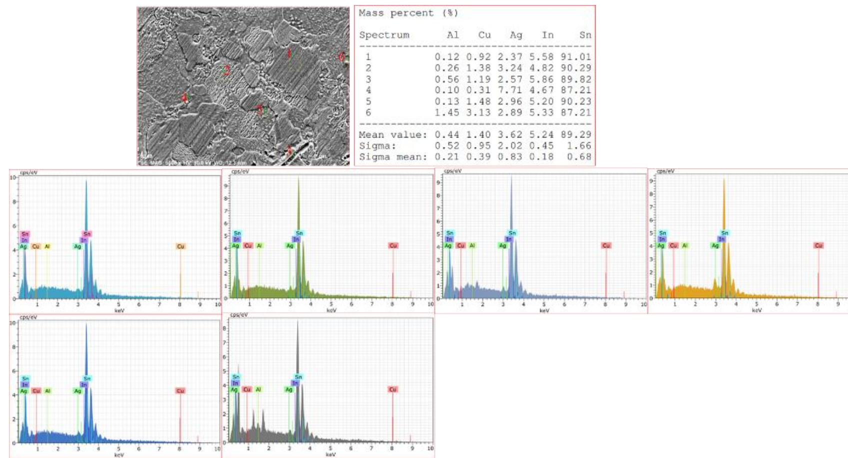

Mass percent (%)

Spectrum	Al	Cu	Ag	In	Sn
1	0.12	0.92	2.37	5.58	91.01
2	0.26	1.38	3.24	4.82	90.29
3	0.56	1.19	2.57	5.86	89.82
4	0.10	0.31	7.71	4.67	87.21
5	0.13	1.48	2.96	5.20	90.23
6	1.45	3.13	2.89	5.33	87.21
Mean value:	0.44	1.40	3.62	5.24	89.29
Sigma:	0.52	0.95	2.02	0.45	1.66
Sigma mean:	0.21	0.39	0.83	0.18	0.68

Figure 5.25. EDX analysis of SAC205-1In-0.9Al alloy before immersion in 1M HCL

5.6.2 Potentiodynamic Polarization Analysis

The potentiodynamic polarization curves of all evolved quinary lead-free solder alloys in a 1M HCL solution are presented in Figure 5.26. These curves show that none of the alloys exhibit any passivation zones. In a passivation zone, the current density must change its direction at a particular potential of anodic polarization and become lower compared to the density immediately before going into the zone. On the other hand, all produced SAC205-1In-xAl alloys only exhibit a pseudo-passivation zone where the current densities stay steady and do not react to fluctuations in scanning potentials, which range nearly from (-0.1) V to the end of the scanning region (+1.0 V). Interestingly, Relative to the NaCl solution, the current density in pseudo-passivation zones is noticeably higher [130]. The observed behavior is due to the highly acidic 1M HCl environment. It is intriguing that the pseudo-passivation region does not terminate at a reactivation point. Figure 5.21 provides clear evidence that the purported passivation zone persists until the end of the scanning zone (+1 V), showcasing a deviation from findings in studies primarily employing NaCl-based solutions [131].

The potentiodynamic polarization measurements yielded quantitative findings detailed in Table 5.14. The corrosion potentials of all the alloys produced in this study were almost equivalent. The corrosion potentials of the newly developed solder alloys exceed those of SAC305 and SAC205-1In due to the higher corrosion current

densities exhibited by the new alloys compared to their predecessors. This increased corrosion current density has led to a higher potential corrosion of the new solder alloys. The newly formulated solder alloys' corrosion potentials can be attributed to the incorporation of aluminum at specific ratios.

By employing Tafel extrapolations, we derived the corrosion current densities and corrosion rate values for each evolved solder alloy. Our observations indicate a consistent trend wherein the corrosion rates decrease with the substitution of tin (Sn) with varying percentages of aluminum (Al) (i.e., 0.3, 0.5, 0.7, and 0.8 wt.%). The corrosion rate of SAC205-1In-0.8Al is the lowest among all produced solder alloys in this study, standing in stark contrast to the 0.9Al% variant. The addition of 0.8 wt.% Al alloy has decreased the corrosion rate compared to SAC305 that was previously made [58], as indicated in Table 5.14. In contrast, the corrosion rate is highest for the 0.9Al% variant due to the high icorr of SAC205-1In-0.9Al; these results highlight the impact of different weight percentages of aluminum on corrosion rates.

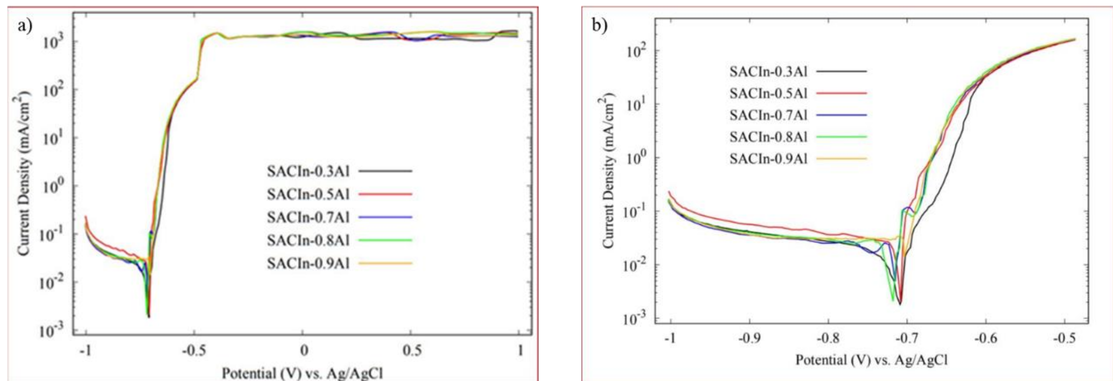

Figure 5.26. Potentiaodynamic polarization curves, a) Potentiodynamic polarization curves of SAC205-1In-xAl (x = 0.3, 0.5, 0.7, 0.8, and 0.9 wt%), b) potentiodynamic polarization curves magnified image.

The corrosion current density (icorr) decreases with increasing Al content in the alloy. Specifically, the icorr values are as follows: 20.8 μA/cm^2 for 0.3 wt% Al, 16.8 μA/cm^2 for 0.8 wt% Al, 18.83 μA/cm^2 for 0.5 wt% Al, 18.5 μA/cm^2 for 0.7 wt% Al, and 30.42 μA/cm^2 for 0.9 wt% Al (as shown in Table 2). Notably, the alloy with 0.8 wt% Al exhibits the smallest corrosion current density. It's worth noting that a low

icorr value signifies a lower corrosion rate, while a higher icorr value indicates a higher corrosion rate [58]. When comparing the corrosion rates, the SAC205-1In-0.8Al alloy demonstrates the lowest corrosion rate among all produced alloys, even less than the corrosion rate of the SAC305 made by previous studies. Therefore, the SAC205-1In-0.8Al is more resistant to the corrosion.

Table 5.14. The corrosion parameters of the produced solder alloy SAC205-1In-xAl

Solder alloys	i_{corr} (μA / cm^2)	CR (mm / year)	E_{corr} (V)
SAC205-1In-0.3Al	20.8	0.5767	-0.71
SAC205-1In-0.5Al	18.83	0.5221	-0.71
SAC205-1In-0.7Al	18.5	0.5129	-0.72
SAC205-1In-0.8Al	16.8	0.4658	-0.72
SAC205-1In-0.9Al	30.42	0.8435	- 0.70
SAC-1In [58]	10.571	0.285	- 0.528
SAC305,[58]	18.095	0.488	-0.525

CCD : Corrosion Current Density ($\mathbf{i_{corr}}$) , CR : Corrosion Rate, E_{corr} : Corrosion Potential

5.6.3 Post-Corrosion Descriptions

The polarization curves indicated that the corrosion characteristics of all solder alloys were nearly identical, as depicted in Figure 5.26. The SEM images of the solder alloys are displayed in Figure 5.27, along with the observed views of the examined lead-free solder alloys following the potentiodynamic tests. When less "Al" is added to the SAC205-1In solder alloy, it results in the formation of an oxide film with a coarse and spherical structure. Specifically, adding 0.3% Al leads to developing an oxide film with these characteristics. This introduction of aluminum to the SAC-In lead-free solder alloy has a notable impact on the surface corrosion product, effectively enhancing passivation capabilities. The resulting development of Al2CuO4 on the surface serves to reduce the solder's overall corrosion sensitivity

[13]. The corrosion resistance and icorr values of SAC205-1In-xAl alloys are affected by the presence of surface phases or oxidations. Upon examining the SEM images in Figure 5.27, an oxide coating begins to develop on the surface as the icorr value decreases after corrosion. The snowy formations observed in SEM examinations correspond to the formation of the oxide film layer [58)]. The SAC205-1In-0.8Al alloy exhibits the best corrosion resistance among all the alloys containing Al. This conclusion is based on the results obtained from all the alloys tested. The introduction of aluminum (Al) into the SAC-1In quaternary lead-free solder alloy leads to the creation of Ag-Al IMCs, specifically Ag2Al and Ag3Al IMCs, as well as Al-Cu IMC phase, identified by Al2Cu and AlCu IMCs. This results in reduced availability of Ag and Cu for the formation of intermetallic compounds with Sn, leading to decreased concentration of Ag3Sn, Cu3Sn, and Cu6Sn5 IMCs.

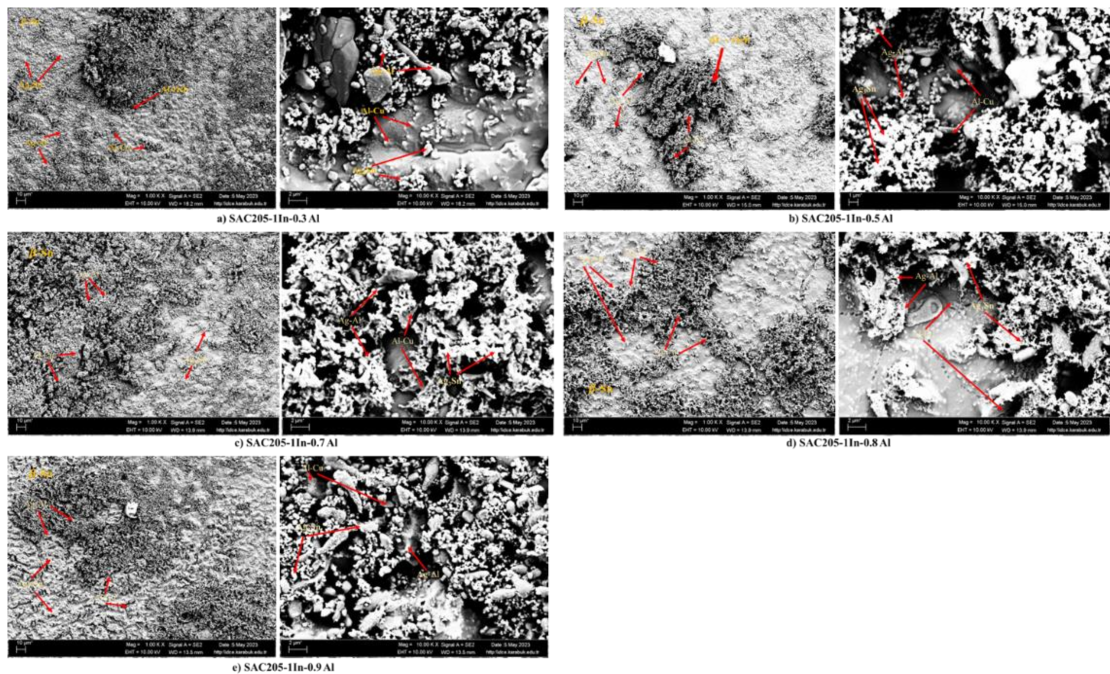

Figure 5.27. SEM images of SACIn-xAl solder alloys after immersion in 1M HCL solution: (a) SAC205-1In-0.3Al, (b) SAC205-1In-0.5Al, (c) SAC205-1In-0.7Al, (d) SAC205-1In-0.8Al, and (e) SAC205-1In-0.9Al.

The images obtained from EDX and depicted in Figures 5.28 through 5.32 provide a visual representation of the mass percentage of elements present in the alloy after immersion in a 1M HCl solution. The observed variations in mass percentage result

from corrosion-induced degradation caused by electrochemical reactions. Furthermore, upon conducting SEM examinations, the formations resembling snow that were observed correspond to the presence of the oxide film layer [58].

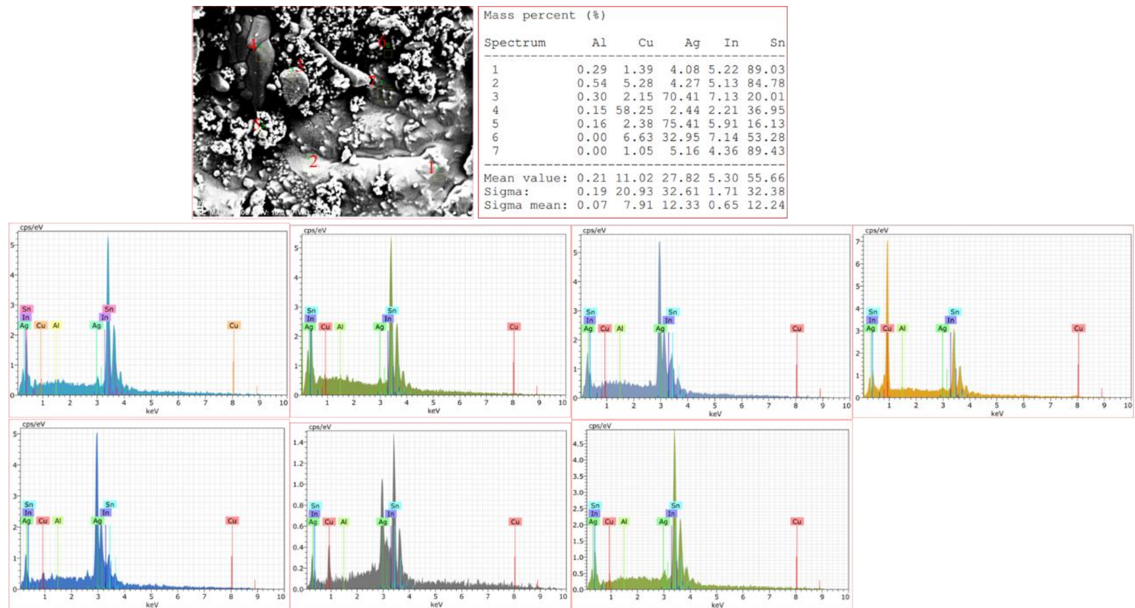

Mass percent (%)

Spectrum	Al	Cu	Ag	In	Sn
1	0.29	1.39	4.08	5.22	89.03
2	0.54	5.28	4.27	5.13	84.78
3	0.30	2.15	70.41	7.13	20.01
4	0.15	58.25	2.44	2.21	36.95
5	0.16	2.38	75.41	5.91	16.13
6	0.00	6.63	32.95	7.14	53.28
7	0.00	1.05	5.16	4.36	89.43
Mean value:	0.21	11.02	27.82	5.30	55.66
Sigma:	0.19	20.93	32.61	1.71	32.38
Sigma mean:	0.07	7.91	12.33	0.65	12.24

Figure 5.28. EDX analysis of the SAC205-1In-0.3Al solder alloy after immersion in a 1M HCL solution.

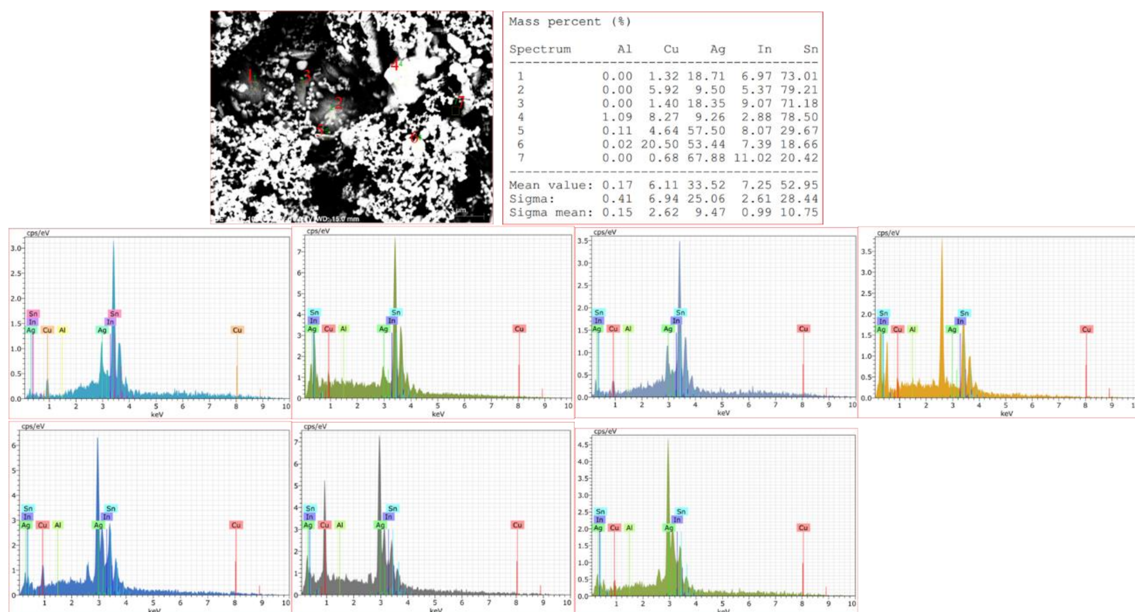

Mass percent (%)

Spectrum	Al	Cu	Ag	In	Sn
1	0.00	1.32	18.71	6.97	73.01
2	0.00	5.92	9.50	5.37	79.21
3	0.00	1.40	18.35	9.07	71.18
4	1.09	8.27	9.26	2.88	78.50
5	0.11	4.64	57.50	8.07	29.67
6	0.02	20.50	53.44	7.39	18.66
7	0.00	0.68	67.88	11.02	20.42
Mean value:	0.17	6.11	33.52	7.25	52.95
Sigma:	0.41	6.94	25.06	2.61	28.44
Sigma mean:	0.15	2.62	9.47	0.99	10.75

Figure 5.29. EDX results of the SAC205-1In-0.5Al solder alloy after immersion in a 1M HCL solution.

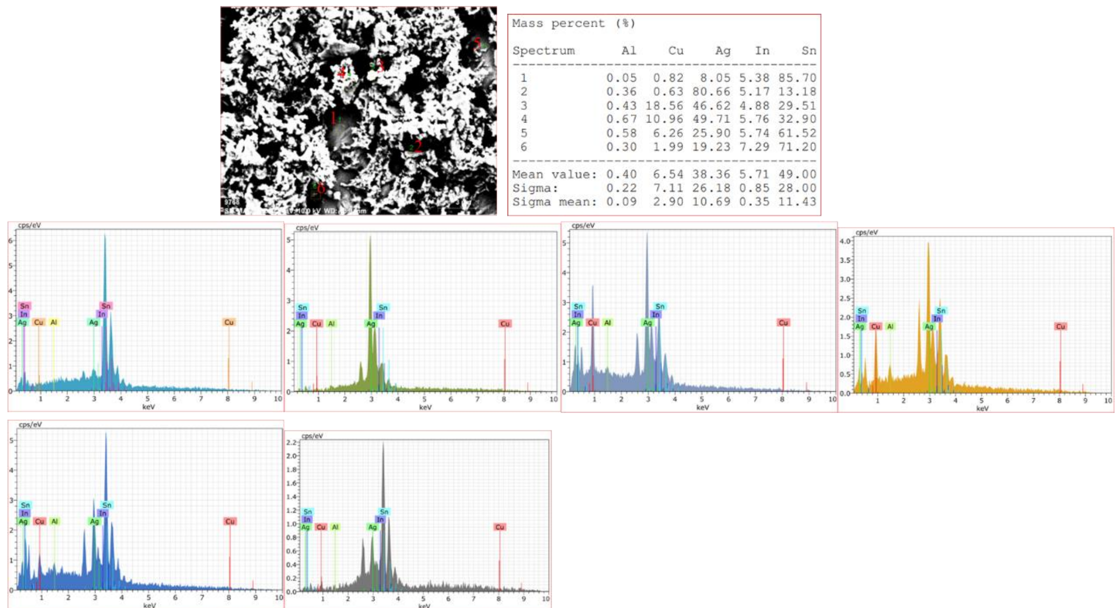

Mass percent (%)

Spectrum	Al	Cu	Ag	In	Sn
1	0.05	0.82	8.05	5.38	85.70
2	0.36	0.63	80.66	5.17	13.18
3	0.43	18.56	46.62	4.88	29.51
4	0.67	10.96	49.71	5.76	32.90
5	0.58	6.26	25.90	5.74	61.52
6	0.30	1.99	19.23	7.29	71.20
Mean value:	0.40	6.54	38.36	5.71	49.00
Sigma:	0.22	7.11	26.18	0.85	28.00
Sigma mean:	0.09	2.90	10.69	0.35	11.43

Figure 5.30. EDX results of the SAC205-1In-0.7Al solder alloy after immersion in a 1M HCL solution.

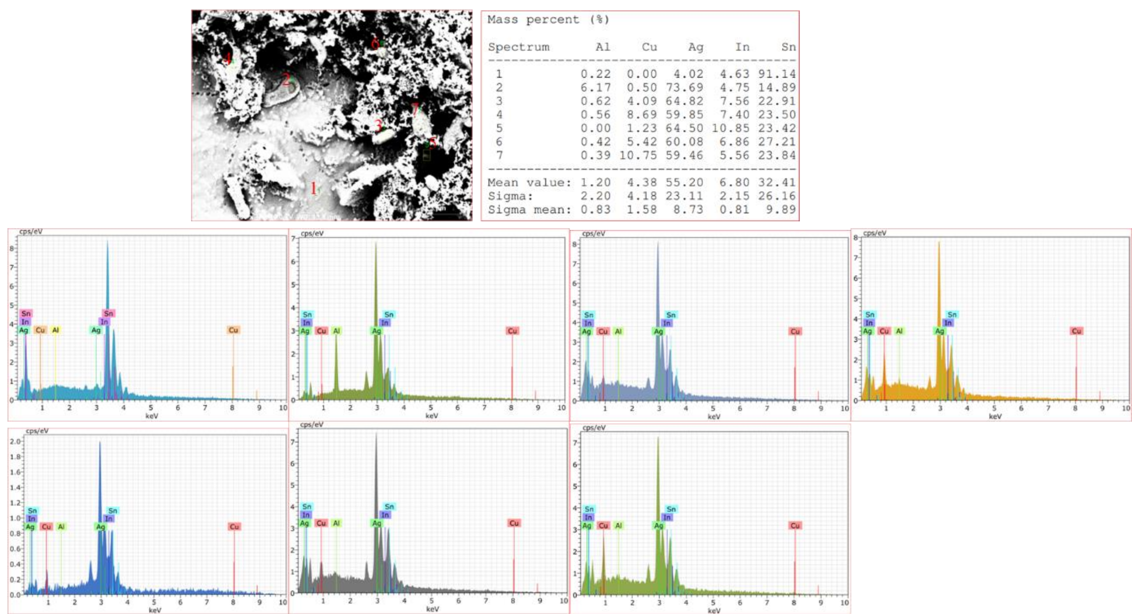

Mass percent (%)

Spectrum	Al	Cu	Ag	In	Sn
1	0.22	0.00	4.02	4.63	91.14
2	6.17	0.50	73.69	4.75	14.89
3	0.62	4.09	64.82	7.56	22.91
4	0.56	8.69	59.85	7.40	23.50
5	0.00	1.23	64.50	10.85	23.42
6	0.42	5.42	60.08	6.86	27.21
7	0.39	10.75	59.46	5.56	23.84
Mean value:	1.20	4.38	55.20	6.80	32.41
Sigma:	2.20	4.18	23.11	2.15	26.16
Sigma mean:	0.83	1.58	8.73	0.81	9.89

Figure 5.31. EDX results of the SAC205-1In-0.8Al solder alloy after immersion in a 1M HCL solution.

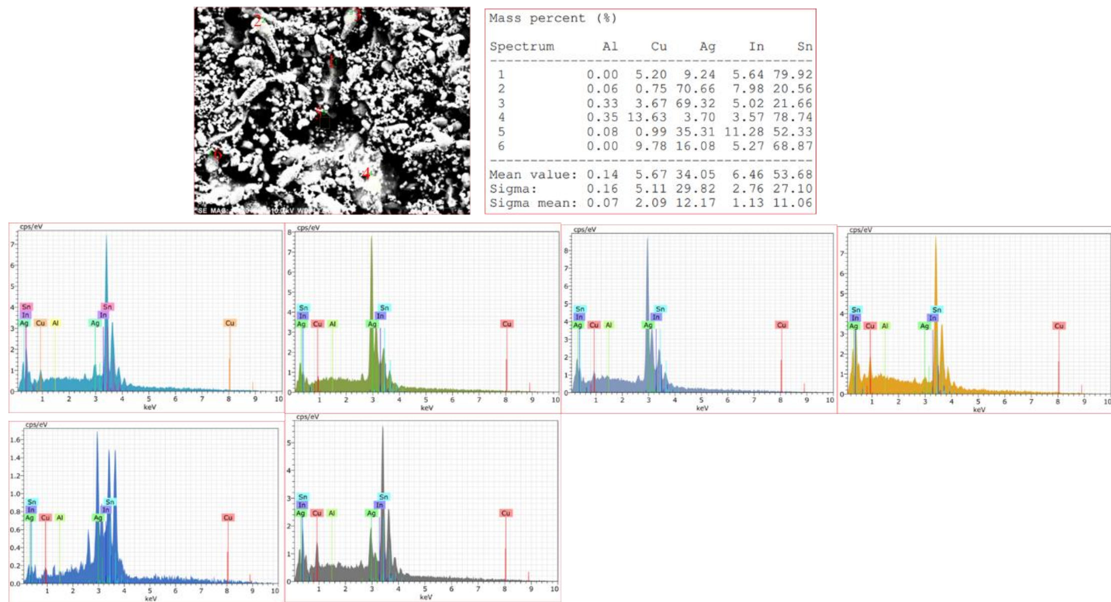

Mass percent (%)

Spectrum	Al	Cu	Ag	In	Sn
1	0.00	5.20	9.24	5.64	79.92
2	0.06	0.75	70.66	7.98	20.56
3	0.33	3.67	69.32	5.02	21.66
4	0.35	13.63	3.70	3.57	78.74
5	0.08	0.99	35.31	11.28	52.33
6	0.00	9.78	16.08	5.27	68.87
Mean value:	0.14	5.67	34.05	6.46	53.68
Sigma:	0.16	5.11	29.82	2.76	27.10
Sigma mean:	0.07	2.09	12.17	1.13	11.06

Figure 5.32. EDX results of the SAC205-1In-0.9Al solder alloy after immersion in a 1M HCL solution.

5.7 ELECTRICAL RESISTIVITY ANALYSIS

The electrical resistivity of cross-sectioned samples of new quinary lead-free solder alloys was measured using a two-point probe technique using a Keith 2400 source meter. The electrical resistivity tests were accomplished at room temperature. The electrical resistivity measurements of produced solder alloys SAC205-1In-xAl where (x = 0.3 wt%, 0.5 wr%, 0.7 wt%, 0.8 wt%, and 0.9 wt%) and SAC205-1In are shown in Appendix B. Twenty measurements of electrical resistivity were taken. The maximum electrical resistivity of the new quinary lead-free solder alloys SAC205-1In-0.3Al, SAC205-1In-0.5Al, SAC205-1In-0.7Al, SAC205-1In-0.8Al, SAC205-1In-0.9Al, and SAC205-1In obtained experimentally are $1.07 \times 10^{-6}\ \Omega.m$, $1.12 \times 10^{-6}\ \Omega.m$, $1.15 \times 10^{-6}\ \Omega.m$, $1.18 \times 10^{-6}\ \Omega.m$, $1.21 \times 10^{-6}\ \Omega.m$, and $1.08 \times 10^{-6}\ \Omega.m$. respectively as shown in Table 5.15.

The addition of aluminum has a noticeable impact on the electrical resistivity of the SAC205-1In solder alloy. With an increase in aluminum, the electrical resistivity gradually increases, reaching its peak at 0.9 wt%, as depicted in Figure 5.33. Notably, the electrical resistivity of all new quinary lead-free solder alloys has

slightly increased compared to the previous SAC305 solder alloy, and the electrical resistivity of SAC205-1In without adding Al. The electrical resistivity of SAC305 was recorded at $1.04 \times 10^{-6}\ \Omega.m$ [57]. The electrical resistivity of composite solder alloys is determined by various factors, including the volume fraction, shape, size, and total electrical resistivity of the material, which is affected by the combined influences of impurity, thermal, and deformation components.

Table 5.15. The maximum electrical resistivity of the new quinary lead-free solder alloys SAC205-1In-xAl obtained experimentally and SAC305.

Solder alloys	SAC305	SACIn-0.0Al	SACIn-0.3Al	SACIn-0.5Al	SACIn-0.7Al	SACIn-0.8Al	SACIn-0.9Al
Resistivity (Ω.m)	1.04E-06 [57]	1.08E-06	1.07E-06	1.12E-06	1.15E-06	1.18E-06	1.21E-06

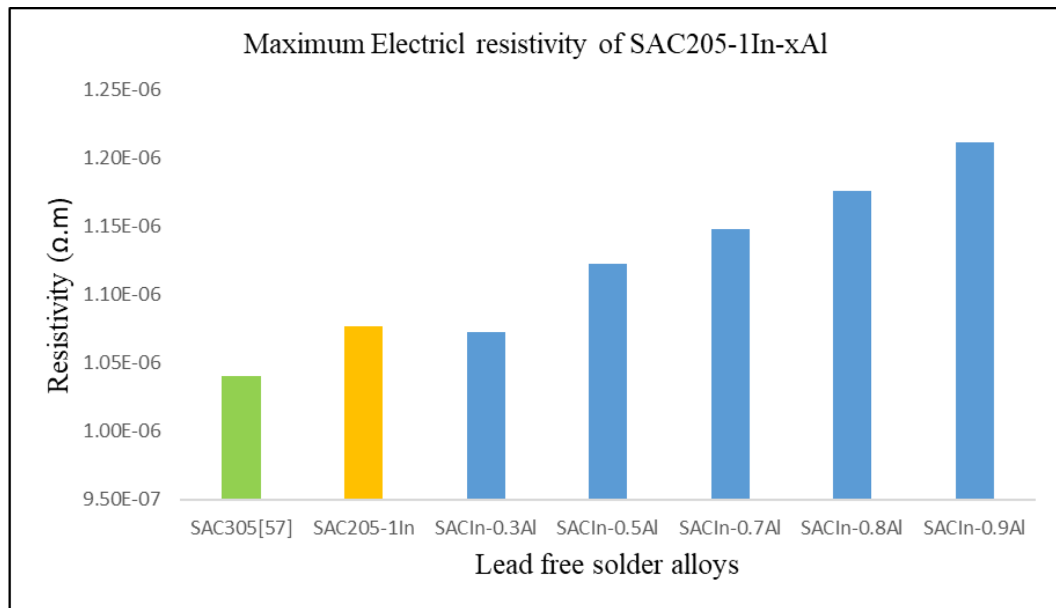

Figure 5.33. Maximum electrical resistivity of new quinary lead-free solder alloys SAC205-1In-xAl (x=0.3, 0.5, 0.7, 0.8 , and 0.9 wt%) and SAC305.

It has been observed that the average resistivity values of 19 readings for five new quinary lead-free solder alloys (SAC205-1In-0.3Al, SAC205-1In-0.5Al, SAC205-1In-0.7Al, SAC205-1In-0.8Al, SAC205-1In-0.9Al, and SAC205-1In) were calculated in Table 5.16. The values were found to be 5.05 x 10^{-07} Ω.m, 5.19 x 10^{-07}

Ω.m, 5.37 x 10^{-07} Ω.m, 5.45 x 10^{-07} Ω.m, 5.66 x 10^{-07} Ω.m, and 5.22 x 10^{-07} Ω.m respectively. It is important to note that resistivity value and conductivity are inversely proportional. Therefore, the solder alloy with 0.3Al added is the best conductor for the current, as it has the lowest resistivity value. (See Table 5.15, Table 5.16, Figure 5.33, and Figure 5.34).

Table 5.16. The average electrical resistivity of SACIn-xAl (x=0.3 wt%, 0.5 wt%, 0.7 wt%, 0.8 wt%, 0.9 wt%).

avg. resistivity of new quinary lead-free solder alloys SAC205-1In-xAl					
0.0 Al	0.3Al	0.5Al	0.7Al	0.8Al	0.9Al
5.22E-07	5.05E-07	5.19E-07	5.37E-07	5.45E-07	5.66E-07

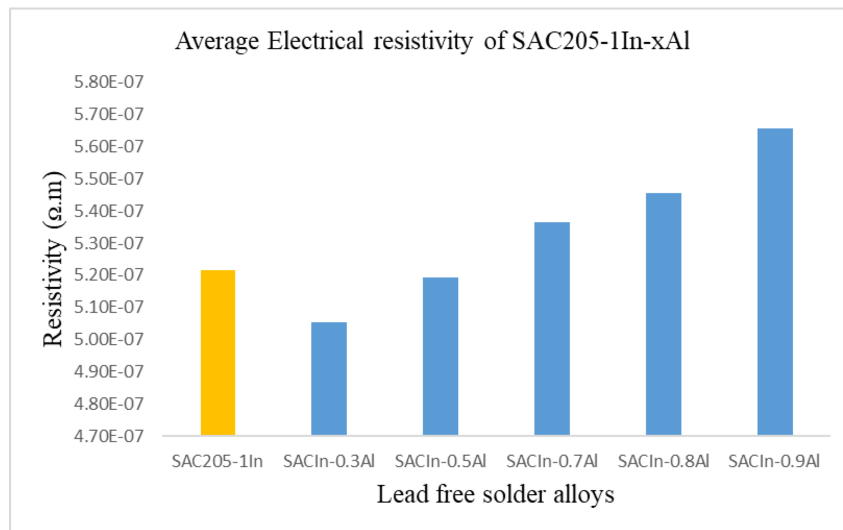

Figure 5.34. Average Electrical resistivity of SAC205-1In-xAl (x=0.3 wt%, 0.5 wt%, 0.7 wt%, 0.8 wt%, 0.9 wt%.

The electrical resistivity increases with decreasing the Ag content from 3.0 wt.% to 1.0 wt.%. This is because the number of low-resistivity Ag3Sn IMCs increases with an increase in the Ag content [63].

The addition of Al to SAC205-1In leads to the creating of CuAl IMC and suppresses the formation of the Ag3Sn and CuSn IMCs phases, and forms Al-Ag and Al-Cu IMCs, the addition of 0.9Al to SAC205-1In reduces the concentration of Ag3Sn and Cu6Sn5 and Cu3Sn more than all produced solder alloys. Therefore, SAC205-1In-

0.9Al has the highest resistivity $1.21 \times 10^{-6}\ \Omega.\mathrm{m}$ than other produced solder alloys SAC205-1In-0.8Al, SAC205-1In-0.7Al, SA205-1CIn-0.5Al, and SAC205-1In-0.3Al that has the lowest electrical resistivity $1.07 \times 10^{-6}\ \Omega.m$, according to the results, the value of electrical resistivity increased by increasing the ratio of Aluminum (Al) as displaced in Fig.5.34 and Table 5.16.
Adding Al suppresses the creating of Ag3Sn and CuSn IMCs phases, producing Al-Ag and Al-Cu, IMCs. The change in the concentration of Ag3Sn and Cu3Sn due to the addition of Al affected the electrical resistivity of the solder alloy [64]. The electrical resistivity of the SAC305 solder alloy was influenced by the volume of Al (wt%). The inclusion of aluminum (Al) did not adversely affect the electrical characteristics of the solder.

5.8 SHEAR STRENGTH RESULTS

Two lead-free solder alloys, SAC205-1In, and new quinary lead-free solder alloys, SAC205-1In-xAl (where x = 0.3 wt%, 0.5 wt%, 0.7 wt%, 0.8 wt%, and 0.9 wt%), were subjected to shear tests using a Zwick Roell device. Copper plates were connected to the jaws of a standard tensometer and pulled across the joint at a crosshead speed of 2.0 mm/min. The shear tests measured the Fmax, Fbreak, maximum elongation, and break elongation; the results are presented in Table 5.17.

The shear strength rises sharply for small elongations until the maximum stress is reached. The samples are not broken at that point; instead, there is a gradual voltage drop (F_{max} and F_{break}), which ends when the internal voltage resistance is zero (maximum shear stress). Due to the geometry of shear and the strong plasticity of Sn alloys, the stress-strain curve has this shape (see Figure 5.35). Similar curves were observed for every alloy composition examined, and its maximum shear was calculated.

The SAC-1In lead-free solder alloy showed a minimum shear strength value of 141.66 MPa without added Al. As for the new quinary solder alloys, the shear stress initially declines with increasing Al percentage at 0.3 wt% and 0.5 wt% Al content. However, a subsequent rise in shear stress occurs at 0.7 wt% Al content, reaching its

peak at 0.8 wt% Al content before declining again at 0.9 wt% Al content as depicted in Figure 5.35. The maximum shear strength was measured as 155.94 MPa for the SACIn-0.8Al solder alloy, as shown in Table 5.17. There was always a strong bond between the solder and the copper layer. Thus, it was clear from all the damaged samples that the failure happened there. The development of IMCs may be one of the factors contributing to the high strength of lead-free solder alloys. The production of Sn-based IMCs of the Cu6Sn5 or Cu3Sn IMC is typically linked to the solder's adhesion to the copper substrate. These lead-free solders have good bonding and wettability properties to Cu substrates because they are Sn-rich. As a result, the solder matrix's mechanical resistance ultimately determines the soldered junctions' mechanical integrity.

Table 5.17. Shear strength test results of produced solder alloys SACIn-xAl.

Solder alloys	Thickness (mm)	En (mm)	F_{max} (N/mm^2)	F_{break} (N/mm^2)	ε_{break} (%)	ε_{max} (%)
SAC-1In	1.5	15	141.66	119.12	0.61	0.60
SACIn-0.3Al	1.5	15	136.54	133.62	0.45	0.44
SACIn-0.5Al	1.5	15	132.97	131.72	0.48	0.48
SACIn-0.7Al	1.5	15	133.72	118.67	0.47	0.46
SACIn-0.8Al	1.5	15	155.94	152.93	0.60	0.59
SACIn-0.9Al	1.5	15	138.21	103.66	0.59	0.57

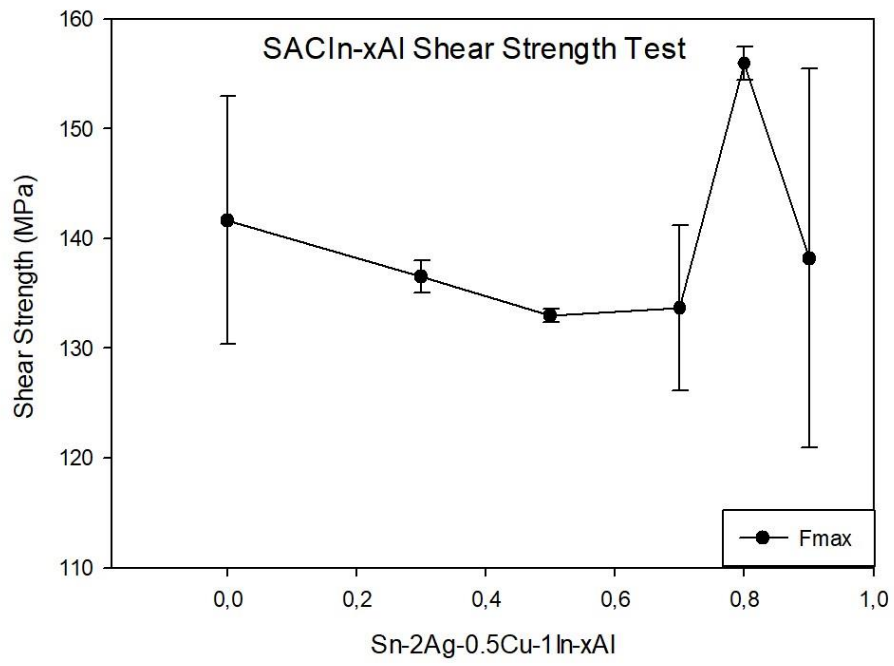

Figure 5.35. Shear strength values of produced solder alloys SAC205-1In-xAl

PART 6

CONCLUSION

Due to environmental concerns, hazardous materials like lead (Pb) in electronics and electrical equipment have been restricted. While lead-free solder has been developed as a substitute, finding replacements for all applications has proven challenging. This study added aluminum to the lead-free solder alloy (Sn-2Ag-0.5Cu-1In) to enhance the performance of SAC solder alloys; through advanced techniques like hybrid drop technique, XRF, XRD, DSC, SEM + EDX analysis, the study explored the new quinary lead-free solder alloy's physical properties, wettability, inter-metallic phases, microstructures, melting temperatures, and other performance factors. The study also analyzed new solder alloys' potentiodynamic polarization, electrical resistivity, and shear strength. This study provides important insights into the existing body of literature by discussing the benefits and drawbacks and comparing findings with previous research. The study findings lead to the following conclusion.

- This study focused on developing and analyzing a range of new quinary lead-free solder alloys. The approach involved incorporating varying quantities of Al into the SAC205-1In, producing new quinary lead-free solder alloys (96.5-x) Sn-2Ag-0.5Cu-1In-xAl. where values of x were tested (0.3 wt%, 0.5 wt%, 0.7 wt%, 0.8 wt%, and 0.9 wt%). XRF analysis was used to thoroughly examine the chemical composition of these alloys, with the resulting data presented in detail in Table 5.1. The optimization of the Sn-Al combination in these new lead-free solder alloys could lead to significant cost reduction.

- Our study employed DSC analysis to ascertain the melting points of newly developed quinary lead-free solder alloys SAC-In-xAl series (with x values of 0.3, 0.5, 0.7, 0.8, and 0.9 wt%). The findings revealed that the melting points of the alloys ranged from 214.3°C to 220.5°C. The study also noted that 3.8

°C decreased the melting point of SAC205-1In-0.3Al to 4.8°C compared to prior studies. In contrast, the melting point of the other quinary lead-free solder alloys manufactured in this study were approximately equivalent to that of SAC205-1In and SAC305. It is crucial to consider that higher melting point solder alloys necessitate elevated temperatures during industrial soldering processes. Adding Al up to 0.3 to SAC205-1In reduced the melting points of solder alloys.

- Incorporating aluminum (Al) into SAC205-1In solder alloys leads to the development of Ag-Al and Cu-Al intermetallic compounds (IMC), ultimately curtailing the growth of Ag3Sn and Cu6-Sn5 IMC. X-ray diffraction (XRD) analysis verified the existence of IMCs such as Ag3Sn, Ag2Al, Ag3Al, Al2Cu, AlCu, Cu3Sn, and Cu6Sn5, which impact the microstructure and concentration of IMC formation within the alloy. These outcomes could enhance the reliability and quality of solder alloys in various applications.

- Wetting tests were conducted for SAC205-1In-xAl (x=0.3, 0.5, 0.7, 0.8, and 0.9 wt%) lead-free solder alloy using the hybrid drop method on a pure copper substrate at temperatures of 275, 300, and 325°C.

- The CA values for the new quinary lead-free solder alloys SAC205-1In-xAl (x=0.3, 0.5, 0.7, 0.8, and 0.9 wt%) were determined at three different temperatures (275 °C, 300 °C, and 325 °C). The lowest average and mean CA of three positive wetting experiments were recorded for each temperature. The lowest average CA of SAC205-1In-0.3Al of three positive wetting experiments for each temperature was 47.84, 42.10, and 39.88, respectively, while the mean CA was 52.61, 45.64, and 42.87, respectively (refer to Table 5.4 for details). The lowest average CA of SAC205-1In-0.5Al of three positive wetting experiments for each temperature was 47.48, 46.50, and 40.12, respectively, while The mean CA was 52.30, 49.09, and 43.06 (refer to Table 5.6 for details). The lowest average CA of SAC205-1In--0.7Al of three positive wetting experiments for each temperature was 61.54, 50.78, and 48.32, respectively, while the mean CA was 63.93, 53.25, and 50.45 (refer to

Table 5.8 for details). In addition, The lowest average CA of SAC205-1In-0.8Al of three positive wetting experiments for each temperature was 50.26, 47.17, and 37.95, respectively, while the mean CA was 52.55, 49.85, and 43.94 (refer to Table 5.10 for details). Finally, the lowest average CA of SAC205-1In-0.9Al of three positive wetting experiments was 50.02, 45.71, and 41.82, respectively, while the mean CA was 52.57, 48.56, and 44.78 (refer to Table 5.12 for details).

- This study found that the SAC205-In-0.3Al solder alloy has the lowest melting point and the highest wettability among all new quinary lead-free solder alloys. SAC205-1In-0.3Al showed the lowest mean contact angle at 42.87 at 325 ^{0}C. It means that the capability of SAC205-1In-0.3Al to spread on a Cu-substrate is higher and faster than other produced solder alloys in this study. Adding aluminum to SAC205-1In increase the melting point. On the other hand, increasing the amount of Al from 0.5 wt% to 0.9 wt% causes a slight increase in the mean contact angle values and melting point of the alloy. The new quinary lead-free solder alloys SAC205-1In-xAl exhibit good wettability with contact angles between 35 and 50 degrees at 275 ^{0}C, 300 ^{0}C, and 325 ^{0}C. The wetting experiments showed that the contact angle decreases as the temperature increases for all new quinary lead-free solder alloys. (See Figure 5.9).

- The SEM analyses found that the IMCs at the interface became more prominent as the temperature increased for each lead-free solder alloy. The SEM-EDX analysis revealed the formation of several IMCs, including Ag_3Sn, Ag_2Al, Ag_3Al, Al_2Cu, AlCu, Cu_3Sn, and Cu_6Sn_5 at the junction of drop solder and the Cu substrate. As per to the literature, the Cu_6Sn_5 IMC can negatively impact joint reliability, but it does create a protective barrier on copper surfaces, which makes them corrosion-resistant. On the other hand, the Cu_3Sn IMC enhances electrical conductivity, mechanical strength, and exhibits high corrosion resistance. Regarding bulk solder alloys, Cu-Al and Ag-Al IMC form more quickly due to the presence of Al. Once Cu-Al and Ag-Al IMC form, less Cu and Ag are available to form IMC with Sn in bulk solder.

Because of their excellent thermal and electrical conductivity, Cu-Al and Ag-Al IMC are popular for conductive or binding compounds.

- The corrosion behavior of new quinary lead-free SAC205-1In-xAl (x = 0.3, 0.5, 0.7, 0.8, and 0.9 wt%) solder alloys was examined in this study under the impact of 1 M HCl. The analyses demonstrated that the corrosion rate of SAC205-1IIn-0.3Al, SAC205-1In-0.5Al, SAC205-1In-0.7Al, and SAC205-1In-0.9Al is slightly higher than that of SAC305 and SAC205-1In. In investigating new quinary lead-free solder alloys, it was observed that the corrosion rate decreases with aluminum's increased replacement of tin. The corrosion rate of SAC205-1In-0.8Al solder alloy (0.4658 mm/year) was found to be the lowest among all alloys studied and even compared to the previously determined corrosion rate of SAC305 (0.488 mm/year). However, it is higher than the corrosion rate of SAC205-1In (0.285 mm/year) determined earlier. The addition of up to 0.9 of aluminum maintained the corrosion resistance of the developed solder alloys within acceptable limits. Furthermore, the introduction of aluminum to the solder alloys resulted in an increase in the (icorr) and (Ecorr) values compared to those of SAC305 and SAC205-1In previously determined by researchers.

- Based on the results of electrical resistivity testing, it has been determined that the maximum electrical resistivity values for the new quinary lead-free solder alloys (SAC205-1In-0.3Al, SAC205-1In-0.5Al, SAC205-1In-0.7Al, SAC205-1In-0.8Al, and SAC205-1In-0.9Al) ranged from $1.07 \times 10^{-6} \Omega.m$ to $1.21 \times 10^{-6} \Omega.m$. It was observed that the electrical resistivity gradually increased as the amount of aluminum increased, with the highest resistivity value of $1.21 \times 10^{-6} \Omega.m$ being achieved with the addition of 0.9 wt% aluminum in SAC205-1In-0.9Al. This particular alloy exhibited a reduction in the concentration of Ag3Sn and Cu-Sn phase (Cu6Sn5 and Cu3Sn), more so than any other alloys produced in this study. Conversely, SAC205-1In-0.3Al had the lowest electrical resistivity $1.07 \times 10^{-6} \Omega.m$, less than the electrical resistivity of SAC205-1In (1.08E-06 $\Omega.m$) without adding

aluminum, making it the most effective conductor for the current. It should be noted that resistivity and conductivity are inversely proportional.

- The SAC-1In solder alloy, which is lead-free, demonstrated a minimum shear strength value of 141.66 MPa when no Al was added. The new quinary solder alloys exhibited a decline in shear stress initially, with an increase in Al percentage at 0.3 wt% and 0.5 wt% Al content. However, at 0.7 wt% Al content, there was a subsequent rise in shear stress, reaching its peak at 0.8 wt% Al content before declining again at 0.9 wt% Al content. The maximum shear strength of the SACIn-0.8Al solder alloy was measured at 155.94 MPa, and it always formed a strong bond with the copper layer. Also, the shear strength of the SAC205-1In-0.3Al, SAC205-1In-0.5Al, SAC205-1n-0.7Al, and SAC205-1In-0.9Al were 136.54 MPa, 132.97 MPa, 133.72 MPa, and 138.21 MPa respectively. CuSn phase which represented by Cu3Sn intermetallic phases is typically produced due to the solder's adhesion to the copper substrate. These lead-free solders have good bonding and wettability properties to Cu substrates, and the solder matrix's mechanical resistance ultimately determines the soldered junctions' mechanical integrity.

PART 7

SUMMARY

Soldering is a technique for combining two or more metallic objects by using another substance (alloy) called solder. This technique is extensively used in the production of electronic devices and has become an indispensable part of modern technology. Since the advent of the electronic age in the 20th century, soldering has become an essential technique for producing electronic devices. Many industrial applications have used solder alloys containing tin, lead, antimony, copper, silver, bismuth, indium, zinc, gold, silicon, and germanium. However, several countries and states have restricted the usage of certain toxic materials, including lead, in electronic devices due to their harmful effects on vital systems in the human body.

There are numerous benefits to using Sn-Pb solder alloy, such as its cost-effectiveness, low melting point, high manufacturability, and strong adhesion to copper (Cu) substrates. However, due to Pb's health and environmental risks, extensive research has been conducted to identify a Pb-free alternative for electronic assemblies. As a result of environmental concerns, government regulations, and market competition, there has been a sustained shift towards using lead-free soldering. Since 2006, many countries have restricted or banned using seven elements, including Pb. The EU's RoHS and WEEE directives aim to promote and develop lead-free solder alloys. The SAC solder alloy is currently the recommended Pb-free option for interconnect manufacturing in the electronics industry.

Several lead-free solder compositions have been created to replace Sn-Pb solder, such as Sn-Bi, Sn-Cu, Sn-Zn, Sn-Ag, Zn-Bi, Sn-Ag-Cu, Sn-Zn-Bi, Sn-Cu-Bi, Sn-Cu-Ni, and others. SAC solder alloys are among the most commonly used lead-free solders due to their exceptional reliability and mechanical properties. However, their high melting point of 217-219°C makes them less preferable than the Sn-Pb solder

alloy, which has a melting point of 183°C. Furthermore, these alloys' high silver (Ag) content increases their production cost.

Two methods can be used to address the drawbacks of SAC solder alloy. The first involves adding elements, such as Ga or rare earth elements, to the SAC alloy to improve its wetting properties and overall performance. The second method involves adding metal and polymer nanoparticles to achieve different properties of the SAC solder.

In our study, we added an Al element to SAC205-1In to overcome SAC's disadvantages and enhance its performance. The ideal lead-free alternatives for soldering should have specific characteristics. They should have a melting temperature similar to that of Sn-Pb solders, good wettability for appropriate metallization during the manufacturing process, similar or better electrical conductivity to transmit electrical signals effectively, adequate mechanical properties to ensure the reliability of electronic products, and should be nontoxic and relatively inexpensive.

This study examines the effect of adding aluminum (Al) to the lead-free solder alloy (Sn-2Ag-0.5Cu-1In) and producing a quinary lead-free solder alloy (96.5-x)Sn–2Ag-0.5Cu-1In–xAl, where x=0.3, 0.5, 0.7, 0.8, and 0.9 wt%. The performance of the produced alloys is then investigated, including their physical properties, wettability, inter-metallic phases, microstructures, melting temperatures, potentiodynamic polarization technique, electrical conductivity analysis, and shear strength. Moreover, it provides new information on the production of new quinary lead-free solder alloys, which have not been previously researched. Additionally, it reveals the production parameters required for industrial output. It makes an essential contribution to the literature by discussing each test's advantages and disadvantages and analyzing the produced alloys' results by comparing them with previous research in the literature.

REFERENCES

1. DHARMA, I. G. B., Hamdi, M., & Ariga, T., The effects of adding silver and indium to lead-free solders. ***Welding journal***, 88(4), 45-48 (2009).

2. Shnawah, D. A., Sabri, M. F. M., & Badruddin, I. A., A review on thermal cycling and drop impact reliability of SAC solder joint in portable electronic products. ***Microelectronics reliability***, 52(1), 90-99 (2012).

3. Kumar, N., & Maurya, A., Development of lead free solder for electronic components based on thermal analysis. ***Materials Today: Proceedings***, 62, 2163-2167 (2022).

4. Amagai, M., WATANABE, M., OMIYA, M., & Kishimoto, K.,. Mechanical Characteristics of Sn-Ag-Based Lead Free Solders. ***journal of the japan institute of electronics packaging***, *5*(6), 551-558 (2002).

5. Cai, Z., Zhang, Y., Suhling, J. C., Lall, P., Johnson, R. W., & Bozack, M. J.. Reduction of lead free solder aging effects using doped SAC alloys. ***In 2010 Proceedings 60th Electronic Components and Technology Conference (ECTC)*** (pp. 1493-1511). IEEE (2010).

6. Balaram, V., Rambabu, U., Reddy, M. R. P., Munirathnam, N. R., & Chatterjee, S., RoHS Regulation: challenges in the measurement of substances of concern in industrial products by different analytical techniques. ***Mapan***, 33, 329-346 (2018).

7. Cheng, S., Huang, C.-M. and Pecht, M., "A review of lead-free solders for electronics applications", ***Microelectronics Reliability***, Vol. 75, pp. 77-95 (2017).

8. Erer, A. M., Oguz, S., & Türen, Y., Influence of bismuth (Bi) addition on wetting characteristics of Sn-3Ag-0.5 Cu solder alloy on Cu substrate. ***Engineering Science and Technology, an International Journal***, *21*(6), 1159-1163 (2018).

9. UYANIK, O., Erer, A. M., & Türen, Y., Effect of Indium on Wettability of Sn-2Ag-0, 5Cu-1In Quaternary Solder Alloy on Cu Substrate. ***El-Cezeri***, *6*(1), 1-7 (2019).

10. Ghosh, S. K., Haseeb, A. S. M. A., & Afifi, A., Effects of metallic nanoparticle doped flux on interfacial intermetallic compounds between Sn-3.0 Ag-0.5 Cu and copper substrate. In *2013* ***IEEE 15th Electronics Packaging Technology Conference (EPTC 2013)*** (pp. 21-26). IEEE (2013).

11. Moser, Z., Gąsior, W., Pstruś, J., & Dębski, A., Wettability studies of Pb-free soldering materials. ***International Journal of Thermophysics***, *29*, 1974-1986 (2008).

12. Yang, L., Zhang, Y., Dai, J., Jing, Y., Ge, J., & Zhang, N., Microstructure, interfacial IMC and mechanical properties of Sn–0.7 Cu–xAl (x= 0–0.075) lead-free solder alloy. ***Materials & Design***, *67*, 209-216 (2015).

13. El-Daly, A. A., & El-Taher, A. M., Evolution of thermal property and creep resistance of Ni and Zn-doped Sn–2.0 Ag–0.5 Cu lead-free solders. ***Materials & Design***, *51*, 789-796 (2013).

14. Efzan Mhd Noor, E., & Singh, A., Review on the effect of alloying element and nanoparticle additions on the properties of Sn-Ag-Cu solder alloys. Soldering & Surface Mount Technology, 26(3), 147-161 (2014).

15. Lee, N. C., Getting ready for lead-free solders. ***Soldering & Surface Mount Technology***, 9(2), 65-69 (1997).

16. Kantarcıoğlu, A., Development of new lead-free solders for electronics industry (***Master's thesis, Middle East Technical University***) (2012).

17. Wu, C. M. L., Yu, D. Q., Law, C. M. T., & Wang, L., Properties of lead-free solder alloys with rare earth element additions. ***Materials Science and Engineering****: R: Reports*, *44*(1), 1-44 (2004).

18. Monsalve E.R., Lead Ingestion hazard in Hand Soldering Environments, in Proceedings of the 8th Annual Soldering Technology and Product Assurance Seminar, ***Naval Weapons Center***, China Lake, CA (1984).

19. Waste Electrical & Electronic Equipment (WEEE)",European Commision, 09th Jun. 2016, ***http://ec.europa.eu/environment/waste/weee/index_en.htm***, Accessed 07th Feb. 2017.

20. Amagai, M., Toyoda, Y. and Tajima, T., “High solder joint reliability with lead free solders”, ***Presented at Proceedings of the 53rd Electronic Components and Technology Conference***, 2003, pp. 317-322 (2003).

21. Terashima, S., Kariya, Y., Hosoi, T. and Tanaka, M., “Effect of silver content on thermal fatigue life of Sn-xAg-0.5Cu flip-chip interconnects”, ***Journal of Electronic Materials***, Vol. 32 No. 12, pp. 1527-1533 (2003).

22. Song, J. M., & Wu, Z. M., Variable eutectic temperature caused by inhomogeneous solute distribution in Sn–Zn system. ***Scripta materialia***, *54*(8), 1479-1483 (2006).

23. Huh, S. H., Kim, K. S., & Suganuma, K., Effect of Ag addition on the microstructural and mechanical properties of Sn-Cu eutectic solder. ***Materials transactions***, *42*(5), 739-744 (2001).

24. Amagai, M.A., study of nanoparticles in Sn–Ag based lead free solders. Microelectron. ***Reliab***., *48*, 1–16 (2008).

25. Moser, Z., Sebo, P., Gąsior, W., Svec, P., & Pstruś, J., Effect of indium on wettability of Sn–Ag–Cu solders. Experiment vs. modeling, Part I. ***Calphad***, *33*(1), 63-68 (2009).

26. Subramanian, K. N., Chen, S. W., Wang, C. H., Lin, S. K., & Chiu, C. N., Phase diagrams of Pb-free solders and their related materials systems. *Lead-Free Electronic Solders:* ***A Special Issue of the Journal of Materials Science: Materials in Electronics***, 19-37 (2007).

27. Rosalbino, F., Angelini, E., Zanicchi, G., Carlini, R., & Marazza, R., Electrochemical corrosion study of Sn–3Ag–3Cu solder alloy in NaCl solution. ***Electrochimica Acta***, 54(28), 7231-7235 (2009).

28. Moser, Z., Fima, P., Bukat, K., Sitek, J., Pstruś, J., Gąsior, W., ... & Gancarz, T., Investigation of the effect of indium addition on wettability of Sn-Ag-Cu solders. ***Soldering & Surface Mount Technology***, 23(1), 22-29 (2011).

29. Kanlayasiri, K., Mongkolwongrojn, M., & Ariga, T., Influence of indium addition on characteristics of Sn–0.3 Ag–0.7 Cu solder alloy. ***Journal of Alloys and Compounds***, 485(1-2), 225-230 (2009).

30. Chuang, C. L., Tsao, L. C., Lin, H. K., & Feng, L. P., Effects of small amount of active Ti element additions on microstructure and property of Sn3. 5Ag0. 5Cu solder. ***Materials Science and Engineering: A***, *558*, 478-484 (2012).

31. Fallahi, H., Nurulakmal, M. S., Arezodar, A. F., & Abdullah, J., Effect of iron and indium on IMC formation and mechanical properties of lead-free solder. ***Materials Science and Engineering: A***, *553*, 22-31 (2012).

32. Lee, L. M., & Mohamad, A. A., Interfacial reaction of Sn-Ag-Cu lead-free solder alloy on Cu: A review. ***Advances in Materials Science and Engineering***, *2013*.

33. Koleňák, R., Augustin, R., Martinkovič, M., & Chachula, M., Comparison study of SAC405 and SAC405+ 0.1% Al lead free solders. ***Soldering & Surface Mount Technology***, 25(3), 175-183 (2013).

34. Lee, H. Y., Sharma, A., Kee, S. H., Lee, Y. W., Moon, J. T., & Jung, J. P., Effect of aluminium additions on wettability and intermetallic compound (IMC) growth of lead free Sn (2 wt.% Ag, 5 wt.% Bi) soldered joints. ***Electronic Materials Letters***, *10*, 997-1004 (2014).

35. Sun, L., & Zhang, L., Properties and microstructures of Sn-Ag-Cu-X lead-free solder joints in electronic packaging. ***Advances in Materials Science and Engineering***, (2015).

36. Sabri, M. F. M., Said, S. B. M., & Shnawah, D. A., Wetting characteristics of Al-containing Sn-1Ag-0.5 Cu solder alloy on Cu substrate using wetting balance and spread area methods. ***Procedia Technology***, *20*, 9-14 (2015).

37. Leong, Y. M., & Haseeb, A. S. M. A., Soldering characteristics and mechanical properties of Sn-1.0 Ag-0.5 Cu solder with minor aluminum addition. ***Materials***, *9*(7), 522 (2016).

38. Maslinda, K., Anasyida, A. S., & Nurulakmal, M. S., Effect of Al addition to bulk microstructure, IMC formation, wetting and mechanical properties of low-Ag SAC solder. ***Journal of Materials Science: Materials in Electronics***, *27*, 489-502 (2016).

39. Sun, L., Zhang, L., Xu, L., Zhong, S. J., Ma, J., & Bao, L., Effect of nano-Al addition on properties and microstructure of low-Ag content Sn–1Ag–0.5 Cu solders. ***Journal of Materials Science: Materials in Electronics***, 27, 7665-7673 (2016).

40. Sayyadi, R., & Naffakh-Moosavy, H., Physical and mechanical properties of synthesized low Ag/lead-free Sn-Ag-Cu-xBi (x= 0, 1, 2.5, 5 wt%) solders. ***Materials Science and Engineering****: A*, *735*, 367-377 (2018).

41. Liao, B., Cen, H., Chen, Z., & Guo, X., Corrosion behavior of Sn-3.0 Ag-0.5 Cu alloy under chlorine-containing thin electrolyte layers. ***Corrosion Science***, 143, 347-361 (2018).

42. Kumar, P. M., Gergely, G., Horváth, D. K., & Gácsi, Z., Investigating the microstructural and mechanical properties of pure lead-free soldering materials (SAC305 & SAC405). ***Powder Metall. Prog***, 18(1), 49-57 (2018).

43. Nasir, S. S. M., Yahaya, M. Z., Erer, A. M., Illés, B., & Mohamad, A. A., Effect of TiO2 nanoparticles on the horizontal hardness properties of Sn-3.0 Ag-0.5 Cu-1.0 TiO2 composite solder. ***Ceramics International***, *45*(15), 18563-18571 (2019).

44. Subri, N. W. B., Sarraf, M., Nasiri-Tabrizi, B., Ali, B., Mohd Sabri, M. F., Basirun, W. J., & Sukiman, N. L, Corrosion insight of iron and bismuth added Sn–1Ag–0.5 Cu lead-free solder alloy. ***Corrosion Engineering, Science and Technology***, 55(1), 35-47 (2020).

45. Gharaibeh, A., Felhősi, I., Keresztes, Z., Harsányi, G., Illés, B., & Medgyes, B.. Electrochemical corrosion of SAC alloys: ***A review. Metals***, 10(10), 1276 (2020).

46. Ali, U., Khan, H., Aamir, M., Giasin, K., Habib, N., & Owais Awan, M., Analysis of microstructure and mechanical properties of bismuth-doped SAC305 lead-free solder alloy at high temperature. ***Metals***, 11(7), 1077 (2021).

47. Kaushik, R. K., Batra, U., & Sharma, J. D., Electrochemical Corrosion Behavior of Sn–1.0 Ag–0.5 Cu and Sn–3.8 Ag–0.7 cu Lead Free Solder Alloys During Storage and Transportation Under Chloride Working Condition. ***Transactions on Electrical and Electronic Materials***, 1-11(2022).

48. Jaiswal, D., Pathote, D., Singh, V., & Behera, C. K., Effect of Al addition on electrochemical behavior of Sn-0.7 Cu-xAl lead-free solders alloys in 3.5 wt.% NaCl solution. ***Journal of Materials Engineering and Performance***, *31*(9), 7550-7560 (2022).

49. Qu, M., Gao, Z., Chen, J., & Cui, Y., Effect of Ni-coated carbon nanotubes addition on the wettability, microhardness, and shear strength of Sn-3.0 Ag-0.5 Cu/Cu lead-free solder joints. ***Journal of Materials Science: Materials in Electronics***, *33*(14), 10866-10879 (2022).

50. Kuang, J. H., Hsu, C. M., & Chiu, W. C., The variation of shear strength of the lead free Sn/3.0 Ag/0.5 Cu solder balls. In 2007 9th ***Electronics Packaging Technology Conference*** (pp. 910-913). IEEE (2007, December).

51. Serkan, O. G. U. Z., Erer, A. M., Türen, Y., & AHLATCI, H., The Effect Of Indium Addition on The Corrosion Kinetics of Sn–3Ag–0.5 Cu Alloy In HCl Acid Solution. ***Avrupa Bilim ve Teknoloji Dergisi***, (34), 28-33 (2022).

52. Mohd Salleh, M. A. A., Hazizi, M. H., Ahmad, Z. A., Hussin, K., & Ahmad, K. R., Wettability, electrical and mechanical properties of 99.3 Sn-0.7 Cu/Si3N4 novel lead-free nanocomposite solder. ***Advanced Materials Research***, *277*, 106-111(2011).

53. Gancarz, T., Fima, P., & Pstruś, J., Thermal expansion, electrical resistivity, and spreading area of Sn-Zn-In alloys. ***Journal of materials engineering and performance***, *23*, 1524-1529 (2014).

54. Yang, W., & Chung, D. D. L., Effect of temperature on the electrical conduction and dielectric behavior of solder. ***Journal of Materials Science: Materials in Electronics***, *32*(5), 6511-6519 (2021).

55. Shalaby, R. M., Munther, M., Al-Bidawi, A. B., & Kamal, M., Effect of aluminum content on structure, transport and mechanical properties of Sn-Zn eutectic lead free solder alloy rapidly solidified from melt. ***Journal: JOURNAL OF ADVANCES IN PHYSICS***, *10*(1) (2015).

56. Yilmaz, S., The geometric resistivity correction factor for several geometrical samples. ***Journal of Semiconductors***, *36*(8), 082001 (2015).

57. Ismail, N., Jalar, A., Afdzaluddin, A., & Bakar, M. A., Electrical resistivity of Sn–3.0 Ag–0.5 Cu solder joint with the incorporation of carbon nanotubes. ***Nanomaterials and Nanotechnology***, 11, 1847980421996539 (2021).

58. Serkan, O. G. U. Z., Erer, A. M., Türen, Y., & AHLATCI, H., The Effect Of Indium Addition on The Corrosion Kinetics of Sn–3Ag–0.5 Cu Alloy In HCl Acid Solution. ***Avrupa Bilim ve Teknoloji Dergisi***, (34), 28-33 (2022).

59. Fayeka, M., Haseeb, A. S. M. A., & Fazal, M. A., Electrochemical corrosion behaviour of Pb-free SAC 105 and SAC 305 solder alloys: a comparative study. ***Sains Malaysiana***, 46(2), 295-302 (2017).

60. Nordin, N. I. M., Said, S. M., Ramli, R., Weide-Zaage, K., Sabri, M. F. M., Mamat, A., ... & Datta, R. S., Impact of aluminium addition on the corrosion behaviour of Sn–1.0 Ag–0.5 Cu lead-free solder. ***RSC advances***, *5*(120), 99058-99064 (2015).

61. Hamidah, I., Solehudin, A., Hamdani, A., Hasanah, L., Khairurrijal, K., Kurniawan, T., ... & Hammouti, B., Corrosion of copper alloys in KOH, NaOH, NaCl, and HCl electrolyte solutions and its impact to the mechanical properties. ***Alexandria Engineering Journal***, *60*(2), 2235-2243 (2021).

62. Abd El Hamid, S. E., Gouda, E. S., & Ghany, N. A. A., Effect of Al and Bi addition on the corrosion behavior, hardness, and melting temperature of lead-free solder alloys. ***Microelectronics Reliability***, *147*, 115051(2023).

63. Amin, N. A. A. M., Shnawah, D. A., Said, S. M., Sabri, M. F. M., & Arof, H., Effect of Ag content and the minor alloying element Fe on the electrical resistivity of Sn–Ag–Cu solder alloy. ***Journal of alloys and compounds***, 599, 114-120 (2014).

64. Shnawah, D. A. A., Sabri, M. F. M., & Badruddin, I. A., Effect of Al addition on the bulk alloy microstructure properties of Sn-1Ag-0.5 Cu solder. ***INFORMACIJE MIDEM-JOURNAL OF MICROELECTRONICS ELECTRONIC COMPONENTS AND MATERIALS***, *42*(2), 88-94 (2012).

65. Schwartz, M. M., & Aircraft, S., Fundamentals of soldering. ***ASM International, ASM Handbook.***, *6*, 126-137 (1993).

66. Abtew, M., & Selvaduray, G., Lead-free solders in microelectronics. ***Materials Science and Engineering: R: Reports***, *27*(5-6), 95-141(2000).

67. Harrison, M. R., Vincent, J. H., & Steen, H. A. H.. Lead-free reflow soldering for electronics assembly. ***Soldering & Surface Mount Technology***, *13*(3), 21-38 (2001).

68. Fritzsche, J., & Peuker, U. A., Wetting and adhesive forces on rough surfaces–an experimental and theoretical study. ***Procedia Engineering***, 102, 45-53 (2015).

69. Erbil, H. Y., "Surface Chemistry of Solid and Liquid Interfaces", ***Blackwell Pub, Oxford, UK, Malden, MA***, 352 (2006).

70. Salaün, F., Devaux, E., Bourbigot, S., & Rumeau, P., Application of contact angle measurement to the manufacture of textiles containing microcapsules. ***Textile research journal***, 79(13), 1202-1212 (2009).

71. Grundke, K., Pöschel, K., Synytska, A., Frenzel, R., Drechsler, A., Nitschke, M., ... & Welzel, P. B., Experimental studies of contact angle hysteresis phenomena on polymer surfaces—Toward the understanding and control of wettability for different applications. ***Advances in colloid and interface science***, 222, 350-376 (2015).

72. Sefiane, K., On the formation of regular patterns from drying droplets and their potential use for bio-medical applications. ***Journal of Bionic Engineering***, 7(4), S82-S93 (2010).

73. Schuster, J. M., Schvezov, C. E., & Rosenberger, M. R., Influence of experimental variables on the measure of contact angle in metals using the sessile drop method. ***Procedia Materials Science***, *8*, 742-751 (2015).

74. Baek, Y., Kang, J., Theato, P., & Yoon, J., Measuring hydrophilicity of RO membranes by contact angles via sessile drop and captive bubble method: A comparative study. ***Desalination***, 303, 23-28 (2012).

75. Tate, T., XXX. On the magnitude of a drop of liquid formed under different circumstances. The London, Edinburgh, and ***Dublin Philosophical Magazine and Journal of Science***, 27(181), 176-180 (1864).

76. Dole, M. A. L. C. O. L. M., Surface tension measurements. ***Physical Methods in Chemical Analysis***, 2, 305-332 (1951).

77. Cao, J. K., & Zhang, Y. B., Improvements in the surface tension measurement using the capillary rise method and its application to water under external magnetic fields. ***Journal of Molecular Liquids***, 382, 121988 (2023).

78. Ruiz-Cabello, F. J. M., ***Efecto de la rugosidad y heterogeneidad superficial en fenómenos de mojado***. Editorial de la Universidad de Granada (2009).

79. Blythe, A. R., Briggs, D., Kendall, C. R., Rance, D. G., & Zichy, V. J. I., Surface modification of polyethylene by electrical discharge treatment and the mechanism of autoadhesion. ***Polymer***, *19*(11), 1273-1278 (1978).

80. Kaelble, D. H., & Cirlin, E. H., Dispersion and polar contributions to surface tension of poly (methylene oxide) and Na-treated polytetrafluoroethylene. **Journal of Polymer Science Part A-2: Polymer Physics,** *9*(2), 363-368 (1971).

81. Rudawska, A., & Jacniacka, E., Analysis for determining surface free energy uncertainty by the Owen–Wendt method. ***International journal of adhesion and adhesives***, *29*(4), 451-457 (2009).

82. Alaqarbeh, M., Adsorption phenomena: definition, mechanisms, and adsorption types: ***short review. RHAZES: Green and Applied Chemistry***, 13, 43-51(2021).

83. Dąbrowski, A.. Adsorption—from theory to practice. ***Advances in colloid and interface science***, 93(1-3), 135-224(2001).

84. Fraissard, J. P. (Ed.)., Physical adsorption: experiment, theory, and applications (Vol. 491). ***Springer Science & Business Media*** (1997).

85. Bolis, V., Fundamentals in adsorption at the solid-gas interface. Concepts and thermodynamics. ***Calorimetry and thermal methods in catalysis***, 3-50(2013).

86. Ho, Y. S., & McKay, G., Sorption of dye from aqueous solution by peat. ***Chemical engineering journal***, 70(2), 115-124 (1998).

87. Usmani, M. A., Khan, I., Gazal, U., Haafiz, M. M., & Bhat, A. H., Interplay of polymer bionanocomposites and significance of ionic liquids for heavy metal removal. In Polymer-Based Nanocomposites for Energy and Environmental Applications. ***Woodhead Publishing*** (pp. 441-463) (2018).

88. Fomina, M., & Gadd, G. M., Biosorption: current perspectives on concept, definition and application. ***Bioresource technology***, 160, 3-14 (2014).

89. Arulvanan, P., Zhong, Z., & Shi, X., Effects of process conditions on reliability, microstructure evolution and failure modes of SnAgCu solder joints. ***Microelectronics Reliability***, 46(2-4), 432-439 (2006).

90. Adetunji, O. R., Ashimolowo, R. A., Aiyedun, P. O., Adesusi, O. M., Adeyemi, H. O., & Oloyede, O. R., Tensile, hardness and microstructural properties of Sn-Pb solder alloys. ***Materials Today: Proceedings***, 44, 321-325 (2021).

91. Zeng, K., & Tu, K. N., Six cases of reliability study of Pb-free solder joints in electronic packaging technology. ***Materials science and engineering: R: reports***, *38*(2), 55-105 (2002).

92. Tu, K. N., Gusak, A. M., & Li, M., Physics and materials challenges for lead-free solders. ***Journal of applied Physics***, *93*(3), 1335-1353(2003).

93. Karakaya, I., & Thompson, W. T.. The Pb− Sn (Lead-Tin) system. ***Journal of Phase Equilibria***, 9, 144-152 (1988).

94. Mayappan, R. A. M. A. N. I., Ismail, A. B., Ahmad, Z. A., Ariga, T., & Hussain, L. B., Wetting properties of Sn-Pb, Sn-Zn and Sn-Zn-Bi lead-free solders. ***Journal Teknologi***, 46(C), 1-14(2007).

95. Kim, H. K., Liou, H. K., & Tu, K. N., Morphology of instability of the wetting tips of eutectic SnBi, eutectic SnPb, and pure Sn on Cu. ***Journal of materials research***, 10(3), 497-504(1995).

96. Wood, E. P., & Nimmo, K. L., In search of new lead-free electronic solders. ***Journal of Electronic Materials***, 23(8), 709-713 (1994).

97. Napp, D., Lead free interconnect materials for the electronics industry. ***In Seventeenth IEEE/CPMT International Electronics Manufacturing Technology Symposium.'Manufacturing Technologies-Present and Future***' (pp. 238-244). IEEE (1995).

98. Nimmo, K., Review of current issues in lead-free soldering. ***The Proceedings of Surface Mount Inter***.(SMI'97), 7-11(1997).

99. Anderson I.E., Sn-Ag-Cu: A Lead Free Solder For Board Applications, ***Proceedings of the NEPCON, Anaheim***, CA, 882-887 (1996).

100. Miller, C. M., Anderson, I. E., & Smith, J. F., A viable tin-lead solder substitute: Sn-Ag-Cu. ***Journal of electronic materials***, *23*, 595-601 (1994).

101. Moon, K. W., Boettinger, W. J., Kattner, U. R., Biancaniello, F. S., & Handwerker, C. A., Experimental and thermodynamic assessment of Sn-Ag-Cu solder alloys. ***Journal of electronic materials***, *29*, 1122-1136 (2000).

102. Ye, L. L., Lai, Z., Liu, J., & Tholen, A., Microstructural coarsening of lead free solder joints during thermal cycling. In ***2000 Proceedings. 50th Electronic Components and Technology Conference (Cat. No. 00CH37070)*** (pp. 134-137). IEEE (2000).

103. Kang, S. K., Lauro, P., Shih, D. Y., Henderson, D. W., & Puttlitz, K. J., Microstructure and mechanical properties of lead-free solders and solder joints used in microelectronic applications. ***IBM Journal of Research and Development***, *49*(4.5), 607-620 (2005).

104. Pal, M. K., Gergely, G., Horváth, D. K., & Gácsi, Z., Microstructural investigations and mechanical properties of pure lead-free (Sn-3.0 Ag-0.5 Cu and Sn-4.0 Ag-0.5 Cu) solder alloy. ***Metallurgical and Materials Engineering***, *24*(1), 27-36 (2018).

105. Sabbar, E. H., Al-Zubaidi, H. A., Aljumaili, A. K., Al-Jumaili, M. H., Al-Jumaili, A. I., & Alsheakh, H., Effects of Ag content on microstructure evolution, intermetallic compound (IMC) and mechanical behaviour of SAC solder joints. ***Microelectronics Reliability***, 147, 115103 (2023).

106. Kim, K. S., Huh, S. H., & Suganuma, K., Effects of intermetallic compounds on properties of Sn–Ag–Cu lead-free soldered joints. ***Journal of Alloys and compounds***, *352*(1-2), 226-236 (2003).

107. Kang, S. K., Shih, D. Y., Donald, N. Y., Henderson, W., Gosselin, T., Sarkhel, A., ... & Choi, W. K., Ag 3 Sn plate formation in the solidification of near-ternary eutectic Sn-Ag-Cu. ***JOM***, *55*, 61-65 (2003).

108. Sundelin, J. J., Nurmi, S. T., Lepistö, T. K., & Ristolainen, E. O., Mechanical and microstructural properties of SnAgCu solder joints. ***Materials Science and Engineering:*** *A*, *420*(1-2), 55-62 (2006).

109. Kamarudin, M., Anasyida, A. S., & Mohd Sharif, N., Effect of aluminium and silicon to IMC formation in low Ag-SAC solder. In **Materials Science Forum. Trans Tech Publications Ltd** (Vol. 819, pp. 63-67) (2015).

110. Chen, Z. W., Gibson, W. M., & Huang, H., High definition x-ray fluorescence: principles and techniques. ***X-ray Optics and Instrumentation***,(2008).

111. Martins, M. A., Pinho, S. P., & Coutinho, J. A., Insights into the nature of eutectic and deep eutectic mixtures. ***Journal of Solution Chemistry*****,** *48*, 962-982 (2019).

112. Zhang, X., Matsuura, H., Tsukihashi, F., & Yuan, Z., Wettability of Sn–Zn, Sn–Ag–Cu and Sn–Bi–Cu Alloys on Copper Substrates. ***Materials Transactions***, *53*(5), 926-931 (2012).

113. Rizvi, M. J., Bailey, C., Chan, Y. C., Islam, M. N., & Lu, H., Effect of adding 0.3 wt% Ni into the Sn–0.7 wt% Cu solder: Part II. Growth of intermetallic layer with Cu during wetting and aging. ***Journal of alloys and compounds***, *438*(1-2), 122-128 (2007).

114. Erer, A. M., Effect of bismuth addition on the corrosion dynamics of Sn–3Ag–0.5 Cu solder alloy in Hydrochloric Acid Solution. ***International Journal of Innovative Engineering Applications***, *5*(1), 40-44 (2021).

115. Ata, P., & Aksöz, S., Lineer ısı akış metoduyla In-Bi intermetalik alaşımlarının ısıl iletkenlik katsayısının ölçümü (***Master's thesis, Nevşehir Hacı Bektaş Veli Üniversitesi***) (2015).

116. Griffiths, D. J.. Introduction to Electrodynamics Fourth Edition (2021).

117. Topsoe H. Geometric factor in four-point resistivity measurement. ***Semiconductor Division No***. 472-13 (Vedbaek), (1968).

118. A. Uhlir, Jr. Bell System Tech. J. 34 P.105-128 (1955).

119. A. Uhlir, Jr. Bell System Tech. J. 34 P.994 (1955).

120. Qiu, H., Hu, X., Li, S., Wan, Y., & Li, Q., Shear strength and fracture surface analysis of lead-free solder joints with high fraction of IMCs. ***Vacuum, 180***, 109611 (2020).

121. Oguz, S., & Erer, A. M., Effect of Al addition on microstructure and wetting properties of quinary lead-free solder alloy systems. ***Physica Scripta***, 98(11), 115929 (2023).

122. Zang, L., Yuan, Z., Xu, H., & Xu, B., Wetting process and interfacial characteristic of Sn–3.0 Ag–0.5 Cu on different substrates at temperatures ranging from 503 K to 673 K. ***Applied Surface Science***, 257(11), 4877-4884 (2011).

123. Wang, T., Zhou, P., Cao, F., Kang, H., Chen, Z., Fu, Y., ... & Yuan, Q., Growth behavior of Cu6Sn5 in Sn–6.5 Cu solders under DC considering trace Al: in situ observation. ***Intermetallics***, *58*, 84-90 (2015).

124. Abdul-Ameer Shnawah, D., Faizul Mohd Sabri, M., Anjum Badruddin, I., & Xing Che, F., The bulk alloy microstructure and tensile properties of Sn-1Ag-0.5 Cu-x Al lead-free solder alloys (x= 0, 1, 1.5 and 2 wt.%). ***Microelectronics international***, *29*(2), 108-116 (2012).

125. Boesenberg, A. J., Anderson, I. E., & Harringa, J. L., Development of Sn-Ag-Cu-X solders for electronic assembly by micro-alloying with Al. ***Journal of electronic materials***, 41, 1868-1881(2012).

126. Pandher, R.S., Lewis, B.G.,Vangaveti, R., & Singlh, B., Drop shock reliability of lead-free alloys effect of micro-additives. ***In 2007 Proceedings 57th Electronic Components and Technology Conference*** (pp.669-676).IEEE (2007).

127. Hodulova, E., Palcut, M., Lechovič, E., Šimeková, B., & Ulrich, K.. Kinetics of intermetallic phase formation at the interface of Sn–Ag–Cu–X (X= Bi, In) solders with Cu substrate. ***Journal of Alloys and Compounds***, 509(25), 7052-7059 (2011).

128. El-Taher, A. M., & Razzk, A. F., Controlling Ag 3 Sn Plate Formation and Its Effect on the Creep Resistance of Sn–3.0 Ag–0.7 Cu Lead-Free Solder by Adding Minor Alloying Elements Fe, Co, Te and Bi. ***Metals and Materials International***, 27, 4294-4305 (2021).

129. Erer, A.M., Effect of bismuth addition on the corrosion dynamics of Sn-3Ag-0.5Cu solder alloy in Hydrochloric Acid Solution. ***International Journal of Innovative Engineering Applications***, 5 (1), 40-44 (2021).

130. Nordin, N. I. M., Said, S. M., Ramli, R., Sabri, M. F. M., Sharif, N. M., Arifin, N. A. F. N. M., & Ibrahim, N. N. S., Microstructure of Sn–1Ag–0.5Cu solder alloy bearing Fe under salt spray test. ***Microelectronics Reliability***, 54(9-10), 2044-2047 (2014).

131. Tsao, L. C., & Chen, C. W., Corrosion characterization of Cu–Sn intermetallics in 3.5 wt.% NaCl solution. ***Corrosion science***, 63, 393-398 (2012).

132. Hadulova,E.,Palcut,M.,Lechovic,E.,Simekova B.,& Ulrich, K, Kinetics of intermetallic phase formationat the interface of Sn-Ag-Cu-x(x=Bi,In) solders with Cu substrate . ***journal of Alloys and Compounds***,509(25), 7052-7059 (2011).

133. Arenas, M. F., & Acoff, V. L., Contact angle measurements of Sn-Ag and Sn-Cu lead-free solders on copper substrates. ***Journal of Electronic Materials***, 33, 1452-1458 (2004).

134. Puttlitz, K. J., & Stalter, K. A., Handbook of lead-free solder technology for microelectronic assemblies. ***CRC Press*** (2004).

135. Glazer, J., Metallurgy of low temperature Pb-free solders for electronic assembly. ***International Materials Reviews***, *40*(2), 65-93 (1995).

136. Hua, F., Lead-Free Solders for Electronic Assembly: Design & Reliability of Solders and Solder Interconnections. In ***Proceedings of a TMS Symposium*** (pp. 65-73) (1997).

137. Artaki, I., Finley, D. W., Jackson, A. M., Ray, U., & Vianco, P. T., ***Wave soldering with Pb-free solders*** (No. SAND-95-1372C; CONF-9508140-4). Sandia National Lab.(SNL-NM), Albuquerque, NM (United States) (1995).

138. Jackson, A. M., Artakl, I., & Vianco, P. T., ***Manufacturing feasibility of several lead-free solders for electronic assembly*** (No. SAND-94-0470C; CONF-940658-1). Sandia National Labs., Albuquerque, NM (United States) (1994).

139. McCormack, M., & Jin, S., Progress in the design of new lead-free solder alloys. ***JOM***, *45*, 36-40 (1993).

140. Harada, M., & Satoh, R., Mechanical characteristics of 96.5 Sn/3.5 Ag solder in microbonding. ***IEEE Transactions on Components, Hybrids, and Manufacturing Technology***, *13*(4), 736-742 (1990).

APPENDIX A.

MEASUREMENTS OF THE CONTACT ANGLE OF SAC205-1In-XAl OBTAINED FROM WETTING EXPERIMENTS

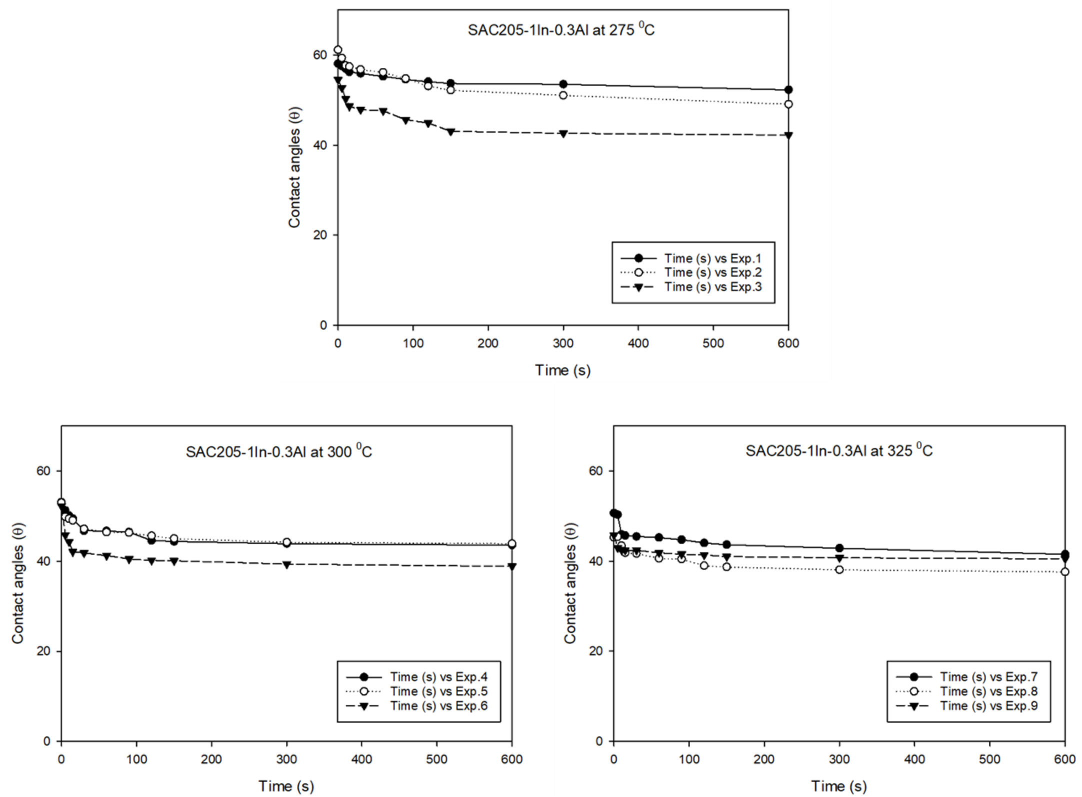

Figure Appendix A.1. Contact angle measurements of SAC205-1In-0.3Al

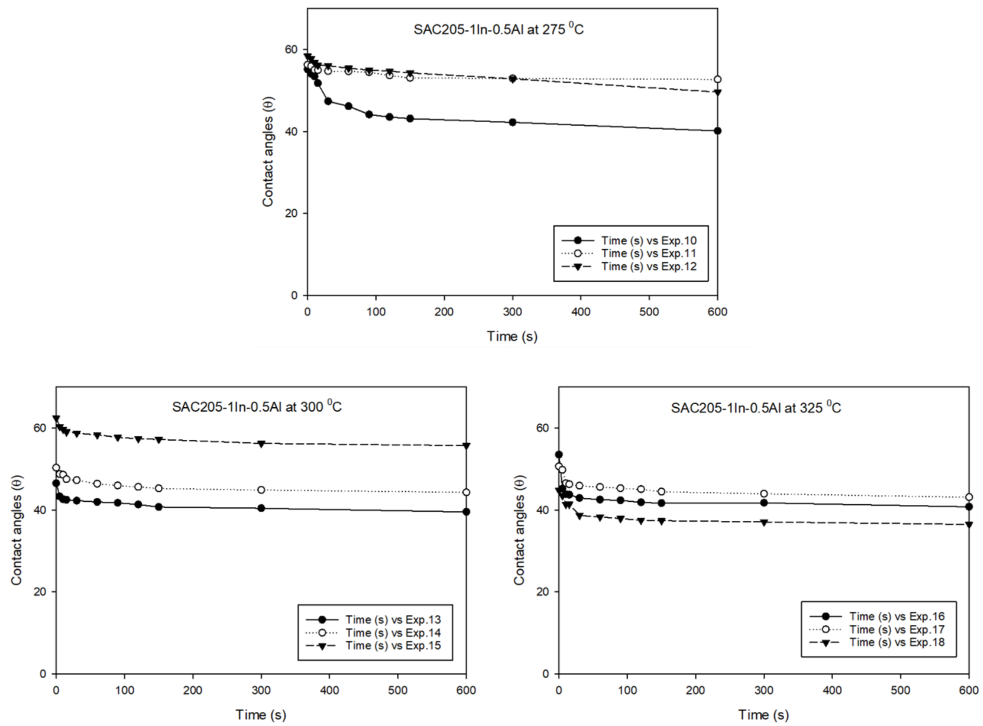

Figure Appendix A.2. Contact angle measurements of SAC205-1In-0.5Al

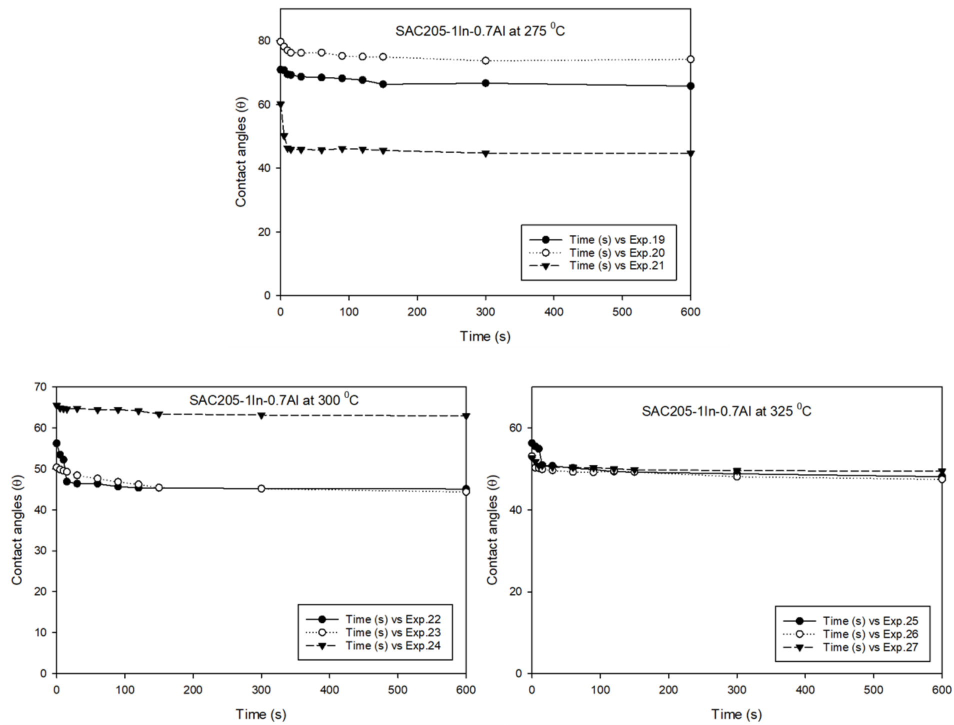

Figure Appendix A.3. Contact angle measurements of SAC205-1In-0.7Al

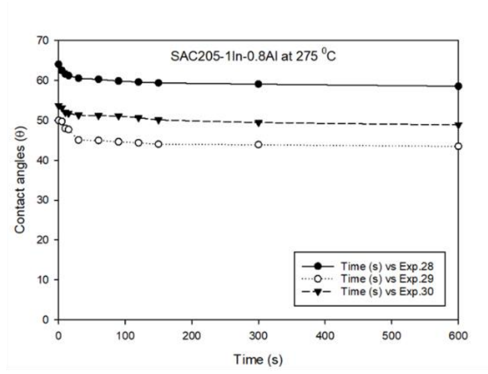

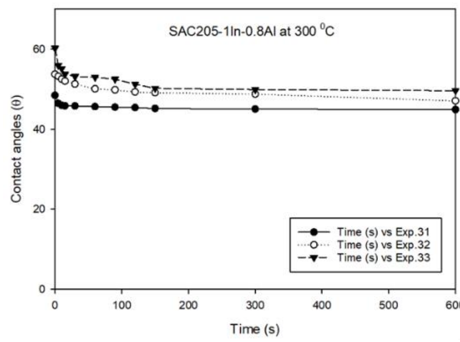

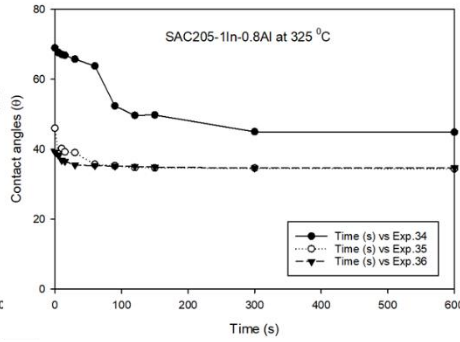

Figure Appendix A.4. Contact angle measurements of SAC205-1In-0.8Al

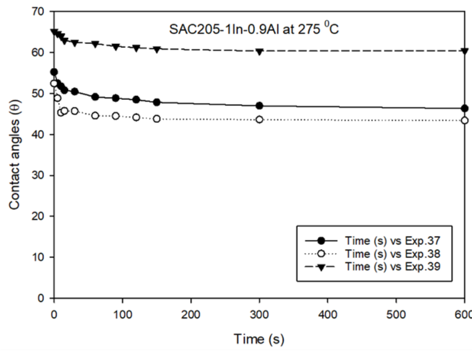

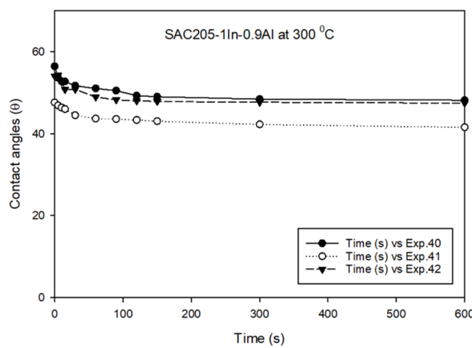

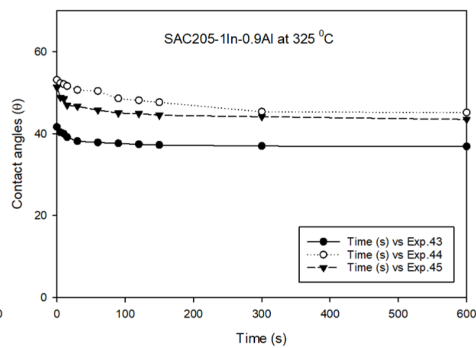

Figure Appendix A.5. Contact angle measurements of SAC205-1In-0.9Al

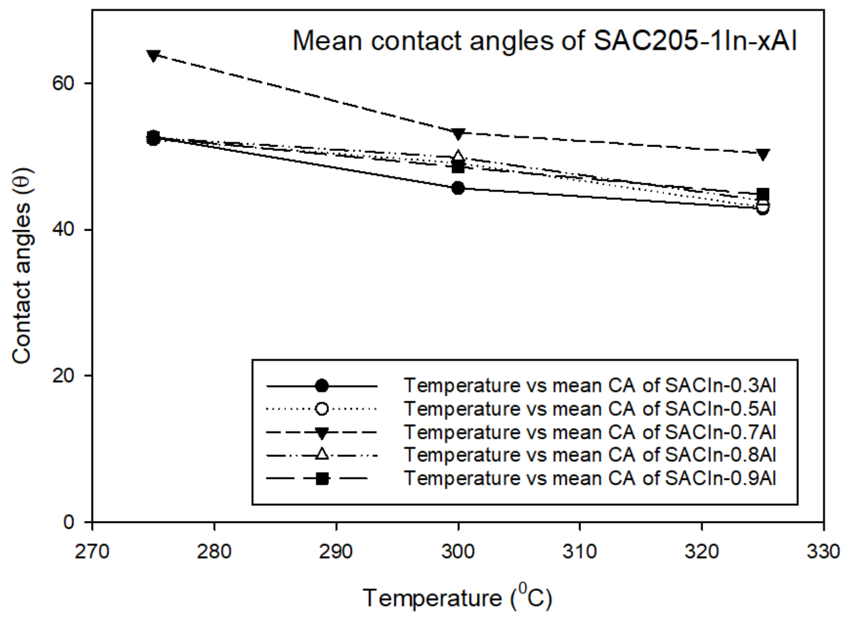

Figure Appendix A.6 Mean contact angles of SAC205-1In-xAl

APPENDIX B.

ELECTRICAL RESISTIVITY MEASUREMENTS OF SAC205-1In-xAl

Table Appendix B.1. Electrical resistivity measurements of SAC205-1In-xAl where (x=0.3, 0.5, 0.7, 0.8, and 0.9 wt%).

Electrical resistivity (ρ) $(\Omega.m)$ of SAC205-1In-xAl					
SAC205-1In-0.0Al	SAC205-1In-0.3Al	SAC205-1In-0.5Al	SAC205-1In-0.7Al	SAC205-1In-0.8Al	SAC205-1In-0.9Al
0.00E+00	0.00E+00	0.00E+00	0.00E+00	0.00E+00	0.00E+00
7.06E-08	6.60E-08	6.87E-08	7.08E-08	7.10E-08	7.49E-08
7.13E-08	6.64E-08	6.87E-08	7.06E-08	7.13E-08	7.41E-08
1.43E-07	1.35E-07	1.39E-07	1.43E-07	1.45E-07	1.51E-07
2.22E-07	2.11E-07	2.15E-07	2.23E-07	2.29E-07	2.34E-07
2.23E-07	2.10E-07	2.13E-07	2.23E-07	2.26E-07	2.34E-07
3.00E-07	2.84E-07	2.90E-07	3.02E-07	3.05E-07	3.18E-07
3.00E-07	2.84E-07	2.91E-07	3.03E-07	3.06E-07	3.18E-07
3.81E-07	3.63E-07	3.72E-07	3.84E-07	3.93E-07	4.07E-07
4.74E-07	4.54E-07	4.63E-07	4.76E-07	4.84E-07	5.02E-07
4.71E-07	4.50E-07	4.68E-07	4.76E-07	4.84E-07	5.02E-07
5.57E-07	5.35E-07	5.47E-07	5.66E-07	5.78E-07	6.02E-07
6.58E-07	6.34E-07	6.55E-07	6.73E-07	6.86E-07	7.09E-07
6.65E-07	6.40E-07	6.50E-07	6.73E-07	6.86E-07	7.16E-07
7.53E-07	7.27E-07	7.56E-07	7.75E-07	7.85E-07	8.19E-07
7.49E-07	7.28E-07	7.45E-07	7.77E-07	7.84E-07	8.22E-07
8.66E-07	8.39E-07	8.62E-07	8.94E-07	9.07E-07	9.42E-07
9.71E-07	9.50E-07	9.69E-07	1.01E-06	1.02E-06	1.06E-06
9.61E-07	9.52E-07	9.69E-07	1.00E-06	1.02E-06	1.05E-06
1.08E-06	1.07E-06	1.12E-06	1.15E-06	1.18E-06	1.21E-06

RESUME

Masoud Giyathaddin OBAID was born in Duhok, Iraq 1980, and he graduated from primary and secondary schools in this city. Then, in 2002, he graduated from Duhok University, College Of Science/physics Department with a B.SC degree in physics., and then, in 2015, he graduated from Dicle University in the Republic of Turkey, Faculty of Natural and Applied Science, with a Master's degree in physics (M.Sc.). Additionally, in 2008, he graduated from Duhok University's College of Arts / English Department with a B.A. Degree in English Arts. In 2012, he graduated from Duhok University's Faculty of Engineering/School of Planning with a high diploma in planning. Then, in 2020, he joined Karabuk University in Turkey to study for a Ph.D. Degree in physics. From 2002 to 2018, he worked as a physics teacher for gifted students at the College of Duhok. In 2018, he became an educational supervisor in the general directorate of education in Duhok City, and up until now, within the period (2017–2019), he worked as a lecturer at the University of Duhok, College of Basic Education, Science Department. During the period (2013–2018), he worked as an educational trainer in the general directorate of education/Duhok.